LINEAR AND NONLINEAR OPTICAL STUDIES OF MOLECULAR ADSORPTION TO SILICA/LIQUID INTERFACES

by

Brittany Lauren Gray Woods

A dissertation submitted in partial fulfillment
of the requirements for the degree

of

Doctor of Philosophy

in

Chemistry

MONTANA STATE UNIVERSITY
Bozeman, Montana

May 2015

DEDICATION

In dedication to my father, who taught me to trust God and to work hard to accomplish my goals. In loving memory of Larry Gray (1946-2002).

ACKNOWLEDGEMENTS

I graciously thank my advisor, Rob Walker, for all the support, patience and dedication he has given me over the years. He always keeps an optimistic view even in the most difficult times. I would also like to thank my committee members, Dr. Pat Callis, Dr. Bern Kohler, Dr. Mary Cloninger, and Dr. Aleks Rebane, and Dr. Stephanie Ewing. I would like to especially thank Dr. Callis for always making time for me; his constant enthusiasm for learning is inspiring.

I extend my gratitude to the members of the Walker Research Group, both past and present, for all the insightful discussions, both scientific and philosophical. I have formed many lasting friendships, but warranting special mentioning is Eric Gobrogge, who has been a constant companion since we started graduate school together. Additionally, I could not have made it through graduate school without the support and friendship from Melissa McIntyre.

And I would not have pursued graduate school without the mentorship of Dr. Nathan Coker, whose dedication and compassion for his students inspired me to become a professor. And finally I would like to thank my family, especially my wonderful and patient husband, Nick. I cannot express how grateful I am that God put him into my life. To my brother and sister, and aunts, uncles, and cousins, I love you and thank you for all the support and care you have provided. And finally, my mother, I thank you for always supporting my decisions, I love you.

TABLE OF CONTENTS

TABLE OF CONTENTS – CONTINUED

TABLE OF CONTENTS – CONTINUED

LIST OF TABLES

Table Page

LIST OF FIGURES

Figure Page

LIST OF FIGURES – CONTINUED

Figure Page

LIST OF FIGURES – CONTINUED

Figure Page

ABSTRACT

Adsorption mechanisms at buried interfaces are difficult to predict *a priori*, with many interactions to consider including those between the substrate and solvent, the substrate and adsorbate, and the solvent and adsorbate. Studies described in this thesis examine the roles these variables have on controlling interfacial behavior, including molecular adsorption and aggregation at solid/liquid interfaces. Specifically, second harmonic generation (SHG) was employed to characterize adsorption environments and adsorption energies at different silica/liquid interfaces, due to the technique's surface specificity. Additionally, time resolved fluorescence was used to quantify emission lifetimes within these same interfacial regions. By systematically changing the substrate, solvent identity, and adsorbate functionality, the impact of each contribution was identified and quantified. Initial studies examined the role played by interfacial pH in controlling adsorption. Above pH 5, silica surfaces become negatively charged and promote two distinct adsorption mechanisms. Adsorption due to these mechanisms requires very long equilibration times (>3hrs). Subsequent experiments studied the role played by solvent identity on interfacial solvation. At a methanol/silica interface a non-polar interfacial environment was produced, independent of solute choice. Non-polar solvents conversely create polar interfacial solvation environments. At these different solid/liquid interfaces, similarly structured coumarin dyes, C151 and C152, were examined. Slight changes in structure lead to differing behaviors at the surface, C151 terminates at monolayer coverage while C152 shows clear signs of multilayer formation. This observation is explained by the difference in hydrogen bonding opportunities for each adsorbate: C151 can accept and donate H-bonds while C152 can only accept H-bonds, resulting in more degrees of freedom for C152 at an interface and thus the possibility of aggregation.

CHAPTER 1

INTRODUCTION

1.1 Motivation

Buried interfaces, such as those between two immiscible liquids or between a solid and a liquid, are challenging to understand as many bulk properties are altered by asymmetric forces between the two adjacent phases. Nevertheless, experimentally identifying how a medium's interfacial properties differ from bulk limits is fundamental to understanding molecularly-based mechanisms of adsorption, surface structure, and surface reactivity.[1-3] Adsorption to a solid/vapor interface reflects simply the interactions between the solute and the substrate. When the system becomes more complex, as in the case of a buried interface, the forces responsible for adsorption become more difficult to interpret. Adsorption from solution to a buried interface requires that a summation of all interactions between the solvent, solute, and substrate be thermodynamically favored. The work presented in this thesis will systemically examine each contribution to isolate how these interactions influence molecular adsorption.

Understanding fundamental properties that promote adsorption has innumerable applications in a wide variety of fields including environmental science, chromatographic separations, corrosion, and biological recognition. Specific examples of applications include the determination of adhesion mechanisms,[4] observing the kinetics and behavior of adsorption of inorganic solutes, and the development of film formation of nanoparticles.[5-7] The work presented in this thesis is more directly applicable to

environmental remediation and chromatographic column development, given the work's focus on silica/aqueous and silica/organic solvent interfaces. [8-10]

Environmental remediation strategies are tailored to either immobilize or dilute harmful solutes. Metal contamination and aggregation, in particular, have been an issue in mining states, such as Kentucky, West Virginia, and even in several areas around Montana.[11-14] New methods are being developed to improve current remediation techniques for removing heavy metals from water and soil samples, an example being interfacial chelation.[13] For this method, surfaces are functionalized with highly specific chelating polymers. These structurally supported membranes allow for improved adsorption and recovery without altering the desirable bulk properties of the polymers.[13] Forced aggregation and immobilization of pollutants can be a useful method of improving the purity of water systems, although removal of these contaminated substrates then becomes an essential requirement for sustained environmental remediation.

Although heavy metal contamination is of great concern, organic pollutants, such as polychlorophenols (PCP) or benzene derivatives, make up about 60% of environmental contaminants.[15-16] In an aqueous environment, these contaminants can have one of three behaviors, as shown in Figure 1.1.[17] If the pollutant has a strong solute-solvent interaction, via hydrogen bonding or dipole-dipole interactions, then the pollutant can remain in solution (Figure 1.1A).[18-20] Another possibility is the solute-substrate interactions are sufficiently strong leading to adsorption (Figure 1.1B). If the molecules in solution continue to be attracted to the interface after the first species adsorb, the adsorbates will begin to aggregate (Figure 1.1C). In each case, there are benefits and

drawbacks from the standpoint of devising remediation strategies: high mobility could cause dilution of benzenes to safe levels but makes environmental remediation difficult and more expensive.[10] If, however, molecules adsorb to the soil, clean-up methods would be simplified, but only in the cases of known spillages. If contamination occurs unknowingly, the pollutant could stay in the environment for years with adverse effects.[21] Determining the mechanisms involved and studying the effects solvent and solute structures have on adsorption and aggregation can lead to improved methodology for water purification systems.

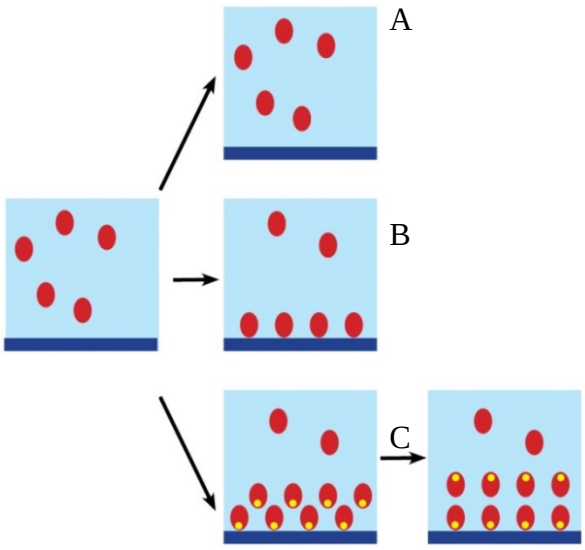

Figure 1.1 A schematic of the options molecules in solution have when they are in proximity to a surface. A) Solutes remain in solution (no adsorption). B) Solutes adsorb to the surface and terminate at a monolayer coverage or C) the solutes have a high affinity for the surface and start to aggregate, either by forming with dipoles directed in the same direction (left) or with canceling dipoles (right).

These same considerations can be applied to the development of chromatographic separation techniques.[22-23] Chromatography, and in particular high performance liquid chromatography (HPLC), uses specially designed columns and solvent mixtures in order to separate solutes in solution.[24] These results can be skewed if solute aggregation or undesirable separation occurs. Aggregation of molecules on column substrates can lead to false reporting of size, molecular mass, and poor separation of solutes.[23] Separation studies using hydrodynamic chromatography have shown the effect aggregation can have on chromatographic techniques in addition to proposing a procedure to reduce aggregation opportunities.[23] Predicting and/or controlling adsorption is a prerequisite for designing column structures that have high selectivity to improve reproducibility and improve accuracy of the results. Not only is the composition of the column structure important for separation but the mobile phase will also play a strong role in controlling how molecules will absorb. Typically, chromatographic methods use silica gels or functionalized silica as the stationary phase, and binary mobile phases such as water:acetonitrile or methanol:water.[25-26] Controlling adsorption requires understanding interfacial solvation. Here, interfacial solvation refers to the noncovalent interactions that an adsorbate experiences with its surroundings. The interface created between the substrate and solvent can have unexpected behavior that influence analyte adsorption. Solvent properties such as polarity, pH, hydrogen bond (H-bond) opportunities, and other bulk solvation properties have been shown to differ greatly at an interface.[1-3, 27-34]

Studies described in this dissertation focus on isolating and characterizing solvent-solute, solvent-substrate, and adsorbate-substrate interactions. Specifically,

experiments alter properties systematically and the changes of molecular adsorption are measured via surface specific and semi-surface specific techniques. One important focus of the work is identifying conditions that either lead to terminal monolayer films or promote formation of multilayers and/or aggregates. As previously mentioned, Figure 1.1 illustrates schematically the different outcomes in systems that can form films. This model is general for any solid/liquid interface and is not specific to the environmental examples given above. A solute can remain in solution, leaving the solvent to fill the surface sites (a). If solutes are stabilized at a surface, they may adsorb to form a terminal monolayer (b), and if solutes are attracted to the species already adsorbed, multilayers will form (c). Multilayer organization will depend sensitively on the structure of the adsorbates themselves. Examples of how molecular structure affects aggregation can be found in the literature describing dye molecule assembly in solutions and at interfaces.[35-38] Aggregation commonly results from enhanced noncovalent interactions between polar monomers. Two common aggregation types are the H-aggregation and J-aggregation. J-aggregate formation (named for Jelley, a pioneer in this field) [35-36, 39-40] results in a red shift of energies compared to the monomeric species, while a blue shift in energetics results in H-aggregation. In this case, the initial H is a descriptive term referring to a blue or hypsochromic shift of absorption spectra.[35-36, 39-40] At surfaces, adsorbates will adopt anisotropic orientations that may either promote or inhibit aggregate formation relative to the tendency of monomers to self-associate in a bulk, isotropic environment. As noted above, aggregation can have important consequences for the fields of separation chemistry and environmental chemistry.

The affinity a solute has for a solid/liquid interface will depend on many factors including the charge and/or dipole density of the substrate, the molecular properties of the solute, and the solvent properties in bulk and at the interface. At interfaces, the solvation environment can be altered due to interactions with the substrate, ordering of solvent molecules, and solvent-solute interactions. Differentiating between interfacial solvation and bulk solvation environment can be difficult, but there is a great need to understand the adsorption environment and mechanisms.[2, 27, 29, 32, 34, 37, 41-48] My dissertation work has focused on studying these differences and, specifically, how the adsorption environment can be drastically altered by slight changes in solvent and solute structure. To study these phenomena we have employed two powerful techniques capable of examining molecular adsorption at various solid/liquid interfaces.

1.2 Summary of Techniques

Observing interfacial chemistry is a difficult task because the signal is limited by the small number of molecules at an interface. Validated mechanistic descriptions of adsorption and interfacial solvation are limited due to a dearth of surface specific techniques capable of probing buried interfaces. Much of the work described in this dissertation exploited the surface specificity of 2nd order nonlinear optical spectroscopy and the approximate surface specificity achieved with total internal reflection (TIR) fluorescence to study adsorption mechanisms and interfacial dynamics. The surface response can further decrease due to adsorbates' dependency on the polarization and incident angle of the incoming beam. The dependency on polarization, however, can

provide valuable information about the average orientation of molecules adsorbed to the surface.

SHG is a nonlinear optical technique that is intrinsically surface specific.[3, 49] In Figure 1.2A, an ultra-fast coherent laser with incident light intensity, I(ω), is used to induce a polarization where the polarization can be expanded as a power series in the strength of the incident electromagnetic field:

$$P = P^{(0)} + P^{(1)} + P^{(2)} + \cdots \quad \text{Eq. 1.1}$$

Here, the total polarization depends on the incident field strength and includes any static polarization, $P^{(0)}$, as well as contributions from induced linear ($P^{(1)}$)and nonlinear polarizations, ($P^{(2)}$, $P^{(3)}$,..etc.). SHG arises from the second order polarization, $P^{(2)}$, which can be related to the intensity of the SH signal, I(2ω) through the following expressions:

$$I(2\omega) \propto \left|P^{(2)}(2\omega)\right|^2 \quad \text{Eq. 1.2}$$

and

$$P^{(2)} = \chi^{(2)} : E(\omega)E(\omega) \quad \text{Eq. 1.3}$$

The second order susceptibility $\chi^{(2)}$, is responsible for the surface specificity of SHG. This term represents a third rank tensor with 27 elements. Third rank tensors are antisymmetric with respect to inversion and require that for each element, $\chi^{(2)}_{i,j,k} = -\chi^{(2)}_{-i,-j,-k}$, where *i,j,k* are the different incident and outgoing field orientations in the laboratory frame of reference. In isotropic environments this condition is satisfied if all elements of the tensor are equal to zero. In an anisotropic environment, such as in noncentrosymmetric materials or at interfaces, SH signal becomes symmetry allowed and the tensor can contain up to three unique, nonzero elements: $\chi^{(2)}_{iiz} = \chi^{(2)}_{izi}, \chi^{(2)}_{zii}$, and $\chi^{(2)}_{zzz}$.

Each of these elements can be separated into nonresonant (NR) and resonant (R) terms where the nonresonant contribution can be treated as a constant over a limited wavelength range:

$$\chi^{(2)} = \chi_{NR}^{(2)} + \chi_{R}^{(2)} \quad \text{Eq. 1.4}$$

$$\chi_{R}^{(2)} \propto N\langle\beta_{ijk}\rangle,\ \beta = \frac{A}{2\omega-\omega-i\Gamma} \quad \text{Eq. 1.5}$$

Here, $\chi_{R}^{(2)}$ is equal to the number of molecules at an interface, N, by the orientationally averaged hyperpolarizability, $\langle\beta_{ijk}\rangle$. β, the molecular hyperpolarizability, is related to the transition matrix element between ground and excited states of a molecule through the A term, where A is the sum of all real excitation energies of the transition matrix elements, $A = \sum \mu_{gk}\mu_{ke}\,\mu_{eg}$, the resonance frequency, 2ω, and the spectral line width, Γ.[50] The resonance wavelength can be compared to the bulk solvatochromic behavior of the adsorbate to determine the local polarity of the interface. The relative homogeneity of the adsorption environment can be inferred from the line width; narrower line widths are assumed to reflect less inhomogeneous broadening.

Raw photon counts generated by SHG are collected and are related back to the incident power (I(ω)), through Equation 1.5 by

$$I(2\omega) \propto \left|\chi^{(2)}\right|^2 I(\omega)^2 \quad \text{Eq. 1.6}$$

From this relationship, we can measure the intensity of the incoming beam I(ω) and collect the second harmonic response I(2ω) and fit the spectra with a combination of Eq. 1.5 and 1.6 to determine the spectroscopic characteristics of the adsorbed species. Additionally, we can use this relationship to calculate adsorption strength. An isotherm is measured by collecting the SH signal as a function of concentration where the square

root of SH signal is proportional to the relative coverage of molecules at the surface. Figure 1.2B and its corresponding inset, show an example of a typical isotherm with monolayer coverage and a SHG spectrum of the system. Assuming ideal conditions, such as a homogenous surface, no interactions between adsorbates, and monolayer coverage of molecules with the same orientation, isotherms can be fitted to a standard Langmuir equation:[51]

$$\frac{q}{Q} = \frac{bc}{1+bc} \qquad \text{Eq. 1.7}$$

where q/Q is the fraction of adsorption sites occupied by solute molecules and is proportional to $\sqrt{I(2\omega)}$. To measure isotherms, the incident (and SH) wavelength remains constant and the SH signal is collected as a function of concentration, c, and then fit to Eq. 1.7 to calculate b, a constant that can be related to the free energy of adsorption, ΔG^o_{ads} through Eq. 1.8.[51]

$$b = e^{\frac{-\Delta G^o_{ads}}{RT}} \qquad \text{Eq. 1.8}$$

$\Delta G^o_{ads}$is the strength of adsorption and in the case of buried interfaces, is the summation of the substrate-adsorbate, substrate-solvent, and the solvent-adsorbate interactions, in addition to any modification of the surface caused by the solvent.

SHG data were fit using programs written for WaveMetric's IGOR Pro. For spectral data, a combination of Eq. 1.4-1.6 were used to fit the data, and for the work presented, data were fit using 4 adjustable parameters: resonance wavelength, amplitude, line width, and the nonresonance term. However, for spectra with multiple peaks the number of adjustable parameters is doubled to take into account any changes of

parameters a second peak introduces. The nonresonance term is typically fit to a single value as the resonance contribution is 10-100 times larger than the nonresonance, however, in some cases the surface response is strong, and the nonresonance term must be treated more carefully. The spectral fitting equation is then adjusted to fit the nonresonance term to a simple function, such as a line. Also written into the IGOR program is an error analysis routine for each parameter.[52] An additional program was written to fit the Langmuir equation to isothermal data and calculated the free energy of adsorption including error analysis.

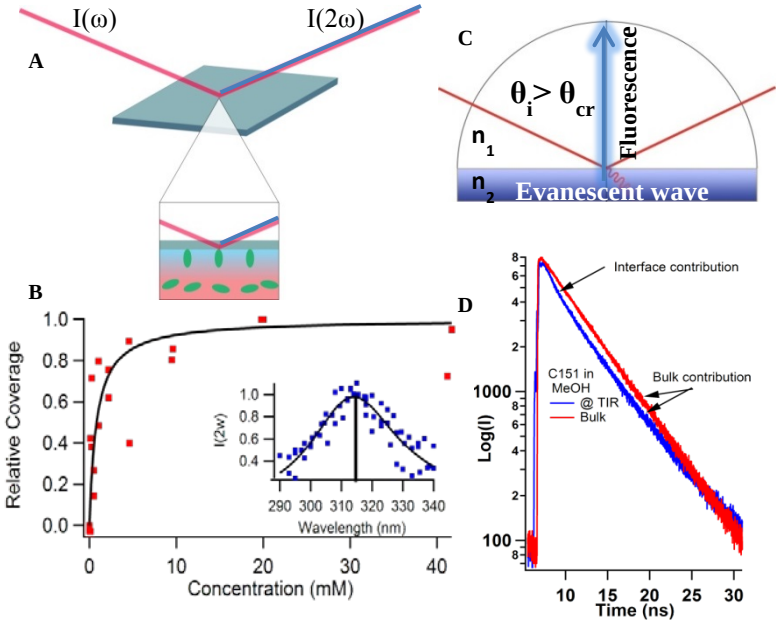

Figure 1.2. A) SHG diagram of an incident beam, I (ω) inducing polarization at an interface and generating SH signal at I (2ω). B) Example SHG data of an isotherm and spectral data (inset). C) Schematic of a TIR geometry. D) Example of TIR decays showing two distinct lifetimes; a bulk contribution and interfacial behavior.

SHG data provide valuable information about the interfacial molecules in their ground electronic state, but to study the photodynamics of these molecules we employ time correlated single photon counting spectroscopy (TCPSC) coupled with a total internal reflection geometry in order to collect interfacial behavior.

Time resolved fluorescence excites a molecule and measures the time required for the molecule to relax radiatively to its electronic ground state. Typically, after exciting to a higher vibrational state in the excited electronic state, molecules rapidly relax to the lowest vibrational state via internal conversion. Internal conversion timescales are quite short, on the order of 10^{-12}s or shorter. [53-54] Electronic excitation, in general, results in a longer lived species whose luminescence can be measured. Although fluorescence lifetimes can range from 10^{-13} to 10^{-4} s, for the purpose of the work presented,[53, 55] we refer to a long lifetime being $\geq$ 5 ns, while a very short lifetime is $\leq$ 1 ns.[56] These limits were chosen based on the lifetimes of the molecules examined in this thesis. A long lifetime would indicate a stable excited state configuration, while a short lifetime would suggest facile non-radiative decay pathways.

Several techniques can be used to collect the fluorescence emission. The technique relevant for studies presented in this dissertation was TCSPC.[53-54] For TCSPC fluorescence, a mode locked laser is used to excite molecules into their excited state configuration and a histogram of the waveform of the decay is collected. The detector, in our case a PMT, is synced to the light source and the collection process starts when an excitation occurs and ends when either an emission photon arrives at the detector or the time window ends.[53-54] The window range is set based on the expected lifetime of the

molecule, longer lifetimes require larger ranges. Once a photon is detected or after the allotted time expires, the arrival times of emission are binned to create a histogram and multiple histograms of the decay are collected for increased accuracy. The log of the intensity of the waveform is plotted against time and should result in either a single line, if there is one lifetime or multiple lines for each lifetime present. In the work presented, the rep rate is 4 MHz and the histogram is collected until the max count reaches 8000 or stops after 5000 s, with 8 ps resolution. The interfacial fluorescence studies are more challenging to collect as there is a drastic decrease in the histogram counts. Typical decays collected in bulk solution can have emission counts on the order of $1x10^5$, this value drops to the order of 10^3 at the interface. To increase counts, the irises are opened and the monochrometer slit widths are increased to the maximum (2 nm), while the signal may increase, increasing the light into the sample chamber also increases the amount of scatter from the optical components.

The effective resolution of TCSPC is dependent on its instrument response function (IRF). The IRF takes into account the inherent electronic noise of the instrument and detector and scatter of excitation source, therefore opening the irises can greatly increase the IRF as light is reflected in the sample chamber. The excitation source for our TCSPC assembly is a Coherent Chameleon Ti:sapphire oscillator (80 MHz rep rate) with a wavelength range of 680-1080 nm. An APE autotracker was use to convert the fundamental beam using either a doubling (SHG) crystal to create a 350-520 nm range or a tripling crystal, creating a 226-340 nm range. The excitation wavelength range for the adsorbates presented here requires only the use of the SHG output and use of the

corresponding modulator (Conoptics Model 350-105).The modulator reduced the repetition rate of the 80 MHz Ti:sapphire laser to a repetition rate of 4 MHz for the TR-TIRF measurements. Fluorescence was collected using a Picoquant PicoHarp 300 detector with the FluoTime 200 software.

Fluorescence data were analyzed using Picoquant's FluoFit fitting software and fitted to a multimodal Gaussian distribution after reconvoluting the data to account for scatter from the IRF. For bulk experiments, the IRF is on the order of 20-50ps. After eliminating contributions from the IRF, data were fit to a sum of exponential decays:

$$I(t) = \sum_{i=1}^{n} A_i e^{-t/\tau_i} \qquad \text{Eq. 1.9}$$

The parameters A_i and τ_i are the amplitude and lifetime of the i^{th} component of the decay, respectfully. Fitting parameters are optimized according to a least squares fit. When making standard, bulk solution measurements, lifetimes can be measured with ±0.05 ns resolution.

Time resolved fluorescence is not a surface specific technique. However, by performing experiments in a total internal reflection geometry (TIR), interfacial time-resolved emission can be measured. As shown in Figure 1.2, for a TIR geometry the incident beam must pass through a material having a higher refractive index ($n_{substrate}>n_{solvent}$) at an incident angle ($\theta_i$) greater than the critical angle (θ_{cr}). With this geometry, the light is reflected but an evanescent field penetrates into the adjacent, low index phase with an amplitude that decreases exponentially. This evanescent wave penetrates and excites molecules at and near the surface on the order of 10^2 nm.[57] The sampling depth is dependent on the wavelength, indices of refraction of the adjacent

media, and the incident angle. The TIR-TCSCP assembly used in these studies has an incident angle range of $72^{o}\pm3$, and a penetration depth of ~100-180 nm for the wavelength range and solvent choices used in this dissertation. The TIR geometry does introduce a higher degree of scatter which increases the IRF to 150-200 ps. In general, data from the TIR assembly can be fit with at least two lifetimes with amplitude accuracies of ±7% and lifetime accuracies of ± 0.20 ns.

My work has used these techniques to observe how slight changes to the substrate, solute, and solvent can alter adsorption behavior. The goal of my research was to explore systematically the fundamental solute, solvent and substrate properties that promote monolayer and multilayer adsorption. Studies described in the following chapters show how the silica/liquid interface is very sensitive the hydrogen bonding capabilities of both the solvent and adsorbate.

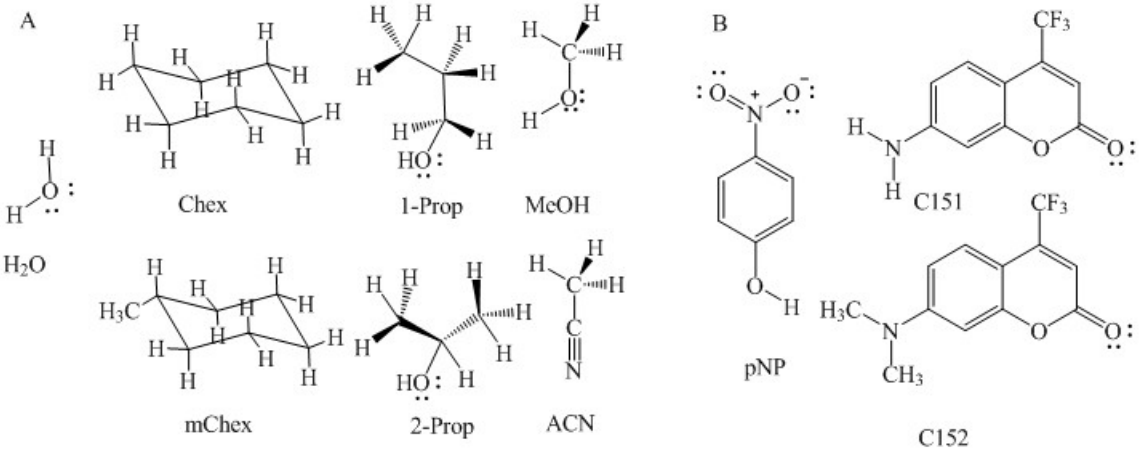

Figure 1.3. A list of all the solvents (A) and solutes (B) discussed in this thesis. The abbreviations for the solvents are as follows, water (H_2O), cyclohexane (Chex), methylcyclohexane (mChex), 1-propanol (1-prop), 2-propanol (2-prop), methanol (MeOH), acetonitrile (ACN). The abbreviations for the solutes are *p*-nitrophenol (pNP), coumarin 151 (C151) and coumarin 152 (C152).

1.3 Polarity Description

There are many descriptions of polarity, such as the π*,[58] $E_T(30)$,[59] P_s,[60] and Z,[61] scales.[62] These scales are empirical and based on spectral data of solvatochromic compounds and therefore are limited in their description of nonspecific (e.g. electrostatic forces) and specific (hydrogen bonding) interactions between the solute and solvent.[62,63] The Onsager polarity function is not based on empirical measurments of specific solutes in solution and instead creates a normalized polarity scale based on the solvent's static dielectric constant, ε, through the following equation:[64]

$$f(\varepsilon) = \frac{2(\varepsilon-1)}{2\varepsilon+1} \qquad \text{Eq. 1.10}$$

The Onsager scale ranges from 0.4 to 1.0, which is given by the dielectric constants of alkanes (~2) to water (~80).[62, 65-66] The work presented in this thesis uses the Onsager function to describe polarity. Although this model lacks the ability to discriminate specific from nonspecific solvation forces, the Onsager function is independent on solute size and shape and allows for an uniform description of solvation effects on adsorption mechanisms.[29, 47] The solvents discussed in this thesis (Figure 1.3) were chosen to observe molecular adsorption effects with varying polarity ($f(\varepsilon)$ of 0.4 (alkanes) to $f(\varepsilon)$=0.98 (water)). In the case of solutes undergoing an increase of transition dipole moment-that is if the ground state molecular dipole is less than that of the excited state dipole- the nonspecific solvation forces will generally result in a decrease of excitation energy in polar solvents, or red shift in spectra.[47, 67] A red shift can also occur if the solvent is a hydrogen bond acceptor, such as acetonitrile and DMSO. This shift in excitation spectra and its dependency on solvation polarity is referred to as a

solvatochromic shift.[29, 66] Figure 1.4 is an energy diagram comparing the solvatochromic shifts of nonspecific solvation interactions (left) and hydrogen bonding, a specific interaction (right). The behavior depicted in Figure 1.3 is predicted for the solutes chosen as interfacial probes (Figure 1.3) as their ground state dipole is less than that of the excited state.

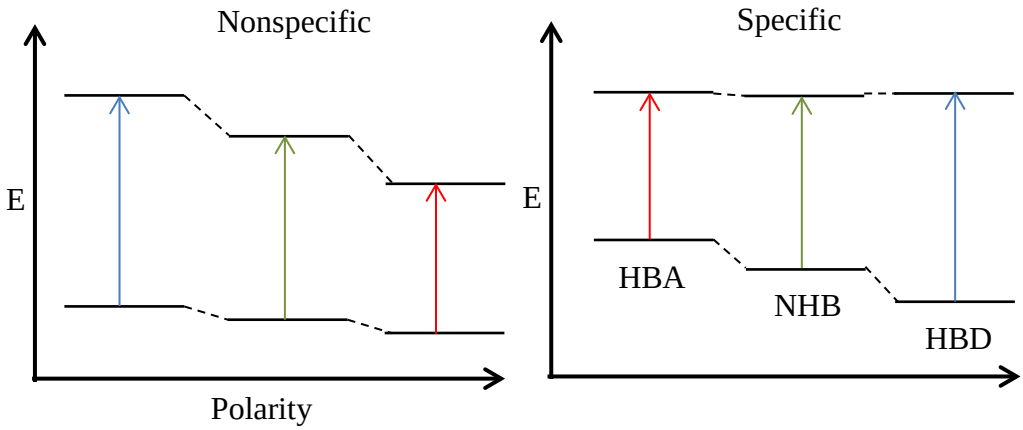

Figure 1.4. Energy diagrams describing the effects of nonspecific interactions (left) and specific interactions (right). The abbreviations are as follows: hydrogen bonding accepting (HBA), non-hydrogen bonding (NHB) and hydrogen bonding donating (HBD) solvents.

1.4 Thesis Organization

Using techniques described in the previous section, my research focuses on understanding solvent effects on molecular adsorption to solid/liquid interfaces and the subtle ways solute and solvent structure control aggregate formation at this boundary. The following section briefly describes topics to be discussed in each chapter. Figure 1.3 depicts the solvents and solutes that will be discussed in this thesis.

Chapter 2. pH Effects on Molecular
Adsorption and Solvation
of p-Nitrophenol at Silica/Aqueous Interfaces.

Chapter 2 presents a series of experiments that examined the role played by interfacial pH in controlling adsorption at the silica/aqueous interface. Silica is a major component of soil, understanding its role in adsorption, especially in various aqueous conditions, can provide valuable insight into the fate of environmental solutes.[68] The silica/aqueous interface was studied at pH 1, 5, 7, and 10.5. At pH 1, terminal silanols are protonated and the surface has a slightly positive charge. As pH increases the silanols become deprotonated, resulting in a negatively charged surface. SHG spectra and isothermal data were collected for p-nitrophenol (pNP), at the silica/aqueous interface for each pH at two equilibration times, after one hour and after three hours. SHG spectra after 1 hr. equilibration showed little pH dependence; only at longer equilibration times did pH effects become prominent in the spectra with the growth of a second binding site in spectra of pH $\geq$ 5. pNP H-bonds to silica through its hydroxyl group. In basic solutions pNP becomes deprotonated and must share a proton with surface oxides, resulting in longer equilibration times. When pNP adsorbs to the deprotonated silica/aqueous interface, two distinctly different silanol sites are sampled, characterized by a weaker and a stronger adsorbate-substrate interaction that appears to be pH dependent.[3]

Chapter 3. Adsorption and
Solvation at Silica/Liquid Interfaces.

This chapter focuses on how organic solvents influence adsorption mechanisms. The results of these studies showed unexpected behavior. Polar protic (1- and 2-

propanol) and nonpolar solvents (cyclohexane and methylcyclohexane) were studied at the silica interface in the presences of well characterize coumarin dyes. At the silica/1- and 2-propanol interfaces, adsorbates were shown to experience a nonpolar interface, while solvents incapable of H-bonding, like cyclohexane, created decidedly polar solvation environments.[1] The latter part of the chapter describes SHG and TIR-TCSPC experiments that studied the interfacial ground electronic state and the dynamics properties of Coumarin 151 (C151) at the methanol/silica interface.[2] C151 has a primary amine at the 7-position and the ability to accept and donate H-bonds. SHG data show C151 at the MeOH/silica boundary experiences a nonpolar interface with relatively strong adsorption as calculated by isothermal data. TIR-TCSPC decays collected at the MeOH/silica interface show two distinct lifetimes, one corresponding to a polar contribution from the bulk and a second lifetime that is similar to the lifetime of C151 in non-polar bulk solutions. This nonpolar interfacial region forms independent of the solute identity, as shown by subsequent SHG studies on various coumarins at the MeOH/silica surface.

Chapter 4. Adsorption and Aggregate Formation at Solid/Liquid Interfaces.

Adsorption mechanisms depend as much on adsorbate identity as on substrate and solvent identity. One property that differentiates solute adsorption mechanisms is an adsorbate's tendency to form either a terminal monolayer or aggregates as bulk solution concentration increases. Of particular interest are two 7-aminocoumarins: C151 and C152. C152 is a tertiary amine that can only accept H-bonds.[1-2] Isothermal data of C151

at the MeOH/silica interface shows typical monolayer coverage with concentration dependent isotherm data similar to that shown in Figure 1.2B. However, as the concentration of C152 at the same interface increases, SH signal decreases sharply, suggesting that C152 begins to self-associate forming aggregates or multilayers with local inversion symmetry. TIR-TCSPC data imply that aggregates experience a different solvation environment than do monomers at monolayer and sub-monolayer coverages. Computational methods were used to provide a semi-quantitative analysis of the most likely aggregate structure. The *ab initio* calculations suggest C152 would preferentially stack with the opposite facing dipoles. This orientation would create an inversion center, explaining the decrease in SHG signal.

By altering the H-bonding capabilities of a solute, one can potentially control aggregation. This has important consequences for environmental testing and biological studies, as pollutants in streams could accumulate in the soil and potentially create an environmental hazard.

Chapter 5. Spectroscopic Solvation
Mechanisms at the Silica/Acetonitrile Interfaces.

The final chapter of the thesis compares the adsorption environment at a silica/polar aprotic interface to the previous data collected at the silica/ polar protic interface. We used C151 and C152 in acetonitrile-a well-studied polar aprotic solvent- to study the effects of hydrogen bonding of both the solvent and solute. Both the SHG and TIR-TCSPC studies on C152 at the silica/acetonitrile interface show C152 experiences a polar adsorption environment. Although SHG data on C151 supports a polar adsorption

region, TIR-TCSPC decays indicate a nonpolar like interface. These conflicting results are surprising. By comparing the silica/acetonitrile data to the silica/methanol studies, we see how the neat silica/solvent environment can greatly influence the ability of the interfacial solvent to stabilize the excited state of the coumarin dyes. The silica/methanol interface was shown to create a nonpolar region. In contrast, the interfacial acetonitrile molecules adsorb to silica and form strongly associating bilayers to silica that can extend several nanometers away from the surface. In addition, acetonitrile molecules are unable to quickly and easily rearrange themselves to stabilize the excited state of C151, resulting in nonpolar-like dynamic properties at a polar interface. We propose that C152 interacts with silica via hydrogen bond accepting, this arrangement would allow the interfacial solvation environment access to stabilize the excited state of C152.

1.5 References

1. Gobrogge, E. A.; Woods, B. L.; Walker, R. A., Liquid Organization And Solvation Properties At Polar Solid/Liquid Interfaces. *Faraday Discussions* **2013**, *167*, 309-327.

2. Roy, D.; Liu, S. L.; Woods, B. L.; Siler, A. R.; Fourkas, J. T.; Weeks, J. D.; Walker, R. A., Nonpolar Adsorption at the Silica/Methanol Interface: Surface Mediated Polarity and Solvent Density across a Strongly Associating Solid/Liquid Boundary. *Journal of Physical Chemistry C* **2013**, *117*, 27052-27061.

3. Woods, B. L.; Walker, R. A., pH Effects on Molecular Adsorption and Solvation of p-Nitrophenol at Silica/Aqueous Interfaces. *Journal of Physical Chemistry A* **2013**, *117*, 6224-6233.

4. Cashman, J. D.; Kennah, E.; Shuto, A.; Winternitz, C.; Springate, C. M. K., Fucoidan Film Safely Inhibits Surgical Adhesions in a Rat Model. *Journal of Surgical Research* **2011**, *171*, 495-503.

5. Bucholz, E. W.; Phillpot, S. R.; Sinnott, S. B., Molecular Dynamics Investigation Of The Lubrication Mechanism Of Carbon Nano-Onions. *Computational Materials Science* **2012**, *54*, 91-96.

6. Picarra, S.; Afonso, C. A. M.; Kurteva, V. B.; Fedorov, A.; Martinho, J. M. G.; Farinha, J. P. S., The Influence Of Nanoparticle Architecture On Latex Film Formation And Healing Properties. *Journal of Colloid and Interface Science* **2012**, *368*, 21-33.

7. Tofan-Lazar, J.; Al-Abadleh, H. A., ATR-FTIR Studies on the Adsorption/Desorption Kinetics of Dimethylarsinic Acid on Iron-(Oxyhydr)oxides. *Journal of Physical Chemistry A* **2012**, *116*, 1596-1604.

8. Li, W.; Liu, D.; Wu, J.; Kim, C.; Fortner, J. D., Aqueous Aggregation and Surface Deposition Processes of Engineered Superparamagnetic Iron Oxide Nanoparticles for Environmental Applications. *Environmental Science & Technology* **2014**, *48*, 11892-11900.

9. Wu, G.; Zhu, X.; Ji, H.; Chen, D., Molecular Modeling Of Interactions Between Heavy Crude Oil And The Soil Organic Matter Coated Quartz Surface. *Chemosphere* **2015**, *119*, 242-9.

10. Franco, C. A.; Martinez, M.; Benjumea, P.; Patino, E.; Cortes, F. B., Water Remediation Based on Oil Adsorption Using Nanosilicates Functionalized with a Petroleum Vacuum Residue. *Adsorption Science & Technology* **2014**, *32*, 197-207.

11. Muncy, B. L.; Price, S. J.; Bonner, S. J.; Barton, C. D., Mountaintop Removal Mining Reduces Stream Salamander Occupancy And Richness In Southeastern Kentucky (USA). *Biological Conservation* **2014**, *180*, 115-121.

12. Perine, A. *An Investigation of Potential Ground and Surface Water Contamination From Stormwater Discharge, City of Missoula, MT.*; Missoula Valley Water Quality District: Missoula, 1998.

13. Tian, F.; Roman, M. J.; Decker, E. A.; Goddard, J. M., Biomimetic Design of Chelating Interfaces. *Journal of Applied Polymer Science* **2015**, *132*.

14. Van Aken, B.; Quaranta, J. D.; Mack, B.; Yu, H.; Ducatman, A. M.; Ziemkiewicz, P. F., Environmental Contaminants in Coal Slurry Intended for Underground Injection in the State of West Virginia. *Journal of Environmental Engineering* **2015**, *141*.

15. EPA Drinking Water Contaminants.

16. Ennist, J. H.; Gobrogge, E. A.; Schlick, K. H.; Walker, R. A.; Cloninger, M. J., Cyclodextrin-Functionalized Chromatographic Materials Tailored for Reversible Adsorption. *Acs Applied Materials & Interfaces* **2014**, *6*, 18087-18097.

17. Arora, P. K.; Bae, H., Bacterial Degradation Of Chlorophenols And Their Derivatives. *Microbial Cell Factories* **2014**, *13*.

18. Corma, A.; Iborra, S.; Velty, A., Chemical Routes For The Transformation Of Biomass Into Chemicals. *Chemical Reviews* **2007**, *107*, 2411-2502.

19. Davis, T. A.; Volesky, B.; Mucci, A., A Review Of The Biochemistry Of Heavy Metal Biosorption By Brown Algae. *Water Research* **2003**, *37*, 4311-4330.

20. Fujishima, A.; Zhang, X.; Tryk, D. A., TiO2 Photocatalysis And Related Surface Phenomena. *Surface Science Reports* **2008**, *63*, 515-582.

21. Soil Screening Guidance: User's Guide. Second Edition ed.; EPA, Ed. Washington, DC, 1996.

22. Grinias, J. P.; Godinho, J. M.; Lunn, D. B.; Jorgenson, J. W., Evaluation Of Preparative Hydrodynamic Chromatography Of Silica Stationary Phase Supports. *Journal of Chromatography A* **2014**, *1370*, 270-273.

23. Lin, M.-C.; Lin, K.-C., Interaction Between Crystal Violet And Anionic Surfactants At Silica/Water Interface Using Evanescent Wave-Cavity Ring-Down Absorption Spectroscopy. *Journal of Colloid and Interface Science* **2012**, *379*, 41-47.

24. Nawrocki, J., The Silanol Group And Its Role In Liquid Chromatography. *Journal of Chromatography A* **1997**, *779*, 29-71.

25. Dawson, R.; Messina, S. M.; Stokes, C.; Salyani, S.; Alcalay, N.; de Fiebre, N. C.; de Fiebre, C. M., Solid-Phase Extraction And HPLC Assay Of Nicotine And Cotinine In Plasma And Brain. *Toxicology Mechanisms and Methods* **2002**, *12*, 45-58.

26. Huber, C. G.; Kleindienst, G.; Bonn, G. K., Application Of Micropellicular Poly-Styrene/Divinylbenzene Stationary Phases For High-Performance Reversed-Phase Liquid Chromotography Electrospray Mass Spectrometry Of Proteins And Peptides. *Chromatographia* **1997**, *44*, 438-448.

27. Brindza, M. R.; Walker, R. A., Differentiating Solvation Mechanisms at Polar Solid/Liquid Interfaces. *Journal of the American Chemical Society* **2009**, *131*, 6207-6214.

28. Eisenthal, K. B., Second Harmonic Spectroscopy Of Aqueous Nano- And Microparticle Interfaces. *Chemical Reviews* **2006**, *106*, 1462-1477.

29. Esenturk, O.; Walker, R. A., Indoline: A Versatile Probe Of Specific And Non-Specific Solvation Forces. *Physical Chemistry Chemical Physics* **2003**, *5*, 2020-2026.

30. Gibbs-Davis, J. M.; Kruk, J. J.; Konek, C. T.; Scheidt, K. A.; Geiger, F. M., Jammed Acid-Base Reactions at Interfaces. *Journal of the American Chemical Society* **2008**, *130*, 15444-15447.

31. Higgins, D. A.; Abrams, M. B.; Byerly, S. K.; Corn, R. M., Resonant 2nd Harmonic-Generation Studies of p-Nitrophenol Adsorption at Condensed-phase Interfaces. *Langmuir* **1992**, *8*, 1994-2000.

32. Horng, P.; Brindza, M. R.; Walker, R. A.; Fourkas, J. T., Behavior of Organic Liquids at Bare and Modified Silica Interfaces. *Journal of Physical Chemistry C* **2010**, *114*, 394-402.

33. Isaienko, O.; Nihonyanagi, S.; Sil, D.; Borguet, E., Observation of the Bending Mode of Interfacial Water at Silica Surfaces by Near-Infrared Vibrational Sum-Frequency Generation Spectroscopy of the Stretch plus Bend Combination Bands. *Journal of Physical Chemistry Letters* **2013**, *4*, 531-535.

34. Marowsky, G.; Steinhoff, R.; Chi, L. F.; Hutter, J.; Wagniere, G., 2ND-Harmonic Generation in Quinquethienyl Monolayers. *Physical Review B* **1988**, *38*, 6274-6278.

35. Verma, P.; Pal, H., Intriguing H-Aggregate and H-Dimer Formation of Coumarin-481 Dye in Aqueous Solution As Evidenced from Photophysical Studies. *Journal of Physical Chemistry A* **2012**, *116*, 4473-4484.

36. Verma, P.; Pal, H., Unusual H-Type Aggregation of Coumarin-481 Dye in Polar Organic Solvents. *Journal of Physical Chemistry A* **2013**, *117*, 12409-12418.

37. Roy, D.; Piontek, S.; Walker, R. A., Surface Induced Changes In Coumarin Solvation And Photochemistry At Polar Solid/Liquid Interfaces. *Physical Chemistry Chemical Physics* **2011**, *13*, 14758-14766.

38. Ariga, K.; Lvov, Y.; Kunitake, T., Assembling Alternate Dye-Polyion Molecular Films By Electrostatic Layer-By-Layer Adsorption. *Journal of the American Chemical Society* **1997**, *119*, 2224-2231.

39. Liu, X.; Cole, J. M.; Chow, P. C. Y.; Zhang, L.; Tan, Y.; Zhao, T., Dye Aggregation And Complex Formation Effects In 7-(Diethylamino)-Coumarin-3-Carboxylic Acid. *Journal of Physical Chemistry C* **2014**, *118*, 13042-13051.

40. Pant, D.; Le Guennec, M.; Illien, B.; Girault, H. H., The pH Dependent Adsorption Of Coumarin 343 At The Water/Dichloroethane Interface. *Physical Chemistry Chemical Physics* **2004**, *6*, 3140-3146.

41. Zhang, X. Y.; Cunningham, M. M.; Walker, R. A., Solvent Polarity At Polar Solid Surfaces: The Role Of Solvent Structure. *Journal of Physical Chemistry B* **2003**, *107*, 3183-3195.

42. Zhang, X. Q.; Yang, W. Y.; You, X. Z.; Wei, Y., Preparation And Characterization Of Self-Assembly Organic Multilayer Films On Silica Surface. *Applied Surface Science* **1995**, *84*, 267-271.

43. Zhang, X.; Steel, W. H.; Walker, R. A., Probing Solvent Polarity Across Strongly Associating Solid/Liquid Interfaces Using Molecular Rulers. *Journal Of Physical Chemistry B* **2003**, *107*, 3829-3836.

44. Wirth, M. J.; Burbage, J. D., Adsorbate Reorientation At A Water(Octadecylsilyl) Silica Interface. *Analytical Chemistry* **1991**, *63*, 1311-1317.

45. Vazquez, R.; Nogueira, R.; Busquets, S.; Mata, J. L.; Saramago, B., Wetting Films Of Polar And Nonpolar Liquids. *Journal of Colloid and Interface Science* **2005**, *284*, 652-657.

46. Vartia, A. A.; Thompson, W. H., Solvation and Spectra of a Charge Transfer Solute in Ethanol Confined within Nanoscale Silica Pores. *Journal of Physical Chemistry B* **2012**, *116*, 5414-5424.

47. Siler, A. R.; Walker, R. A., Effects of Solvent Structure on Interfacial Polarity at Strongly Associating Silica/Alcohol Interfaces. *Journal of Physical Chemistry C* **2011**, *115*, 9637-9643.

48. Shang, X. M.; Benderskii, A. V.; Eisenthal, K. B., Ultrafast Solvation Dynamics At Silica/Liquid Interfaces Probed By Time-Resolved Second Harmonic Generation. *Journal of Physical Chemistry B* **2001**, *105*, 11578-11585.

49. Bloembergen, N., 2ND Harmonic Reflected Light. *Optica Acta* **1966**, *13*, 311-322.

50. Benjamin, I., Inhomogeneous Broadening Of Electronic Spectra At Liquid Interfaces. *Chemical Physics Letters* **2011**, *515*, 56-61.

51. Hiemenz, P. C., *Principles Of Colloid And Surface Chemistry*, 2 ed.; Marcel Dekker, Inc: New York 1986; Vol. 9, p 792.

52. Taylor, J. R., *An Introduction To Error Analysis: The Study Of Uncertainties In Physical Measurements*, 2nd ed.; University Science Boooks: Sausalito, Ca, 1997.

53. Lakowicz, J., *Principles of Fluorescence Spectroscopy*, Third ed.; Springer Science +Business Media, LLC: New York, 2006.

54. Becker, W., Advanced Time Correlated Single Photon Counting Techniques. In *Advanced Time Correlated Single Photon Counting Techniques*, A.W. Castleman, J., J.P. Toennies, and W. Zinth, Ed. Springer Berlin, Germany, 2006; p 414.

55. Harris, D. C., *Exploring Chemical Analysis*, 3rd ed.; W.H. Freeman and Company: New York, NY, 2005.

56. Nad, S.; Kumbhakar, M.; Pal, H., Photophysical Properties Of Coumarin-152 And Coumarin-481 Dyes: Unusual Behavior In Nonpolar And In Higher Polarity Solvents. *Journal of Physical Chemistry A* **2003**, *107*, 4808-4816.

57. Hecht, E., *Optics*, 4th ed.; Pearson Education, Inc: San Francisco, CA, 2002.

58. Buncel, E.; Rajagopal, S., Studies Of Azo And Azoxy Dyestuffs .19. Solvatochromic Studies Of Novel Azo Merocyanine Dyes - The Pi-Star-Azo-Scale Of Solvent Polarity. *Journal of Organic Chemistry* **1989**, *54*, 798-809.

59. Marcus, Y., The Effectiveness Of Solvents As Hydrogen-Bond Donors. *Journal of Solution Chemistry* **1991**, *20*, 929-944.

60. Freed, B. K.; Biesecker, J.; Middleton, W. J., Spectral Polarity Index - A New Method For Determining The Relative Polarity Of Solvents 1. *Journal of Fluorine Chemistry* **1990**, *48*, 63-75.

61. Kosower, E. M., The Effect Of Solvent On Spectra .1. A New Empirical Measure Of Solvent Polarity - Z-Values. *Journal of the American Chemical Society* **1958**, *80*, 3253-3260.

62. Reichardt, C., Solvatochromic Dyes As Solvent Polarity Indicators. *Chemical Reviews* **1994**, *94*, 2319-2358.

63. Mellein, B. R.; Aki, S. N. V. K.; Ladewski, R. L.; Brennecke, J. F., Solvatochromic Studies Of Ionic Liquid/Organic Mixtures. *Journal of Physical Chemistry B* **2007**, *111*, 131-138.

64. Onsager, L., Electric Moments Of Molecules In Liquids. *Journal of the American Chemical Society* **1936**, *58*, 1486-1493.

65. *CRC Handbook of Chemistry and Physics*, 90 ed.; Taylor and Francis Group, LLC: Boca Raton, Fl, 2009-2010.

66. Suppan, P., Solvatochromic Shifts - The Influence Of The Medium On The Energy Of Electronic States. *Journal of Photochemistry and Photobiology a-Chemistry* **1990**, *50*, 293-330.

67. Steel, W. H., Y.Y. Lau, C.L. Beildeck, R.A. Walker, Solvent Polarity Across Weakly Associating Interfaces. *Journal Of Physical Chemistry B* **2004**, *108*, 13370-13378.

68. Urio, R. d. P.; Masini, J. C., Evaluation Of Sequential Injection Chromatography For Reversed Phase Separation Of Triazine Herbicides Exploiting Monolithic And Core-Shell Columns. *Talanta* **2015**, *131*, 528-534.

CHAPTER TWO

pH EFFECTS ON MOLECULAR ADSORPTION AND SOLVATION OF P-NITROPHENOL AT SILICA/AQUEOUS INTERFACES

Contributions of Authors and Co-Authors

Manuscript in Chapter 2

Author: B. Lauren Woods

Contributions: Collected and analyzed all experimental data and author.

Co-Author: Rob Walker

Contributions: Assisted with data analysis and edited manuscript at all stages.

Manuscript Information Page

B. Lauren Woods, Robert Walker
Journal of Physical Chemistry A
Status of Manuscript:
____ Prepared for submission to a peer-reviewed journal
____ Officially submitted to a peer-review journal
____ Accepted by a peer-reviewed journal
_X__ Published in a peer-reviewed journal

Publisher: ACS
Date of Submission: 15 January 2013
Date Accepted: 5 May 2013
Volume 117, Issue 29, May 2013, 6224-6233
The following chapter has been published in the Journal of Physical Chemistry A and appears in this thesis/dissertation with the journal's permission.

CHAPTER TWO

pH EFFECTS ON MOLECULAR ADSORPTION AND SOLVATION OF P-NITROPHENOL AT SILICA/AQUEOUS INTERFACES

Abstract

Resonance enhanced second harmonic generation (SHG) was used to examine the effects of solution pH and surface charge on *para*-nitrophenol (pNP) adsorption to silica/aqueous interfaces. During the early stages of monolayer formation, SHG spectra of interfacial pNP showed a single resonant excitation wavelength at approximately 313 nm regardless of solution pH. This resonance wavelength of adsorbed species is lower than the 318 nm excitation maximum of pNP in bulk aqueous solution. Experiments were performed at pH concentrations of 1.0, 5.0, 7.0, and 10.5. Under these conditions, the silica surface carried a surface charge that ranged from slightly positive (pH = 1) to strongly negative (pH = 10.5) due to protonation/deprotonation of surface silanol groups. Over the course of 1-3 hours, SHG spectra of pNP evolved so that spectra from interfaces fully equilibrated with solution pH showed two clear resonance features with wavelengths of approximately 310 nm and 330 nm. These wavelengths imply that adsorbed pNP samples two discrete local solvation environments at the silica/aqueous interface. Based on the solvatochromic behavior of pNP in different bulk solvents, the shorter wavelength feature corresponds to a local environment having an effective dielectric constant of 9.5 (similar to that of dichloromethane), while the longer wavelength feature lies outside of pNP's standard solvatochromic window. This longer

wavelength result implies an effective dielectric constant greater than that of bulk water *or* an adsorption mechanism that has pNP adsorbates sharing a proton with surface silanol groups (and adopting an electronic structure that begins to resemble that of its deprotonated form, *p*-nitrophenoxide). The longer wavelength feature is weakest in the low pH systems when the surface is either neutral or slightly positively charged and most prominent at the negatively charged silica/aqueous (pH=10.5) interface. pNP adsorption isotherms for all systems showed approximate Langmuir behavior. Using concentration dependent data from both low and intermediate pH led to calculated adsorption energies of -19 ± 2 kJ/mole for all pH values except pH 10.5 where ΔG^{o}_{ads} fell to –6 ± 2 kJ/mole. Taken together, these spectroscopic and adsorption studies of pNP adsorption to silica/aqueous interfaces as a function of aqueous pH show that interfacial acid/base chemistry can require hours to reach equilibrium and that the silica surface presents hydrogen bonding solutes such as pNP with two distinct adsorption sites. The invariance of pNP's SHG spectra to bulk solution pH suggests that pNP solvation is dominated by substrate/solute interactions with the adjacent solvent having very little influence on adsorbed solute properties.

2.1 Introduction

Molecular adsorption at solid/liquid interfaces depends on a subtle balance between solute-solvent, solute-substrate, and substrate-solvent interactions. Understanding how each of these associations contributes to the overall affinity of a solute for different solid/liquid interfaces has far reaching consequences for phenomena

as diverse as adhesion,[69-70] biomineralization,[71-73] chromatographic separation,[74] and heterogeneous catalysis.[75] In order to predict whether or not solutes will adsorb to a solid/liquid interface *and* what sort of environment an adsorbate will experience at this boundary, one must know adsorption and solvation energies of both the solute *and* the solvent as well as how the anisotropy intrinsic to the interface changes solvent properties relative to bulk solution limits.[41] Furthermore, all of these quantities must be known accurately, because determining whether or not solutes are surface active requires evaluating small differences between what can be large numbers. This task becomes even more challenging when solvent structure at the surface can be affected by specific solvation forces such as hydrogen bonding[27] and nonspecific forces arising from surface charge.[76-78] (Figure 2.1)

Many models have been developed to explore adsorption mechanisms.[79-83] Although these models have helped cultivate our understanding of interfacial behavior, they typically consider only a subset of the forces responsible for molecular adsorption to solid/liquid interfaces. Some studies focus primarily on adsorbate/substrate interactions,[82-83] while other work treats more rigorously the energetics and structure of solvent/substrate interactions.[79-80]

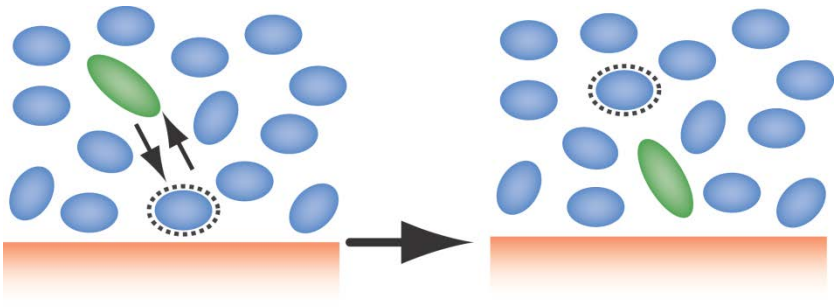

$$\Delta G_{tot} = \Delta G_{ads,u} - \Delta G_{solv,u} + \Delta G_{solv,v} - \Delta G_{ads,v} + \Delta G^*$$

Figure 2.1. A schematic representation of molecular adsorption to the solid/ liquid interface. The total change in system free energy (ΔG_{tot}) must take into account association between the solute (u) and substrate ($\Delta G_{ads,u}$), the (partial) loss of solvation energy as the solute loses some of its solvation sphere ($-\Delta G_{solv,u}$), the loss of adsorption energy between the displaced solvent (v) and substrate ($\Delta G_{ads,v}$) and the gain in solvation energy as the displaced solvent re-solvates in bulk solution ($\Delta G_{solv,v}$). ΔG^* accounts for nonadditive changes in interfacial solvent properties induced by the substrate.

In order to adsorb to an interface, a solute's association with the surface and surrounding solvent must be more energetically favorable than remaining solvated in bulk solution. With regards to silica/aqueous interfaces – the subject of this work - X-ray methods such as X-ray absorption near edge spectroscopy (XANES)[84] and X-ray photoelectron spectroscopy (XPS)[79] and theory have provided molecular-level insight into substrate and interfacial solvent structure, and some studies have explored how this structure changes as a function of pH.[76, 85-87] Other techniques including optical and potentiometric methods have also examined water structure at silica and other mineral surfaces as a function of pH.[41, 78-79, 85, 87-88] However, none of these studies have addressed specifically how changes in solvent structure and surface charge affect the tendency of solutes to adsorb to the interface, nor have experiments examining the silica/aqueous

interface clarified how the local environment surrounding adsorbed solutes differs from bulk solution limits.

At pH < 2 silica's surface silanol groups are fully protonated with some silanol groups carrying an additional proton (as $-SiOH_2^+$) and the surface has a small positive charge. Deprotonation of the terminal silanols occurs at high pH, creating a net negative surface charge.[88-91] The potential of zero charge for silica/aqueous interfaces has been reported for aqueous pH between 2 and 4.[91-92] While different studies report differences in the quantitative acid/base properties of silica surfaces, most find that silica's surface acidity is characterized by two pK_a values, one that is slightly acidic (pH ~ 5) and one that is more basic (pH ~8).[88, 90] Nonlinear optical studies reported by Ong, *et al.* show strong enhancement of the second order polarization by the static electric field from the charged surface. SHG data showing enhancement of the nonresonant second order susceptibility pass through two equivalence points, one with a pK_a of 4.5 and another at a pK_a of 8.5.[88] Based on the magnitude of these changes, the authors conclude that the more acidic pK_a accounts for 19% of the surface silanol groups while 81% of the surface silanol groups are characterized by the more basic pK_a. Potentiometric titrations performed by Meties and coworkers[90] report that 15% of the terminal silanol sites had a pK_a of 5.5 and the remaining 85% had a pK_a of 9.0. More recent experiments performed by Azam et. al. tested the effects of the composition of the aqueous phase has on the ratio between the pK_as.[93] According to these studies, the ratio is sensitive to the specific ion in solution. While the origins of these two distinct silanol groups have not been determined directly, data from the SHG experiments were used to propose that the acidic pK_a arises

from isolated silanol groups while the basic pK_a should be assigned to surface silanol groups that are hydrogen bonded to neighbors.[88] (Figure 2.2)

As pH increase the terminal Si-OH becomes deprotonated and at high pH the surface becomes rough and increase in heterogeneous,[94] thus new slides are used for each experiment involving high pH. Given the chemical changes that occur at the silica/aqueous interface as a function of pH, one might expect interfacial solvation of adsorbed solutes to change also. To observe the effects of aqueous phase pH and surface charge on interfacial adsorption and solvation, experiments described below measure the affinity of *p*-nitrophenol (pNP) for the silica/aqueous interface and record the resonance enhanced SHG spectra of the adsorbates at four different bulk pH concentrations. pNP is a solute having well defined acid/base properties and solvatochromic behavior. pNP's solvatochromic window for electronic excitation extends from 288 nm in nonpolar, low dielectric solvents such as alkanes to 318 nm for polar solvents including DMSO and water. The fact that pNP's excitation wavelength in polar solvents is independent of hydrogen bonding conditions shows that the solute's electronic structure is controlled exclusively by the surrounding dielectric properties rather than specific, localized solute-solvent interactions.

With a pK_a of 7.2, pNP is almost exclusively neutral at low pH but in basic conditions, pNP will be in its anionic form, *p*-nitrophenoxide (pNP^-).[65] As an aqueous solution of pNP becomes more basic, the solution assumes a bright yellow color corresponding to a shift in the absorbance spectrum from λ_{max} of 317 nm ($pH \leq 5$) to λ_{max}

of 400 nm. (Figure 2.3) The relative amounts of pNP and pNP^- in solution as a function of pH can be calculated easily.

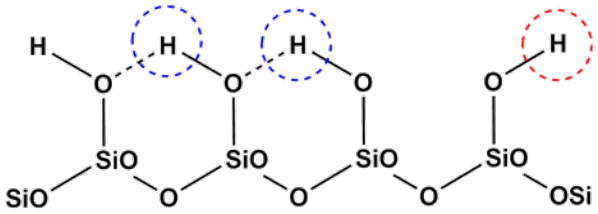

Figure 2.2. Based on nonlinear optical studies, Ong, *et al.*[22] propose that the hydroxylated silica surface has two different silanol sites. One type of terminal silanol is hydrogen bonded to neighbors (blue) and has a pK_a of 8.5. The other type of surface silanol is isolated (red) and has a lower pK_a of approximately 4.5.

In the studies presented below, we investigate adsorption and solvation of *p*-nitrophenol (pNP) at silica/aqueous interfaces as a function of solution phase pH. Motivating this work is an extensive body of literature that has characterized the silica/aqueous interface in terms of solvent structure,[88, 95] dynamics, [77, 96] the effect of surface charge,[30, 87, 96] and the role played by these systems in analytical separation schemes.[70, 73] Specifically, our studies seek to identify how (or if) molecular adsorption to silica/aqueous interfaces depends on interfacial charge and how interfacial charge affects interfacial solvation. In this context, the term 'solvation' is used to describe the noncovalent interactions that a solute has with its surroundings, regardless of whether those interactions are with the solvent or the solid substrate.

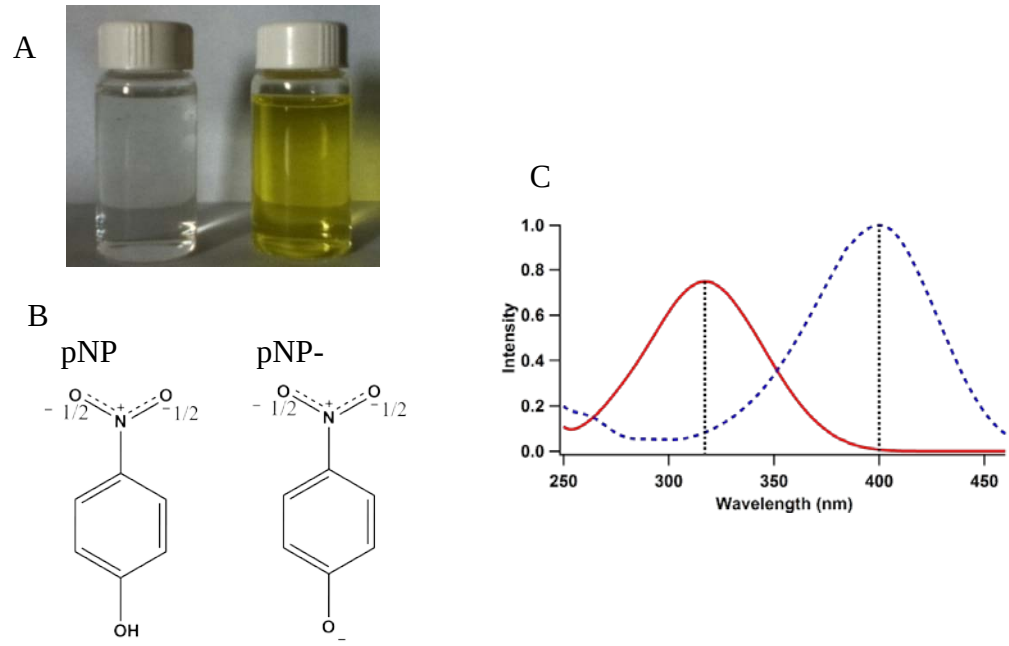

Figure 2.3. A) Comparison of pNP and pNP^-, ~2 mM of pNP in pH 1 (left) and pH 10.7 (right); B) Structure of protonated and deprotonated pNP; C) UV/Vis spectra of pNP in acidic conditions (red, solid line) and basic solution (blue, dashed line). When pNP is deprotonated the electronic resonance wavelength shifts from 317 nm to 400 nm.

Resonance enhanced SHG spectra of pNP adsorbed to silica/aqueous interfaces proved to be time dependent with the SHG spectra changing shape over the course of hours. During the early stages of adsorption, spectra of interfacial pNP were characterized by a single excitation wavelength (313 nm) implying a single type of adsorption site. Furthermore, the approximate resonance wavelengths were largely pH independent and reflected a local polarity more consistent with acetonitrile than with bulk aqueous solution. Over the course of 1-3 hours, SHG spectra evolved to show two distinct excitation wavelengths, one at 310 nm and another at 330 nm. These data suggest that pNP adsorbed to fully equilibrated silica/aqueous interfaces samples two

markedly different local dielectric environments. Silica surfaces are known to be highly heterogeneous,[94] but data presented in this work show how this heterogeneity directly impacts molecular adsorption *and* solvation. Furthermore, similarities between pNP spectra from the equilibrated silica/aqueous interface and the silica/vapor interface illustrate that the heterogeneity sampled by pNP depends almost exclusively on solute/substrate interactions. These results are discussed in the context of cooperative acid-base behavior between the solute and substrate and the importance of allowing for any long-time changes required to establish equilibrium at silica/aqueous interfaces.

2.2 Experimental Methods

MP Biomedical grade pNP was purchased from Aldrich and used as received. Solutions of pH 1.0, 5.0, 7.0, and 10.7 (all $\pm$0.2) were made using ACS grade hydrochloric acid and 1 M sodium hydroxide solution (made from ACS grade NaOH pellets). A PASCO Xplorer GLX data logger coupled with a PASPort high-resolution pH/ORP/ISE amplifier was used to monitor the solution's pH. Buffers were not used to maintain the pH balance thus requiring that all solutions be used immediately upon preparation. (Buffering solutes have been shown to affect solute adsorption in ways that can mask specific solute/substrate interactions.[97-98]) Silica slides were cleaned using a 50/50 sulfuric/nitric acid mixture and rinsed thoroughly with deionized water (Milipore, 18.2 MΩ). The slide was then affixed in the sample cell in direct contact with the pNP containing aqueous solution and allowed to equilibrate for one or three hours. Resonance-enhanced SHG signal was induced using a Libra-HE laser (Coherent, 85 femtosecond

pulses, 1 kHz repetition rate) coupled to a visible optical parametric amplifier (Coherent OPerA Solo) and collected using a PMT. Incident power before the sample ranges from 0. 5mW to 3.5 mW, with an average energy density of 1.38 mW/mm at the sample surface. Additional details about this system can be found in earlier reports[47] and in Appendix A. Bulk absorption data was recorded using a Hitachi U-3010 UV/Vis spectrophotometer.

Resonance enhanced SHG is a popular method used to study adsorption and interfacial solvation,[41, 47, 49] and has been used to identify how surfaces change solvation environments from bulk solution limits.[28, 34, 47] Shifts in excitation wavelength describe the local polarity sampled by solvatochromic solutes at the silica/aqueous interface and the strength of the solute's SHG signal is related to the population and average orientation of adsorbed solutes. The intensity of the SHG response, I(2ω), is related directly to the intensity of the incident light I(ω) through the induced 2nd order polarization $P^{(2)}(2\omega)$:

$$I(2\omega) = \left|P^{(2)}(2\omega)\right|^2 = \left|\chi^{(2)} : E(\omega)E(\omega)\right|^2 = \left|\chi^{(2)}\right|^2 I(\omega)^2 \qquad \text{Eq. 2.1}$$

where $P^{(2)}(2\omega)$ is the induced second order polarization. $P^{(2)}(2\omega)$ is proportional to the system's 2nd order susceptibility, $\chi^{(2)}$, and the intensity of the incident field at frequency ω, I(ω). $\chi^{(2)}$ is a third rank tensor that can be separated into resonant and non-resonant susceptibilities. The non-resonant (NR) susceptibility is intrinsic to any boundary where symmetry is broken and can reflect the behavior of the solvent and/or substrate but is inherently macroscopic. The NR portion is typically assumed to be single valued, but can

also be fitted to a linear function.[99-100] The resonant portion depends on properties of the adsorbates:

$$\chi_R^{(2)} = N < \beta_{ijk} >,\ \beta = \frac{A}{w_0 - w - i\Gamma} \qquad \text{Eq. 2.2}$$

Here, A is a constant associated with SH amplitude, ω_o is the resonant frequency of the transition, ω is the frequency of the incident light, and Γ is the linewidth. $<\beta>$ represents the orientationally averaged molecular hyperpolarizability of interfacial adsorbates. Analysis of our spectroscopic data exploited all three of the molecular fitting parameters: ω_o served as a measure of the local polarity surrounding the adsorbed pNP while Γ was interpreted in terms of the heterogeneity associated with the adsorption environment. In instances where SHG spectra showed two resonance features, the ratio of amplitudes (A_1/A_2) indicated the relative contributions from distinct adsorption sites.

Solute adsorption can be quantified with an adsorption isotherm. Assuming that the average orientation of adsorbed pNP remains constant as a function of surface coverage, the square root of the SH intensity is proportional to the surface concentration. (Equation 2.1) Plotting $I(2\omega)^{1/2}$ vs. bulk concentration one can calculate adsorption energies after choosing an appropriate model. Isotherm data presented below were evaluated using several different models (including Freundlich, Langmuir-Freundlich, and Temkin fits)[51] but the quality of the fits did not unambiguously favor one model over another. Adsorption energies reported in this work are the result of fitting data to a Langmuir model despite the acknowledged limitations of Langmuir adsorption, namely that surfaces must be homogeneous, that solutes behave ideally and the molecular adsorption ceases after a monolayer is formed.

In the Langmuir model (Equation 2.3),

$$\frac{q}{Q} = \frac{bc}{1 + bc} \qquad \text{Eq. 2.3}$$

q is the adsorption capacity , Q is the maximum saturation capacity, b is a fitting parameter related to the adsorption energy, c is the bulk concentration, and the ratio of q/Q is proportional to the square root of the normalized signal. b can then be used in the following equation to solve for the free energy of adsorption (ΔG^{o}_{ads}) (Equation 2.4):

$$b = e^{\frac{-\Delta G^{o}_{ads}}{RT}} \qquad \text{Eq. 2.4}$$

All fitting and data analysis was performed using Igor Pro v.6.02 (WaveMetrics, Inc.).

2.3 Results and Discussion

To understand what role the aqueous solvent plays in controlling interfacial solvation of adsorbed pNP, we first measured the SHG spectrum of pNP adsorbed to the silica/vapor interface. (Figure 2.4) To prepare this sample, a 4 mM solution of pNP in hexanes was allowed to equilibrate with a clean silica slide, and the hexanes were then allowed to evaporate. The silica slide with the adsorbed pNP was placed into the experimental assembly without any solvent present. While we acknowledge that the silica surface will retain some amount of adsorbed water vapor, we believe, based on data from silica/aqueous systems, that these silica/vapor data reflect primarily direct substrate/solute interactions. In the absence of a bulk aqueous phase, the pNP spectrum shows two peaks, one at 310 nm and the other at 330 nm. The appearance of two peaks implies that in the absence of a bulk solvent, pNP adsorbs to the surface through two different mechanisms with the shorter wavelength feature indicating weaker interactions

between the solute and substrate and the longer wavelength value indicating strong substrate/solute association.

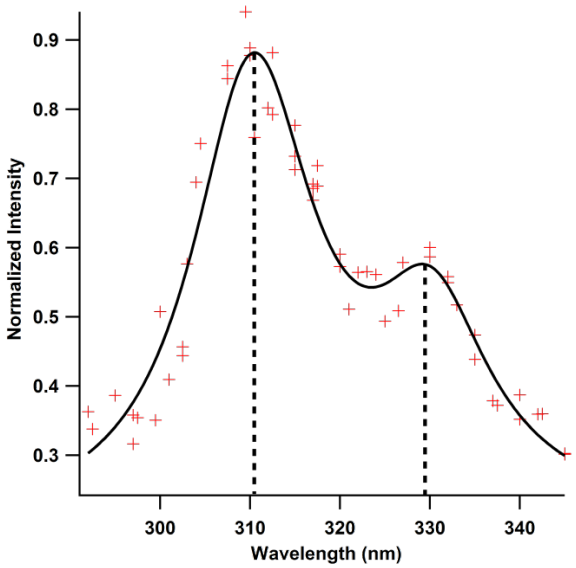

Figure 2.4. SHG spectrum for pNP at the solid/vapor interface. There are two peaks, one at 310 nm and a second peak at 330 nm. Additional details about the fitting parameters are reported in Table 2.2.

This two-site description of pNP adsorption to the silica/vapor interface also supports the studies cited above that found the acid/base properties of the silanol terminated surface to be dominated by two distinct pK_a values. Given the negative dipole from the $–NO_2$ terminal, the most likely scenario to describe the interaction of pNP with the silanol group would be via the hydroxyl end of the pNP. This assumption is strengthened after analysis of adsorption strength, which corresponds to the energy associated with hydrogen bonding. If hydrogen bonding between the pNP and surface silanol groups is the primary mechanism responsible for solute adsorption, then we assign the shorter wavelength feature in the pNP SHG spectrum to pNP adsorbed to the more acidic silanol groups, while the longer wavelength feature is due to pNP serving as a

strong hydrogen bond donor to siloxides. These assignments are based on careful analysis of changes in relative amplitudes of the two features at silica/aqueous interfaces as a function of aqueous phase pH. (*Vide infra.*)

Table 2.1. Distribution, adsorption and spectroscopic data for pNP after 1 hour equilibration time. Values for bulk solute concentration (= pNP + pNP^-), peak wavelength, line width(Γ), and the adsorption energy(ΔG^o_{ads}) as a function of pH following equilibration for 1 hour. The ratio of pNP to its deprotonated form shows a decrease in pNP in favor of pNP- as pH increases, but affects neither the resonance wavelength nor adsorption energy. Increases in heterogeneity are indicated by increases in line width.

pH	Bulk Conc. (mM)	pNP/pNP-	Peak wavelength (nm)	Γ (nm)	ΔG^o_{ads} (kJ/mol)
1.0	25	$10^{6.2}$	314 ± 2	37±1	-21±1
5.0	25	$10^{2.2}$	313 ± 2	37±1	-17 ±2
7.0	50	$10^{0.2}$	309 ± 3	44±1	-17 ±2
10.5	100	$10^{-3.3}$	316 ± 3	61±1	-5.8±2

The first question to resolve when considering pNP adsorption to silica/aqueous interfaces is whether or not pNP adsorbs at all. pNP is moderately soluble in aqueous solution with a solubility limit of 15.8 g/L (= 0.11 M) and an octanol water partitioning coefficient (log P = 1.91) that is relatively small compared to those of similarly sized aromatic solutes.[101] To assess pNP's affinity for silica/aqueous interfaces, resonance enhanced SH intensity (I(2ω)) was recorded as a function of concentration. Plotting the square root of the signal as a function of pNP concentration allowed us to calculate ΔG^o_{ads} for the different silica/aqueous systems using Eqns. 2.3-2.4. One complication that we needed to take into account was that as pH increases the amount of pNP decreases due to deprotonation of the phenol to form the anionic phenoxide. Given a pK_a of 7.2, we

calculated ratios of pNP/pNP^- as a function of pH, and results are reported in Table 2.1. This effect was significant primarily for the high pH experiments (at pH = 10.5) and, to a much lesser extent, for neutral pH (pH = 7). Our determination of ΔG^o_{ads} considered only the amount of neutral pNP in solution. Isotherms were measured after an hour of equilibration for pH 10.5, 7, 5, and 1. (Figure 2.5) The values of ΔG^o_{ads} for these experiments are also reported in Table 2.1. Under acidic and neutral conditions, ΔG^o_{ads} remained relatively constant at -19 kJ/mole. Signals reported in Figure 2.5 are necessarily from neutral pNP that are subject to interfacial asymmetry. Experiments cannot identify solutes in the near interfacial region which sees an anisotropic environment. However, at pH 10.5 the adsorption energy increased to -6 kJ/mole, a result that can be understood in terms of competing equilibria between pNP adsorption and pNP/pNP^- in bulk solution. The smaller ΔG^o_{ads} value at high pH indicates that (the small amount of) neutral pNP feels less of a driving force to adsorb to the negatively charged silica/aqueous interface.

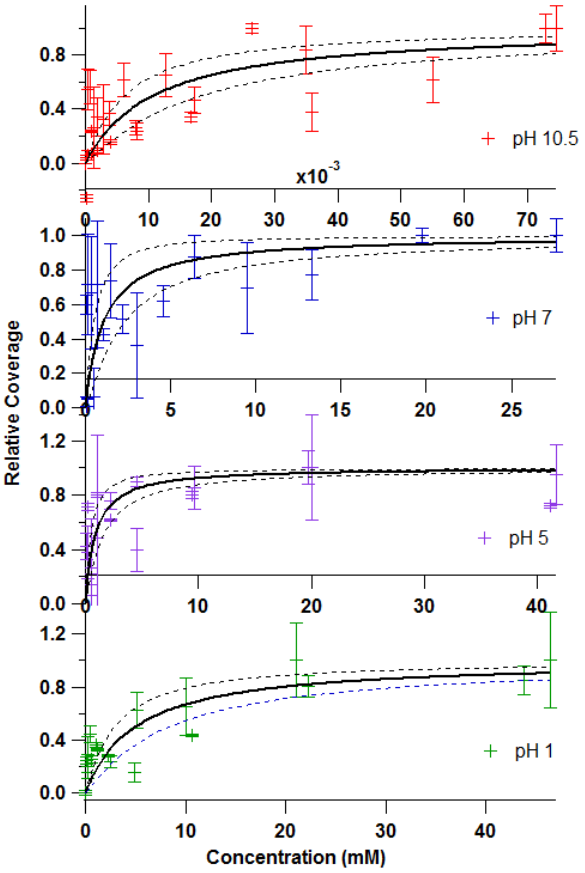

Figure 2.5. Isothermal data were collected at 315 nm with an equilibration time of 1 hr. for pH 10.5 (top), 7.0, 5.0, 1.0 (bottom). All isotherms were fitted using the Langmuir fit, represented by a solid black line. ΔG^{o}_{ads} are reported in Table 2.1.

An important point to note is that at pH = 10.5, only 0.1% of all solutes in solution are in the neutral form and the majority anions are not expected to have strong SH resonant enhancement at wavelengths below ~340 nm. (Figure 2.3) Furthermore, Coulombic repulsion between the negatively charged silica surface and the pNP^- anion should minimize adsorption of the majority anionic solute. Consequently, any resonance enhancement observed in the SH spectra from silica/high-pH aqueous interfaces can result only from preferential adsorption of the small number of neutral solutes in solution

or from the silanol groups that remain protonated at the surface donating their proton to pNP^- forming a solute that becomes nominally neutral.

SHG spectra were recorded from silica/aqueous interfaces for aqueous solutions having pH concentrations of 1.0, 5.0, 7.0, 10.5 (all ±0.2). Concentrations of pNP were chosen so that the surface would have full monolayer coverage. Spectra were acquired after allowing approximately one hour for equilibration and the data were fit to Equations 2.1-2.2. (Figure 2.6 and Table 2.1) (For the pH 7 and 10.5 solutions, we increased bulk pNP concentrations from 25 mM to $\geq$50 mM in order to obtain SH spectra having resolvable contrast between intensities on and off resonance.) The spectra are characterized by a single resonance feature that ranged from 309 nm (pH7) to 316 nm (pH 10.5). Excitation wavelength maxima from the lower pH systems fell between these two limits. The spectra show no systematic shift in resonance wavelength and the linewidths are broader than what one usually observes for solutes adsorbed to silica/liquid interfaces.[47, 50, 77] The data suggest that after ~1 hour, adsorbed pNP samples a single, heterogeneous environment that is polar but slightly less polar than bulk aqueous solution. The linewidth broadens noticeably as the pH rises leading us to conclude that the silica surface presents a more heterogeneous adsorption environment under more basic conditions. Adsorption energies ranged from -6 kJ/mole to -21 kJ/mole but did not show any systematic variation with $\lambda_{SH,max}$, or Γ.

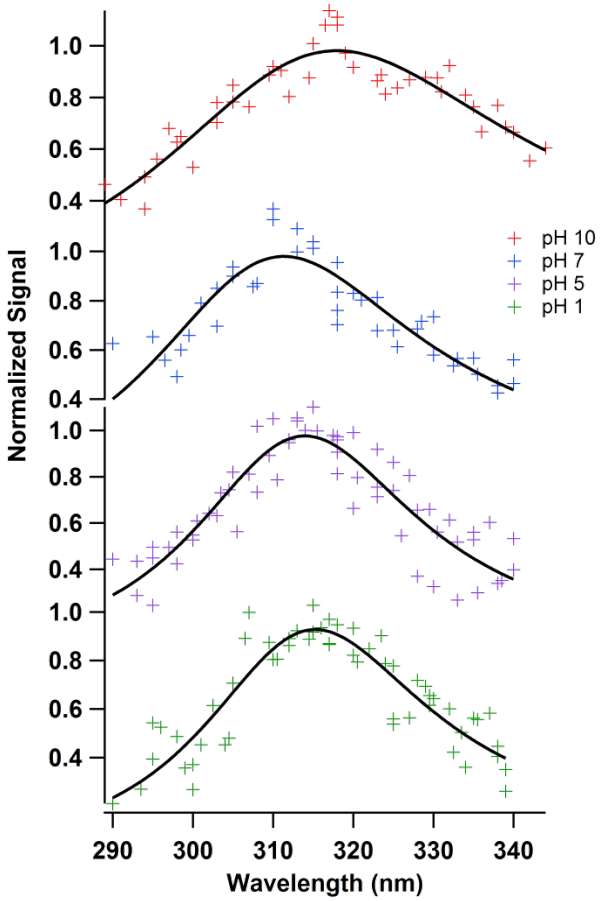

Figure 2.6. SHG data for pNP in increasing pH solutions (bottom to top). The resonance peak for all spectra was around 314 nm.

The apparent insensitivity of spectroscopic features to aqueous pH and the dramatic differences between the silica/aqueous and silica/vapor spectra raise concerns that perhaps the silica surface is not fully equilibrated after allowing only 1 hour of equilibration. To test the time-dependent condition of the silica surface as a function of pH, control experiments were performed to measure the nonresonant $\chi^{(2)}$ response of neat silica/aqueous interfaces as a function of pH but in the absence of a solute. As reported first by Eisenthal and coworkers, as the aqueous solution becomes more basic, the nonresonant SH field created at a silica/aqueous interface increases by more than an order

of magnitude from pH 2 to pH 14, passing through two equivalence points at pH values of 4.5 and 8.5.[88] In our control experiments, the relative nonresonant SH intensities from the silica/aqueous interfaces at pH 1.0 and 10.5 were approximately equal after one hour of equilibration. Only after *three* hours did the SH response from the interface from the two different systems show the contrast comparable to that reported in Reference [88]. (Data from these experiments are presented in Appendix A.)

Precedent exists for believing that acid/base equilibration at silica aqueous interfaces can require hours. Geiger and coworkers[30] have shown previously the effects of aqueous solution ionic strength can have on charged state of the silica/aqueous interface at various pHs. The authors explained their results in terms of strong ion-surface interactions that kinetically inhibit the interface's approach to equilibrium. Our experiments studying adsorption and solvation at silica/aqueous interfaces are performed with deionized water, but addition of either HCl or NaOH to create acidic or basic solutions, respectively can lead to Na^+ or Cl^- concentrations as high as ~0.3 M, comparable to concentrations used in by Geiger and coworkers. Consequently, the specific "jamming" effects reported in Reference 30 may play a role in explaining long equilibration times, although similar pNP behavior was observed under all pH conditions even when the ionic strength was quite low (e.g. pH = 5). The effects of specific adsorbed ions on molecular interactions with a silica substrate remain a subject still under investigation.

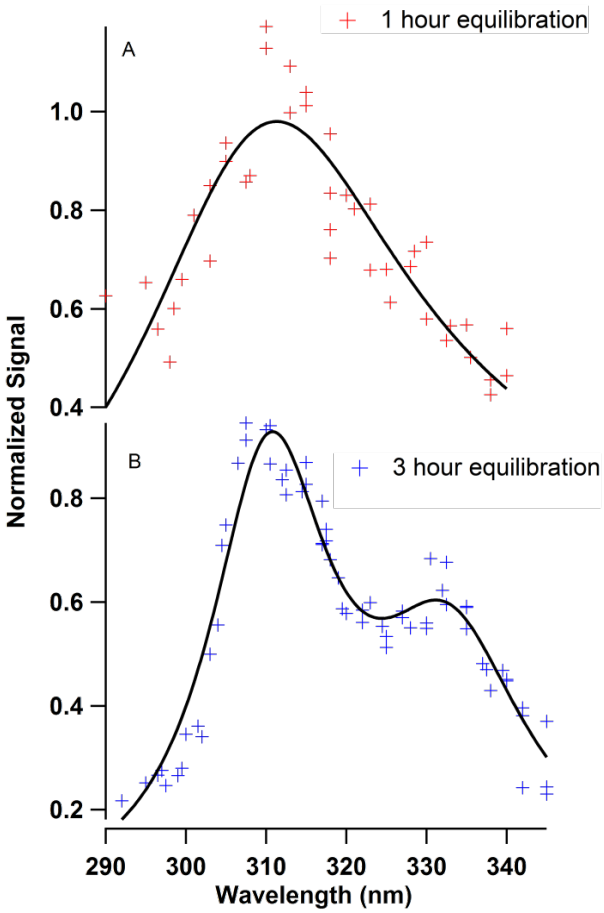

Figure 2.7. SHG spectra of 50mM pNP adsorbed to the silica/aqueous interface from a pH 7 solution after one hour equilibration time (A) and three hours equilibration (B). Details about fitting parameters are described in the text.

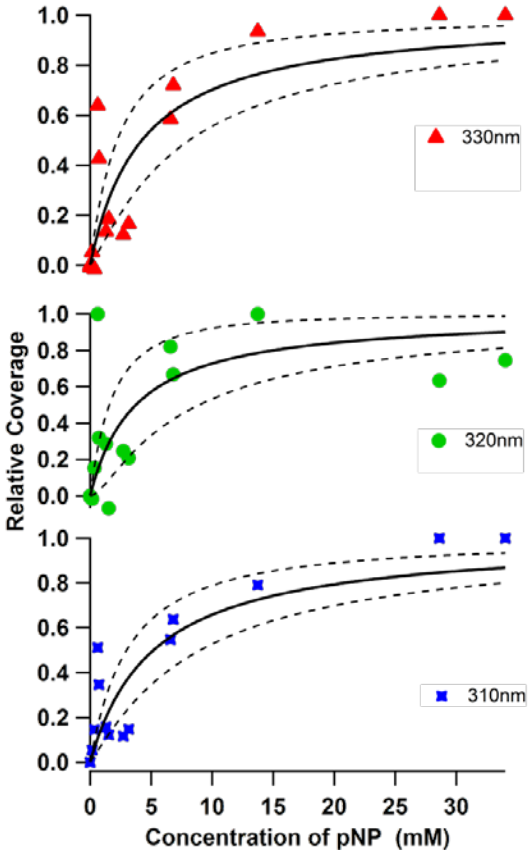

Figure 2.8. Isothermal data collected for pH 7 after 3 hours of equilibration. Data were collected at the two resonant peaks (310 nm and 330 nm) along with 320 nm. The values of the ΔG^{o}_{ads} for 310 nm, 320 nm, and 330 nm data are -21±1 kJ/mol, -20±3 kJ/mol, and -21±2 kJ/mol respectively.

Figure 2.7 shows the SH spectra of pNP adsorbed to the silica/aqueous (pH 7) interface after 1 hour and 3 hours of equilibration. (Spectra taken at even longer equilibration times show no change from the 3 hour spectrum.) In contrast to the 1-hour spectrum with a single electronic resonance, the 3-hour spectrum shows *two* clear resonance wavelengths at 310 nm and 330 nm. These features match the wavelengths and linewidths of the two resonances observed for pNP adsorbed to the silica/vapor

interface (Figure 2.4). The amplitude ratios are different (with the silica/vapor spectrum having more relative amplitude in the shorter wavelength feature) but are still within a standard deviation of each other. This result implies that once fully equilibrated, pNP adsorption and solvation at silica/aqueous interface is largely independent of the surrounding solvent *and* surface charge state. It should be noted there could be the possibility of nanobubble formation at the surface could be inducing the similarities,[102-103] but from our set-up we have no conclusive way to determine bubble formation. In addition, given the statistic distribution of bubble coverage (~24% in basic solution)[102], we would expect to see a higher degree of variation in repeated measurements.

Furthermore, comparing relative amplitudes of pNP in pH 7 and pH 5 shows distinct ratios and although some could argue the large error bars suggest some overlap, the systematic change in behavior is more tied to chemical interactions than the possibility of a nanobubble domain. We propose that the emergence of two distinct adsorbed populations is the result of chemistry occurring *at the interface* rather than differences in the kinetics or thermodynamics associated with adsorption *from* bulk solution. Figure 2.8 reports isotherm data acquired at three different wavelengths (310 nm, 320 nm and 330 nm) for the silica/aqueous (pH7) system measured after 3 hours of equilibration. If one site was being populated preferentially or if nonresonant contributions to the second order susceptibility were affecting the spectra through constructive or destructive interference, we would expect the 320 nm data to deviate significantly from the 310 and 330 nm data. Instead, however, isotherm data for all three wavelengths are virtually superimposable. From these results, we propose that the silica

surface equilibrated with bulk solution presents pNP with two distinct solvation environments, one that is less polar than the bulk aqueous phase and one that is more polar. Furthermore, these sites arise following early-time, nonspecific pNP adsorption followed by the surface becoming fully equilibrated with bulk solution pH and creating the two different sites. The distribution of these adsorption sites changes with aqueous phase pH suggesting that the two different adsorption sites are correlated with populations of neutral (-Si-OH) and deprotonated (-Si-O^-) silanol groups at the silica surface. The adsorption energies calculated from both the short and long wavelength features are equivalent.

Table 2.2. Data for pNP after 3 hr equilibration time and for S/V interface. Values for peak wavelengths, line widths (Γ), and the ratio of amplitudes for each spectrum in Figure 2.9. For comparison, the values from the solid/vapor experiment have also been included.

pH	Bulk Conc.(mM)	λ_1(nm)	Γ_1(nm)	λ_2(nm)	Γ_2(nm)	A_1/A_2
1.0	25	310±1	14±1	328±5	38±2	3± 2
5.0	25	311±1	18±1	333±1	9±1	3±2
7.0	50	310±1	16±1	331±1	19±1	1.3±0.2
10.5	100	309±1	13±1	331±1	16±1	1.2±0.8
S/V	4	310±1	17±1	330±1	16±1	1.9±0.6

Spectra of pNP adsorbed to all of the silica/aqueous interfaces were taken after 3 hours and are shown in Figure 2.9. As with the pH 7 data, all spectra show evidence of two resonance wavelengths although for the acidic silica/aqueous (pH 1) interface the long wavelength feature appeared only as a shoulder to the dominant resonance at

310 nm. Values for the resonance peak locations and line widths are reported in Table 2. The peak locations vary very little, implying that adsorbed pNP is sensitive primarily to local effects and not influenced significantly by bulk pH *or* by general properties such as the interfacial Helmholtz layer or Debye length.[51] When taking into account the behavior of the resonance amplitudes as a function of bulk solution pH, these observations suggest two different hydrogen bonding mechanisms for the short and long wavelength resonances. (Figure 2.10)

Also included in Table 2.2 are the A_1/A_2 ratios for the intensity amplitudes as a function of pH, where A_1 and A_2 are the amplitudes of the 310 nm and 330 nm features, respectively, as determined from fitting the data to Equations 2.1-2.2. A general observation is that at higher pH, the A_1/A_2 ratio is smaller suggesting that the long wavelength feature is associated with the deprotonated surface silanol groups. Data from the two acidic silica/aqueous systems (pH = 1 and 5) show large amplitude ratios, but these data also have a high degree of uncertainty associated with them. Fitting for acidic conditions were problematic and showed no strong preference for a specific parameter. Repeated efforts to fit the pH 5 spectrum lead to the following observations: amplitude fits are flexible, but linewidth and peak wavelengths tended to remain relatively consistent throughout the fitting process. We note that the quality of the fit for the pH 1 data is particularly poor and fails to capture the very sharp edge at short wavelengths. The origin of this effect is uncertain, although we note that only for the acidic system does the silica surface have a slight, formal positive charge. However,

efforts to include a 3rd specific adsorption site with physically meaningful spectroscopic parameters did not improve the quality of either the pH 1 or pH 5 fits.

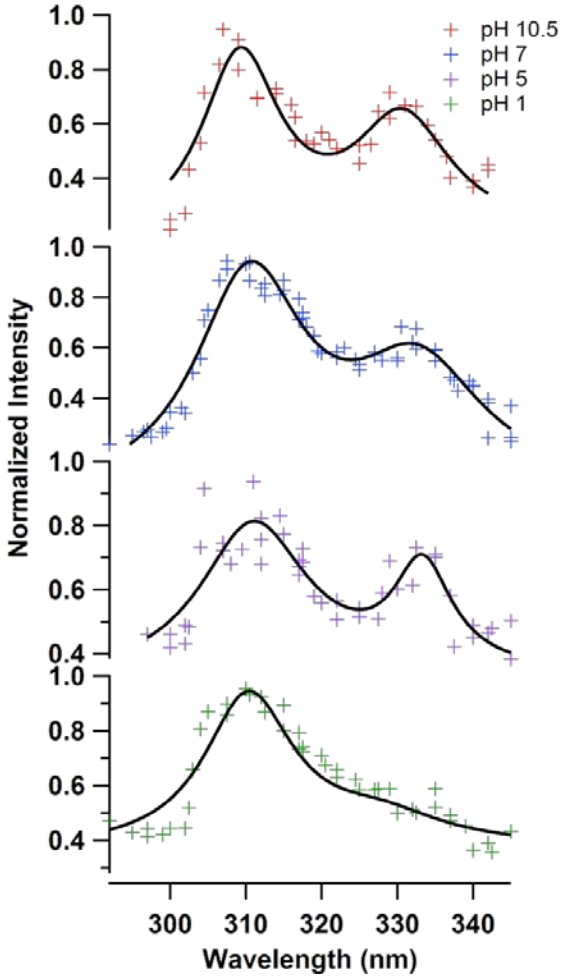

Figure 2.9. After 3 hours of equilibration, the first peak on all the pH experiments are slightly blue shifted from ~315nm to 310nm. At 330nm, a second peak is present in all the experiments, although at pH 1 it can only be seen as a shoulder.

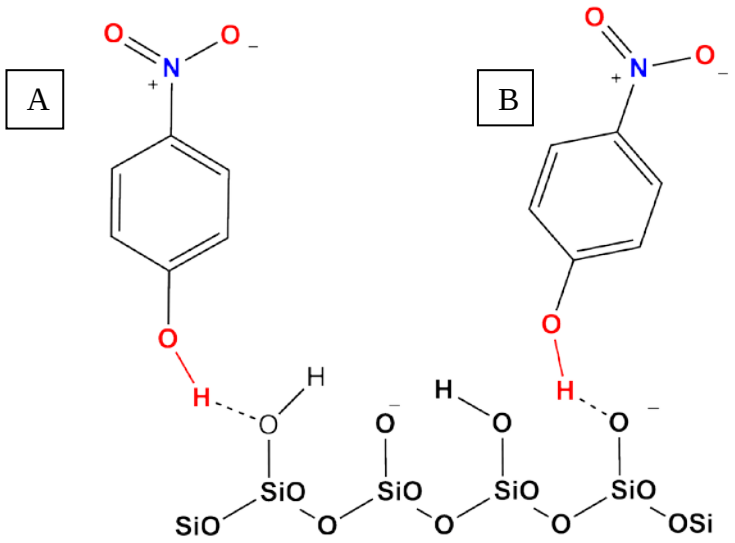

Figure 2.10. Schematic illustration representing the two populations associated with pNP adsorption to the fully equilibrated silica/aqueous interface. (A) The terminal silanol and pNP are both in their neutral forms and share a hydrogen. (B) As the surface becomes deprotonated, a negative charge is built up, the second adsorption mechanism is assigned to pNP- H-bonding to Si-OH or a deprotonated O- bonding to a protonated pNP.

When reporting results from nonlinear optical spectra having two features reasonably close in resonance frequency, one needs to consider carefully the coherent contribution of each transition and the possibility that spectra may contain significant constructive or destructive interference from the two resonances with each other and/or with any nonresonant background. In spectra containing only isolated resonance features, interference between $\chi^{(2)}_{res}$ and $\chi^{(2)}_{NR}$ can lead to pronounced asymmetry with an extreme example being derivative-shaped resonance transitions such as those observed in nonlinear vibrational spectra of alkyl monolayers on metals.[104] Similar interferences have also been observed in SH spectra.[27, 47, 105-106] In the event that a SHG spectrum contains contributions from two adsorbate populations, constructive and destructive

interference can result from both resonant terms of the $\chi^{(2)}$ tensor as well as the nonresonant contribution. Depending on the relative signs of the two resonant terms line shapes may show constructive or destructive, derivative-like behavior. The data in Figures 2.8 and 2.9 have been fit to Equation 2.2 while considering all permutations of resonant and nonresonant $\chi^{(2)}$ contributions. To within the limits of experimental reproducibility, we believe that the spectra in Figure 2.8 all reflect contributions from two distinct populations of pNP sharing similar net orientations adsorbed to silica/aqueous interfaces.

Furthermore, the effects of the nonresonant susceptibility, although non-zero, do not strongly affect the measured resonant behavior. One reason that the features in the 3-hour spectra do not show strong evidence of interference is that the resonances are consistently narrower than in the 1 hour spectra. These findings imply that the two adsorption sites (illustrated schematically in Figure 2.10) at the fully equilibrated silica/aqueous interface are more homogeneous than the environment sampled after only 1 hour of equilibration.

2.4 Conclusions

Summarizing the findings from our studies of pNP adsorption to silica/aqueous interfaces as a function of aqueous phase pH, we conclude that while initial adsorption may occur indiscriminately, the resulting equilibration between adsorbed solutes and the silica substrate is neither simple nor rapid. Furthermore, interactions that adsorbed pNP solutes experience at the interface appear to be dominated almost exclusively by close

association with the silica substrate with the aqueous solvent playing primarily a spectator's role. Specific observations from this work include the following:

- pNP adsorbed to the silica/vapor interface samples two distinctly different environments with one characterized by weaker interactions (leading to a shorter wavelength resonance in the SH spectrum) and one characterized by strong interactions between the solute and substrate that push the pNP resonance wavelength beyond the polar limit of the solute's solvatochromic window.
- Equilibration of adsorbed pNP at the silica/aqueous interface requires up to 3 hrs regardless of aqueous phase pH.
- During the initial stages of adsorption, pNP samples a single albeit heterogeneous environment that is slightly less polar than bulk aqueous solution given an observed shift in pNP's excitation to shorter wavelengths. If modeled using a Langmuir isotherm, pNP adsorption is thermodynamically favored with a ΔG^{o}_{ads} of ~-20 kJ/mole except under alkaline conditions (pH10.5) where ΔG^{o}_{ads} is -6 kJ/mole.
- Once fully equilibrated with the silica/aqueous, pNP samples two distinct environments, one polar and one nonpolar. While the nature of these two environments does not depend on bulk aqueous pH, their relative importance changes with changing pH. At low pH, pNP adsorbed to the less polar site makes a larger contribution to the SH spectrum and at higher pH, contributions from the more polar site become more pronounced. These findings correlate with the two types of surface silanol groups reported to exist at the hydroxylated silica surface.

The silica/aqueous interface represents a complex, heterogeneous environment that create different mechanisms for solute adsorption from aqueous solution. Furthermore, adsorbed solutes and the surface can require hours to equilibrate fully. Given the importance of molecular adsorption to silica surfaces in fields as diverse as geochemistry, separation science and environmental remediation, a molecularly-based understanding of solute/substrate interactions will require extensive and quantitative studies. Results presented in this work and elsewhere have begun to unravel some of the relevant issues – time, ionic strength, pH – associated with chemistry occurring at the solid/liquid interface. Our findings and their implications motivate continued efforts to develop validated, predictive models that can accurately describe molecular adsorption to these ubiquitous and complicated boundaries.

2.5 Acknowledgements

The authors would like to gratefully thank the NSF for support. The authors thank A. Renee Siler for contributions toward experimental set-up and David Halat who assisted with analysis and programing.

Supporting Information Available. This information is available free of charge via the Internet at http://pubs.acs.org and can be found in Appendix 1

2.6. References

27. Brindza, M. R.; Walker, R. A., Differentiating Solvation Mechanisms at Polar Solid/Liquid Interfaces. *Journal of the American Chemical Society* **2009**, *131*, 6207-6214.

28. Eisenthal, K. B., Second Harmonic Spectroscopy Of Aqueous Nano- And Microparticle Interfaces. *Chemical Reviews* **2006**, *106*, 1462-1477.

30. Gibbs-Davis, J. M.; Kruk, J. J.; Konek, C. T.; Scheidt, K. A.; Geiger, F. M., Jammed Acid-Base Reactions at Interfaces. *Journal of the American Chemical Society* **2008**, *130*, 15444-15447.

34. Marowsky, G.; Steinhoff, R.; Chi, L. F.; Hutter, J.; Wagniere, G., 2ND-Harmonic Generation in Quinquethienyl Monolayers. *Physical Review B* **1988**, *38*, 6274-6278.

41. Zhang, X. Y.; Cunningham, M. M.; Walker, R. A., Solvent Polarity At Polar Solid Surfaces: The Role Of Solvent Structure. *Journal of Physical Chemistry B* **2003**, *107*, 3183-3195.

47. Siler, A. R.; Walker, R. A., Effects of Solvent Structure on Interfacial Polarity at Strongly Associating Silica/Alcohol Interfaces. *Journal of Physical Chemistry C* **2011**, *115*, 9637-9643.

49. Bloembergen, N., 2ND Harmonic Reflected Light. *Optica Acta* **1966**, *13*, 311-322.

50. Benjamin, I., Inhomogeneous Broadening Of Electronic Spectra At Liquid Interfaces. *Chemical Physics Letters* **2011**, *515*, 56-61.

51. Hiemenz, P. C., *Principles Of Colloid And Surface Chemistry*, 2 ed.; Marcel Dekker, Inc: New York 1986; Vol. 9, p 792.

65. *CRC Handbook of Chemistry and Physics*, 90 ed.; Taylor and Francis Group, LLC: Boca Raton, Fl, 2009-2010.

69. Escudero, C.; Salmeron, M., From Solid-Vacuum To Solid-Gas And Solid-Liquid Interfaces: In Situ Studies Of Structure And Dynamics Under Relevant Conditions. *Surface Science* **2013**, *607*, 2-9.

70. Weetall, H. H., Preparation of Immobilized Proteins Covalently Coupled Through Silane Coupling Agents to Inorganic Supports. *Applied Biochemistry and Biotechnology* **1993**, *41*, 157-188.

71. Chen, Z.; Li, Z.; Lin, Y.; Yin, M.; Ren, J.; Qu, X., Biomineralization Inspired Surface Engineering Of Nanocarriers For pH-Responsive, Targeted Drug Delivery. *Biomaterials* **2013**, *34*, 1364-71.

72. Mann, S., Molecular Technntonics in Biomineralization and Biomimetic Materials Chemistry. *Nature* **1993**, *365*, 499-505.

73. Znidarsic, W. J.; Chen, I. W.; Shastri, V. P., Influence Of Surface Charge And Protein Intermediary Layer On The Formation Of Biomimetic Calcium Phosphate On Silica Nanoparticles. *Journal of Materials Chemistry* **2012**, *22*, 19562-19569.

74. Yang, H.; Vovk, G.; Coombs, N.; Sokolov, I.; Ozin, G. A., Synthesis Of Mesoporous Silica Spheres Under Quiescent Aqueous Acidic Conditions. *Journal of Materials Chemistry* **1998**, *8*, 743-750.

75. Destoop, I.; Ghijsens, E.; Katayama, K.; Tahara, K.; Mali, K. S.; Tobe, Y.; De Feyter, S., Solvent-Induced Homochirality In Surface-Confined Low-Density Nanoporous Molecular Networks. *Journal of the American Chemical Society* **2012**, *134*, 19568-71.

76. Hopkins, A. J.; McFearin, C. L.; Richmond, G. L., Investigations Of The Solid-Aqueous Interface With Vibrational Sum-Frequency Spectroscopy. *Current Opinion in Solid State & Materials Science* **2005**, *9*, 19-27.

77. Mondal, S. K.; Yamaguchi, S.; Tahara, T., Molecules at the Air/Water Interface Experience a More Inhomogeneous Solvation Environment than in Bulk Solvents: A Quantitative Band Shape Analysis of Interfacial Electronic Spectra Obtained by HD-ESFG. *Journal of Physical Chemistry C* **2011**, *115*, 3083-3089.

78. Jena, K. C.; Covert, P. A.; Hore, D. K., The Effect of Salt on the Water Structure at a Charged Solid Surface: Differentiating Second- and Third-order Nonlinear Contributions. *Journal of Physical Chemistry Letters* **2011**, *2*, 1056-1061.

79. Duval, Y.; Mielczarski, J. A.; Pokrovsky, O. S.; Mielczarski, E.; Ehrhardt, J. J., Evidence Of The Existence Of Three Types Of Species At The Quartz-Aqueous Solution Interface At pH 0-10: XPS Surface Group Quantification And Surface Complexation Modeling. *Journal of Physical Chemistry B* **2002**, *106*, 2937-2945.

80. Koopal, L. K., Wetting of Solid Surfaces: Fundamentals and Charge effects. *Advances in Colloid and Interface Science* **2012**, *179*, 29-42.

81. Liu, Q.; Yuan, S. L.; Yan, H.; Zhao, X., Mechanism of Oil Detachment from a Silica Surface in Aqueous Surfactant Solutions: Molecular Dynamics Simulations. *Journal of Physical Chemistry B* **2012**, *116*, 2867-2875.

82. Manne, S.; Gaub, H. E., Molecular-Organization Of Surfactants At Solid-Liquid Interfaces. *Science* **1995**, *270*, 1480-1482.

83. Tiberg, F.; Jonsson, B.; Tang, J.; Lindman, B., Ellipsometry Studies Of The Self-Assembly Of Nonionic Surfactants At The Silica Water Interface-Equilibrium Aspects. *Langmuir* **1994**, *10*, 2294-2300.

84. Brown, M. A.; Huthwelker, T.; Redondo, A. B.; Janousch, M.; Faubel, M.; Arrell, C. A.; Scarongella, M.; Chergui, M.; van Bokhoven, J. A., Changes in the Silanol Protonation State Measured In Situ at the Silica-Aqueous Interface. *Journal of Physical Chemistry Letters* **2012**, *3*, 231-235.

85. Drach, M.; Andrzejewska, A.; Narkiewicz-Michalek, J.; Rudzinski, W.; Koopal, L. K., Theoretical Modeling Of Cationic Surfactants Aggregation At The Silica/Aqueous Solution Interface: Effects Of pH And Ionic Strength. *Physical Chemistry Chemical Physics* **2002**, *4*, 5846-5855.

86. Pokrovsky, O. S.; Golubev, S. V.; Mielczarski, J. A., Kinetic Evidences Of The Existence Of Positively Charged Species At The Quartz-Aqueous Solution Interface. *Journal of Colloid and Interface Science* **2006**, *296*, 189-194.

87. Sulpizi, M.; Gaigeot, M. P.; Sprik, M., The Silica-Water Interface: How the Silanols Determine the Surface Acidity and Modulate the Water Properties. *J. Chem. Theory Comput.* **2012**, *8*, 1037-1047.

88. Ong, S. W.; Zhao, X. L.; Eisenthal, K. B., Polarization of Water-Molecules at a Charged Interface-2nd Harmonic Studies of Silica Water Interface. *Chemical Physics Letters* **1992**, *191*, 327-335.

89. Allen, L. H.; Matijevi.E, Stability of Colloidal Silica: Effect of Hydroyzable Cations. *Journal of Colloid and Interface Science* **1971**, *35*, 66-&.

90. Allen, L. H.; Matijevi.E; Meties, L., Exchange Of Na+ For Silanolic Protons Of Silica. *Journal of Inorganic & Nuclear Chemistry* **1971**, *33*, 1293-&.

91. Horiuchi, H.; Nikolov, A.; Wasan, D. T., Calculation Of The Surface Potential And Surface Charge Density By Measurement Of The Three-Phase Contact Angle. *Journal of Colloid and Interface Science* **2012**, *385*, 218-224.

92. Iler, R. K., *The Chemistry Of Silica: Solubility, Polymerization, Colloid And Surface Properties, And Biochemistry* John Wiley & Sons, 1979.

93. Azam, M. S.; Weeraman, C. N.; Gibbs-Davis, J. M., Specific Cation Effects on the Bimodal Acid-Base Behavior of the Silica/Water Interface. *Journal of Physical Chemistry Letters* **2012**, *3*, 1269-1274.

94. Li, I.; Bandara, J.; Shultz, M. J., Time Evolution Studies Of The H2O/Quartz Interface Using Sum Frequency Generation, Atomic Force Microscopy, And Molecular Dynamics. *Langmuir* **2004**, *20*, 10474-10480.

95. Zhao, X. L.; Ong, S. W.; Eisenthal, K. B., Polarization of Water-Molecules at a Charged Interface-2nd Harmonic Studies of Charged Monolayers at the Air-Water Interface. *Chemical Physics Letters* **1993**, *202*, 513-520.

96. Zhao, X. L.; Ong, S. W.; Wang, H. F.; Eisenthal, K. B., New Method For Determination Of Surface pKa Using 2nd Harmonic Generation. *Chemical Physics Letters* **1993**, *214*, 203-207.

97. Green, J. S.; Jorgenson, J. W., Minimizing Adsorption Of Proteins On Fused-Silica In Capillary Zone Electrophoresis By The Addition Of Alkali-Metal Salts To The Buffers. *Journal of Chromatography* **1989**, *478*, 63-70.

98. Yakovleva, J.; Davidsson, R.; Lobanova, A.; Bengtsson, M.; Eremin, S.; Laurell, T.; Emneus, J., Microfluidic Enzyme Immunoassay Using Silicon Microchip With Immobilized Antibodies And Chemiluminescence Detection. *Analytical Chemistry* **2002**, *74*, 2994-3004.

99. Busson, B.; Tadjeddine, A., Non-Uniqueness of Parameters Extracted from Resonant Second-Order Nonlinear Optical Spectroscopies. *Journal of Physical Chemistry C* **2009**, *113*, 21895-21902.

100. Can, S. Z.; Chang, C. F.; Walker, R. A., Spontaneous Formation Of DPPC Monolayers At Aqueous/Vapor Interfaces And The Impact Of Charged Surfactants. *Biochimica Et Biophysica Acta-Biomembranes* **2008**, *1778*, 2368-2377.

101. Moridani, M. Y.; Siraki, A.; Chevaldina, T.; Scobie, H.; O'Brien, P. J., Quantitative Structure Toxicity Relationships For Catechols In Isolated Rat Hepatocytes. *Chemico-Biological Interactions* **2004**, *147*, 297-307.

102. Mazumder, M.; Bhushan, B., Propensity And Geometrical Distribution Of Surface Nanobubbles: Effect Of Electrolyte, Roughness, pH, And Substrate Bias. *Soft Matter* **2011**, *7*, 9184-9196.

103. Yang, J.; Duan, J.; Fornasiero, D.; Ralston, J., Kinetics Of Co2 Nanobubble Formation At The Solid/Water Interface. *Physical Chemistry Chemical Physics* **2007**, *9*, 6327-6332.

104. Yang, C. S. C.; Richter, L. J.; Stephenson, J. C.; Briggman, K. A., In Situ, Vibrationally Resonant Sum Frequency Spectroscopy Study Of The Self-Assembly Of Dioctadecyl Disulfide On Gold. *Langmuir* **2002**, *18*, 7549-7556.

105. Malin, J. N.; Geiger, F. M., Uranyl Adsorption and Speciation at the Fused Silica/Water Interface Studied by Resonantly Enhanced Second Harmonic Generation and the Chi((3)) Method. *Journal of Physical Chemistry A* **2010**, *114*, 1797-1805.

106. Steinhurst, D. A.; Owrutsky, J. C., Second Harmonic Generation From Oxazine Dyes At The Air/Water Interface. *Journal of Physical Chemistry B* **2001**, *105*, 3062-3072.

CHAPTER 3

ADSORPTION AND SOLVATION AT SILICA/LIQUID INTERFACES

3.1 Introduction

In Chapter 2 we explored the influence of the substrate in adsorption by examining the silica/aqueous interface after inducing surface charges by altering the bulk solution pH. From these experiments we learned that by modifying the surface, the adsorption kinetics and molecular environment can be drastically altered. The silica/aqueous interface, however, is difficult to evaluate given the heterogeneity of surface sites and complicated acid-base behavior. Rather than examine the diversity of surface SiOH groups and their complex (and changing) behavior on solution pH, the rest of my thesis research examines chemical behavior at silica/non-aqueous interfaces, where we systematically change the functionality of the solvent and adsorbate to isolate the role of each variable in molecular adsorption. When exposed to an organic solvent, we assume that all surface silanol groups remain protonated. Chapter 3 is a combination of published and unpublished data collected at silica/alkane and silica/alcohol interfaces, using well characterized laser dyes. Specifically, results in this chapter delve into how interfacial solvation structure can be difficult to predict *a priori* as the solid surface can force adjacent solvent molecules to adopt structures not found in bulk solution.

This re-organization of interfacial molecules is sensitive to both geometric and dipolar considerations, as well as the differences between solute-solute and solute-

substrate affinities. Small alterations of these intra- and inter-phase interactions can have pronounced effects that extend far into solution, causing changes to the interfacial anisotropy and causing other properties of the interfacial environment to change from bulk solution limits.

These adsorption properties play critical roles in separation science and in the development of exposure estimates used for regulatory purposes. For example, functionalized surfaces designed for improved HPLC performance show distinct differences in analyte retention and tailing depending on whether the eluting solvent is a water-acetonitrile mixture or a water-methanol mixture.[107] Simulations have attributed these differences to a competition between solute adsorption to the solid/liquid interface and solute partitioning into a column's hydrophobic layer,[108] but the predictive capabilities of this model and others remain untested. In a related application, estimates of organic pollutant bioavailability depend on partitioning between two media such as soil and water or soil and air.[109] Partitioning models, however, are often parameterized by linear free energy relationships that fail to distinguish among different types of interactions such as hydrogen bonding, dipole pairing, steric constraints, and hydrophobic effects.[110]

Two limiting cases can be used to describe adsorption and solvation at solid/liquid interfaces. An *additive* model of adsorption considers the idealized energetics of separate pairs of components – solute/substrate (with no solvent), solute/solvent (with no substrate), and solvent/substrate (with no solute).[41, 111-112] Based on this information alone, a model then tries to predict whether or not adsorption is favorable. This scheme

represents an "averaged" description of adsorption and can be used to assess quickly if solutes are likely to adsorb spontaneously from solution.[41, 77, 111] Furthermore, interfacial properties can be predicted simply by extrapolating from the corresponding properties of both bulk phases. Predictions using this approach can be quite accurate if the solvent and substrate do not have localized, directional interactions.

Alternatively, a *cooperative* model of adsorption starts by acknowledging that a substrate alters the properties of the adjacent solvent creating an interfacial region that cannot be described by weighted averages of bulk properties.[113] Extreme examples include silica/*n*-alcohol ($n \geq 3$) solid/liquid interfaces where interfacial properties are dominated by a high viscosity, alkane-like environment.[27, 43, 48, 114-116] This nonpolar boundary arises from strong hydrogen bonding between the alcohol and silica silanol groups and the van der Waals interactions between adjacent alkyl chains.

Macroscopic measurements have shown how surfaces can influence the weak forces underlying solvent wetting.[32, 45, 80, 117-122] Although these contact angle studies provide valuable insight into dipolar interactions and dispersive forces, these experiments lack molecular specificity and the ability to characterize molecular organization across a solid/liquid interface. From these macroscopic observations and empirical parameterizations,[32, 45, 80, 117-122] one is left to infer details about liquid structure. The studies described in this chapter employ nonlinear and linear techniques that are either inherently surface specific or pseudo-surface specific in order to characterize and examine, from a molecular perspective, the role solvent polarity has in molecular adsorption. The experiments compare various alkane and polar protic alcohol solvents

using two well-characterized adsorbates. These liquids were chosen to explore how competition between liquid/substrate association and steric effects between solvent monomers at the surface impact solute monomer structure and orientation.

3.1.1 Solvents

In the most general sense, liquids at solid/liquid interfaces can be categorized as being either weakly associating or strongly associating.[27, 66, 123] Weakly associating liquids will interact with a solid substrate through induced dipole or dispersion forces. While weakly associating liquids may wet a polar substrate, they tend to do so incompletely and form films with measurable contact angles.[124-126] Strongly associating liquids, in contrast, will completely wet a polar substrate due to hydrogen bonding or more general dipolar forces that promote spreading. The studies presented here used cyclohexane (Chex) and methylcyclohexane (mChex) to characterize the interfacial behavior of weakly associating solvents. For comparison, 1- and 2- propanol (1- and 2-prop, respectively) and methanol (MeOH) were used to examine interfacial solvation between silica and strongly associating liquids. The molecular structures for the solvents can be found in Figure 3.1A.

Liquid structure that has been altered by a surface will have different solvating properties than the bulk solvent, where solvent species are free to organize without anisotropic constraints. In this context, solvation describes the non-covalent interactions a solute has with its surrounding molecules. Numerous spectroscopic studies and simulations report that local dielectric properties, hydrogen bonding opportunities and reorientation dynamics sampled by solutes adsorbed to silica/liquid interfaces differ

significantly from bulk solution limits.[27, 37, 67, 88, 127-131] Many of the experimental results, however, are rationalized in terms of assumed or anticipated solvent organization rather than directly measured structure.

For example, slow solute reorientation at the silica/butanol[48] and sapphire/butanol[132] interfaces has been attributed to a restrictive environment created by strong hydrogen bonding between the liquid and the solid substrate, but solvent structure has not been measured directly. From a molecular perspective, questions about liquid structure and organization at a solid/liquid interface can be nuanced. X-ray scattering experiments performed by Doerr, *et al.* reported that the silicon oxide/liquid cyclohexane interface was characterized by a dense, solid-like cyclohexane layer in direct contact with the substrate followed by a reduced density region that extended ~3-4 nm into the bulk.[133] *n*-Decane density at the same solid surface approached bulk values in only one solvent layer and showed no further anomalies as a function of distance away from the solid surface. In contrast to both cyclohexane and *n*-decane, *n*-hexane experienced significant solvent depletion within the first solvent layers and this low-density region persisted ~3 nm into bulk solution. These results were interpreted in terms of differences between liquid packing densities (ρ^*)[133] with cyclohexane being able to form much denser films than either *n*-decane or *n*-hexane. Data from surface force apparatus measurements also showed that n-alkanes ($n \geq 8$) formed layered structures when confined between silica and mica surfaces, whereas thin liquid films of branched alkanes were much more unstable and were readily expelled from between the two surfaces.[133-137] Again, data

were interpreted with “geometric” explanations that considered solvent packing and organization as the primary contributors to liquid behavior at an interface.

Liquid organization at solid/liquid alkane interfaces appears to depend sensitively on molecular shape. However, strongly associating liquids such as alcohols, amines, and nitriles exploit dipole-dipole interactions and hydrogen bonds between the liquid and the substrate to create regions having structural and dynamic properties that differ significantly from bulk liquid limits. Atomic Force Microscopy (AFM) measurements of alcohol solutions at the silica surface report that *n*-alcohols with n > 3 stand upright and form hydrophobic films at the solid/liquid interface.[138-139] At the related silica/methanol interface, surface-specific vibrational spectra imply that methanol forms a tightly coordinated bilayer structure where methyl groups from the first, hydrogen-bonded solvent layer point away from the silica surface and methyl groups from the second solvent layer are directed towards the silica surface. Effects from the silica surface on methanol structure are assumed to extend no further than two solvent layers into bulk solution.[140-141] However, another proposed interaction mechanism between methanol and silica suggests the nonpolar region was formed via hydrogen bonding.[2] This mechanism will be explored further in Section 3.3 and is discussed here only briefly. Methanol can hydrogen bond to the silica substrate and cannot exploit lateral, van der Waal’s interactions to form the Langmuir-film structure observed at silica/*n*-alcohol interfaces.[27, 48, 116] Molecular dynamics (MD) and Monte Carlo simulations have been performed for systems with methanol in silica nanopores.[142-144, 145-147] In these simulations, methanol molecules are strongly correlated to the silica surface via hydrogen bonds with silanol

groups, resulting in slower orientational and translation dynamics. For methanol confined in silica nanopores, however, the liquid structure depends on both general properties of the silica surface and on details of the confined geometry. The relative importance of these contributions cannot be decoupled in a straightforward way. Whichever method is chosen to explain the silica/methanol interactions, both computational and experimental data suggest that a polar solvent can form a nonpolar adsorption environment.

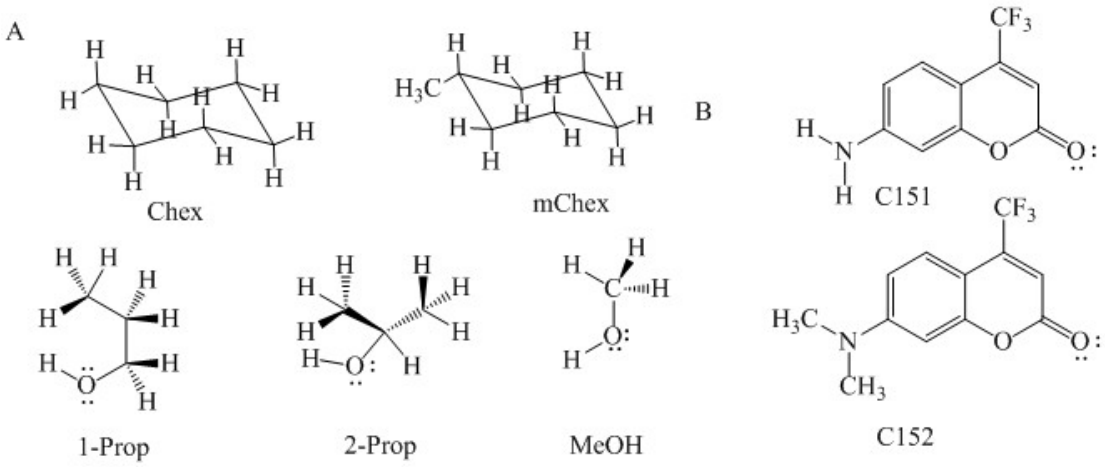

Figure 3.1 Solvents studied in this work are shown in (A); solvation effects were studied using 7-amino-4-(trifluoromethyl)coumarin (C151) and 7-Dimethylamino-4-(trifluoromethyl)coumarin (C152)

Similarly, several studies have examined solvatochromatic shifts in a solute's excitation wavelength to infer details about the local polarity at and across solid/liquid interfaces.[148-149] Again however, conclusions about why a given solid/liquid interface is more or less polar than a bulk solution limit rely upon indirect evidence from bulk liquid studies or simulations. This chapter will take the discussion further and examine various

silica/liquid interfaces in the presence of adsorbates to determine the role solvent choice has on adsorption behavior.

3.1.2 Adsorbates

The solvents chosen, Figure 3.1A, differ in intermolecular steric interactions and were expected to influence monomer organization and solvation at silanol-terminated, polar silica surfaces. Well-characterized coumarin dyes (Figure 3.1B) were chosen to study these interfaces because of the dyes' large Stokes shifts and sensitivity towards the local polarity both in the ground electronic state and excited state.[56, 150-161] If the silica-liquid interactions are strong, then the solute will sample a polarity that is sensitive to the anisotropic solvent structure induced by the silica substrate. If, however, silica-solute interactions are stronger than those between the silica and the liquid, then the interfacial polarity experienced by the solute will be dominated by the effects of the surface silanol groups.

Coumarin dyes, and in particular 7-aminocoumarins, have high quantum yields in appropriate solvents and well-studied excited states. Many 7-aminocoumarins form an intramolecular charge transfer state in polar solvents.[47-49,162-164,58] The studies discussed in this chapter focused on two 7-aminocoumarins, coumarin 151 (C151), a primary amine, and C152, a tertiary amine. These chromophores have electronic structures that are extremely sensitive to the local solvation environment. Solvatochromic effects shift C151's excitation wavelength from ~360 nm in alkane solvents to ~410 nm in DMSO.[165-166] Furthermore, in polar solvents, C151 has a relatively high quantum yield ($\Phi \sim 0.65$) and a long fluorescence lifetime (~5 ns), but in alkane solvents, C151 shows weaker

fluorescence with a more dominant, shorter emission lifetime (~1 ns).[165-166] These differences have been attributed to an excited state intramolecular charge transfer (ICT) conformer that is stabilized in polar media.[153-154, 165-167]

C152 also has an ICT conformation, however, experimental and computational data show that C152 forms a twisted ICT (or TICT) state in polar solvents.[1, 37, 56, 160, 168] The stabilization of the TICT results in a low Φ of <0.2 and a short (sub-ns) lifetime in polar solvents. In contrast, the quantum yield nears unity in non-polar solvents and the resulting lifetime increases to ~4 ns.[56] C152 is a useful probe for studying interfacial dynamics and interfacial polarity given C152's large change in dipole moment (~5 Debye).[154] The large change in dipole moment following photoexcitation results in a large solvatochromatic shift in both excitation and emission spectra. In polar solvents, C152 excites at 400 nm and emits at 513 nm; in nonpolar solvents the peak excitation and emission wavelengths blue shift to 370 nm and 425 nm, respectively. [154]

3.2 Experimental

Anhydrous methylcyclohexane was purchased from Sigma Aldrich, >99% cyclohexane was purchased from Acros, HPLC grade 2-propanol was received from EMP, and the 1-propanol was purchased from Fisher. Solutions were also made using spectral grade methanol (purity >99%). Laser grade coumarin 151 and coumarin 152 were obtained from Exciton. All liquids and solutes were used as received. The SHG experiments used silica slides from SPI Inc, fluorescence experiments used silica hemispheres from ISP. The slides, hemispheres and their corresponding Kel-F sample

cells were cleaned using a 50/50 (by volume) sulfuric/nitric acid mixture and rinsed thoroughly with deionized water (Milipore, 18.2 MΩ). The slides and hemispheres were then affixed in the sample cell in direct contact with the liquid phase containing a pure liquid or a solution with a given coumarin solute.

SHG experiments employ a Libra-HE Ti:sapphire laser (Coherent, ~3.3 W 85 fs pulse duration, 1 kHz repetition rate) coupled to a visible optical parametric amplifier (Coherent OPerA Solo) to generate visible light. Resonance-enhanced second harmonic generation (SHG) signal was collected using a PMT coupled to photon counting electronics. Incident power of the visible light before the sample ranged from 0.5 mW to 3.5 mW and for the solute used in these studies, SHG experiments covered a SH wavelength range of 350-408 nm. Additional details about the SHG assembly can be found in Chapter 2 and Appendix A.[169]

In addition to SHG, we employed time-resolved fluorescence to study the dynamics properties of C151 at the silica/methanol interface. Time-resolved fluorescence is not inherently surface specific, however, when coupled to a total internal reflection geometry (TIR), we are able to probe interfacial dynamics. The fluorescence instrumentation and TIR set-up was discussed briefly in Chapter 1 and the instrumentation schematic and a detail description of the time correlated single photon counting (TCPSC) are found in Chapter 4.

3.3 Results and Discussion

Bulk excitation and emission data of C151 and C152 were recorded using JY

Horiba Fluorolog 3 fluorimeter to determine the bulk solvatochromatic range of these solutes. The fluorescence data collect were in agreement with values found in literature.[56, 155, 159] The bulk solvatochromatic range was used as a benchmark comparison to infer the local interfacial polarity sampled by the adsorbates. SHG spectra of the coumarins were measured to determine the effective excitation wavelengths.

3.3.1 C151 and C152 at the Silica/Cyclohexane and Silica/Methylcyclohexane Interfaces

The SHG spectrum of C151 adsorbed to the silica/Chex interface reports an excitation wavelength of 400 ± 2 nm, data that fall near the long-wavelength, polar edge of C151's solvatochromic window. (Figure 3.2A) A SHG spectrum could not be collected at the silica/mChex interface. After scanning the full wavelength range available, the data appeared to rise as the wavelength increased, however, a Lorentzian feature was not produced. Unfortunately, the SHG set-up is limited in its ability to measure at longer wavelengths, therefore we are unable to determine if the signal will eventually decrease. The intensity appeared to increase as the wavelength approached the red limit, suggesting that the environment at the silica/mChex interface may be even more polar.

The SHG experiments were reproduced using C152 to determine if the polar behavior of these alkane structures is solute dependent. C152 at the silica/Chex interface experiences a polar environment, as shown by the resonance peak at 399±2 nm, unlike C151, the silica/mChex interface produced a discernable spectrum.

The resonance wavelength for C152 at the silica/mChex interface was also at 399±2 nm, indicating a polar interfacial region. (Spectral data can be found in Table 3.1) Several possible interpretations can explain how these alkanes produced a polar adsorption environment.

Unlike cyclohexane and methylcyclohexane, coumarins can associate with surface silanol groups through dipole-dipole interactions and hydrogen bonding. The solvatochromic behavior of C152 does not allow us to discern whether or not dipolar association between the adsorbate and the surface involves hydrogen bond donation and/or acceptance from the surface silanol groups. In bulk polar media, C152's excitation wavelength is ~400 nm regardless of whether the solvent is a strong hydrogen bond donor (such as H_2O) or acceptor (such as DMSO). Instead, all one can deduce from the SHG spectra and the C152's bulk solution behavior is that C152 solvation at the silica/Chex and silica/mChex interfaces is dominated by a distinctly polar environment, likely created by the high density of surface dipoles. If hydrogen bonding interactions between the surface silanols and C152's carbonyl (in the 2- position) and/or amine (in the 7- position) are strong enough to displace interfacial solvent species, then the extremely polar environment reported at these silica/alkane interfaces can be can assigned to strong substrate/solute interactions.

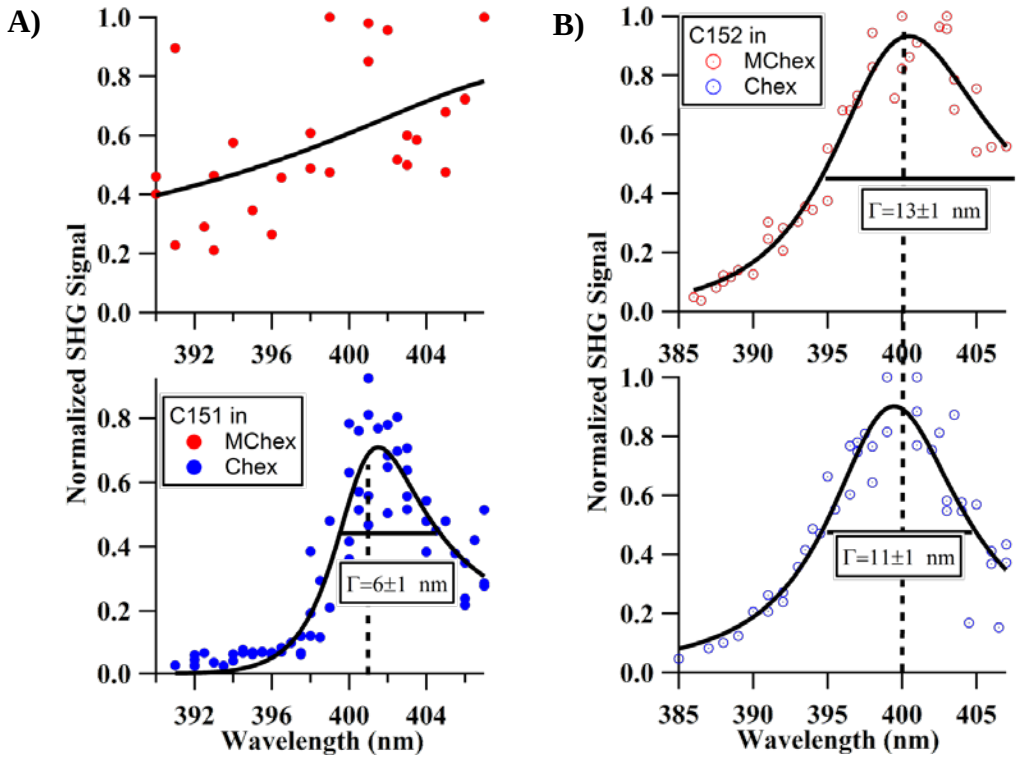

Figure 3.2: SHG spectra of coumarin 151 (A) and coumarin 152 (B) at the silica/mChex and at the silica/chex interfaces.

Table 3.1: SHG spectral data of coumarin 151 and coumarin 152 at the silica/mChex and at the silica/chex interfaces.

	C151			C152		
Solvent	Conc. (μM)	λ (nm)	Γ (nm)	Conc. (μM)	λ (nm)	Γ (nm)
Chex	4.37	400±2	6±1	14.00	399±2	11±1
Mchex	13.09	----	---	31.10	399±2	13±1

An alternative explanation for the polar environment sampled by C152 at the silica/alkane interfaces is that the C152 is simply solvated by thin layer of water bound to the silica surface itself. (For reference, the excitation wavelength of C152 in aqueous solution is 398 nm.) Thin water films have been reported by Schlangen and

others and we cannot discount the possibility that adventitious water might be present at the silica/alkane interfaces sampled in this work.[41, 42] Several independent observations, however, lead us to believe that trace interfacial water is not playing a significant role in either liquid organization or interfacial solvation.

First, while C152 is not able to discern between polar solvents, C151 has a relatively large solvatochromatic shift between solvents that can donate and accept hydrogen bonds. In polar solvents such as acetonitrile and methanol, C151's λ_{exc} is ~380-390 nm.[159] In strong hydrogen bond accepting solvents such as DMSO, λ_{exc} for C151 is red shifted to 410 nm and in solvents capable of donating strong hydrogen bonds such as water, λ_{exc} shifts to shorter wavelengths (369 nm). Such effects have been explored previously and can be understood in terms of hydrogen bonding at the amine position.[156, 170-171] In the current context, these differences in solvatochromic behavior can serve as an indicator of hydrogen bonding opportunities for the adsorbed solute. As indicated in Figure 3.2, C151 is sensitive to the high dipole density presented by the silica surface and is likely to be donating hydrogen bonds to surface silanols. Were significant water present at the silica/cyclohexane interface, we would expect C151 to show an SHG resonance closer to the 369 nm aqueous limit.

Secondly, Vibrational Sum Frequency Generation (VSFG) spectroscopy was used to measure the neat solvent/silica interface. VSFG is an additional second order nonlinear optical technique that is inherently surface specific, and while SHG is used to probe the electronic transition, VSFG measures vibrational spectra of molecules in environments lacking inversion symmetry. VSFG spectra were collected at both the

neat silica/Chex and silica/mChex interfaces and no discernible water feature was observed. Water adsorbed to a silica surface shows a strong broad SFG signal centered at 3140 cm^{-1}, and is assigned to tetrahedrally-coordinated water in a strong hydrogen bonding environment.[33, 172-173] As reported by vibrational data collected by Gobrogge,[1] there was little to no evidence of the water adsorption feature at the silica/Chex and silica/mChex interfaces.

Also warranting mention are spectral hole burning experiments performed by Kohler and coworkers showing the possibility of long chain alkanes creating a static electric field.[174-176] Experiments performed using octatetraene in n-hexane reported large splittings of photochemical hole burning spectra that appears to have linear dependence on electric field strength. The experiments were conducting using an externally applied field, which could have induced the large splittings. Further investigations have shown the electric field was in fact produced by the alkane chains.[175] This static field could influence the adsorption environment and could be a possible explanation of the 'polar like' interfacial region C151 and C152 experience.

3.3.2 C151 and C152 at the Silica/1-Propanol and Silica/2-Propanol Interfaces

SHG spectra of C151 and C152 adsorbed to the silica/ 1- and 2-propanol interfaces are shown in Figure 3.3. Some of the noise in the data between 355-365 nm arose from a necessary switch between filter sets. SHG data in this region were all normalized to the non-resonant response of a clean gold surface and data show clear resonance enhancement at shorter wavelengths. As shown in Figure 3.3

and Table 3.2, excitation wavelengths were calculated C151 and C152 at the silica/1-propanol and 2-propanol interfaces, in addition to calculations of their respective line widths. For reference the excitation wavelengths of C151 and C152 in bulk propanol are 384nm and 398 nm, respectively.[56, 159] In fact, the SHG data show that the coumarins adsorbed to the silica/ 1- and 2-propanol interfaces samples an environment that is even less polar than bulk alkane solvents.

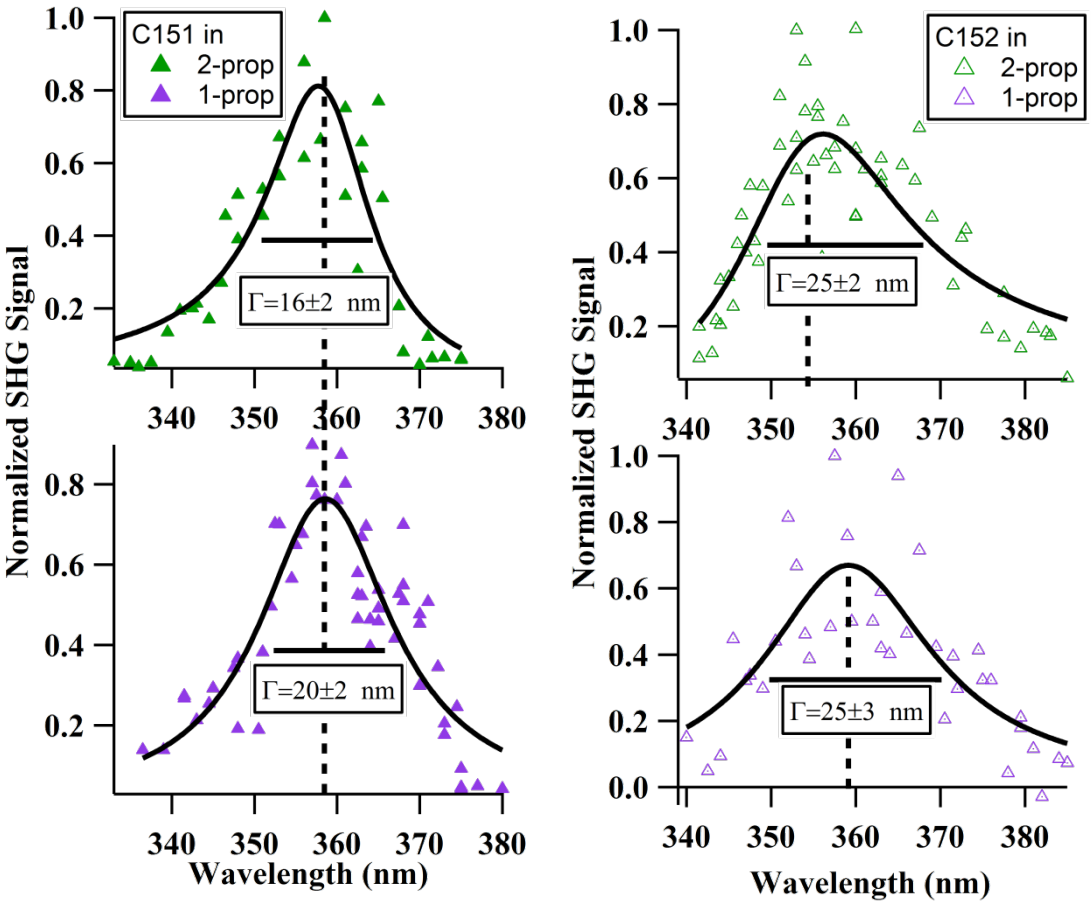

Figure 3.3: SHG spectra of coumarin 151 (A) and coumarin 152 (B) at the silica/1-prop and at the silica/2-prop interfaces.

Such behavior is not unprecedented. Earlier studies of solvent polarity across strongly associating silica/n-alcohol and aqueous/*n*-alcohol interfaces reported the existence of extremely nonpolar environments for $n \geq 8$. Experiments using variable length surfactants that systematically varied solute location across the interface suggested that the width of this nonpolar region extended approximately one solvent length away from the surface.[115, 177] The origin of this low dielectric region had been attributed to a scarcity of hydrogen bonding across the interfacial region. If the propanol isomers hydrogen bond strongly to the silica surface forming a nonpolar film, then any adsorbed solutes will experience an environment that is significantly less polar than the bulk liquid. Furthermore, if solvent density experiences partial depletion or conformational restrictions relative to bulk limits, then the local dielectric environment can be even rarer than in solutions of alkanes. This picture is consistent with the proposed organization of 1- and 2-propanol at the silica/liquid interface deduced from VSFG data.[1]

Table 3.2: SHG spectra results of coumarin 151 and coumarin 152 at the silica/1-prop and at the silica/2-prop interfaces.

	C151			C152		
Solvent	Conc. (μM)	λ (nm)	Γ (nm)	Conc. (μM)	λ (nm)	Γ (nm)
1-prop	17.45	359±2	20±2	279.90	356±2	22.4±2
2-prop	8.73	359±2	16±1	108.86	352±2	23.2±2

Several observations warrant mentioning. First, the interfacial polarity reported by adsorbed C151/C152 tracks inversely with bulk solvent polarity: silica/propanol interfaces appear extremely nonpolar to the adsorbates while

silica/cyclohexane interfaces provide a local polarity consistent with what one would expect of high dielectric solvents. Second, line widths are closely correlated with SHG resonance wavelengths. SHG line widths at the nonpolar, silica/propanol interfaces are ~20 nm (FWHM), a result that is narrower than excitation line widths in bulk solution (~40 nm) but consistent with previously reported SHG spectra. At the polar silica/alkane interfaces, however, the SHG line widths are remarkably narrow at ~12 nm. The origin of this effect is uncertain, but if the coumarins adsorbs to the silica surface by accepting hydrogen bonds through both the 2- position carbonyl and 7- position amine *and* if the surrounding solvent monomers are restricted in their motion, then the narrow line widths may reflect a very low degree of inhomogeneous broadening.

As a final observation relevant to the silica/propanol interfaces, we note that both 1- and 2-propanol have nonpolar 'tails' that can contribute directly to the creation of the nonpolar interface. The influence of this 'tail' can easily be determined by observing the silica/methanol interface. Methanol is the smallest alcohol, with the smallest hydrophilic: hydrophobic ratio, therefore the hydrophobic effects should be least pronounced.

For the experiments described below, we employed SHG and time-resolved fluorescence to observe the steady state and emissive behavior of C151 in methanol. The time resolved fluorescence instrumentation was discussed in the introduction and details about the assembly will be presented in detail in Chapter 4, but a brief description is given here. Time correlated single photon counting (TCPSC)

spectroscopy measures lifetimes of C151 in bulk and at the silica/methanol interface. Time-resolved fluorescence is not inherently surface specific. Consequently, this project required the design and construction a total internal reflection geometry assembly to collect TCSPC emission. The TIR-TCSPC excites molecules at the surface and some depth into the bulk region. The TIR penetration depth is dependent on the wavelength, incident angle, and indices of refraction of the solvent and substrate. For our current set-up the indices of refractions for Chex, mChex, and 1-/2-prop are too large to collect TIR data.

3.4 C151 at the Silica/Methanol Interface

In the work presented below, resonance enhanced second harmonic generation (SHG) is used to probe adsorption and solvation of C151 at the silica/methanol solid/liquid interface. The excitation wavelength measured from adsorbed C151 implies that the interface formed between these two polar media – silica and methanol – is distinctly nonpolar. Furthermore, time resolved fluorescence measurements carried out in a TIR geometry show that the emission of adsorbed C151 is consistent with an environment that cannot stabilize the ICT state. The origin of this nonpolar region is identified explicitly by molecular dynamics simulations. Collectively, these findings present a complete picture of how surfaces and solvents conspire to create distinctive environments having properties that differ from bulk solution limits. These boundaries require that solute behavior be described by a cooperative model of adsorption and solvation.

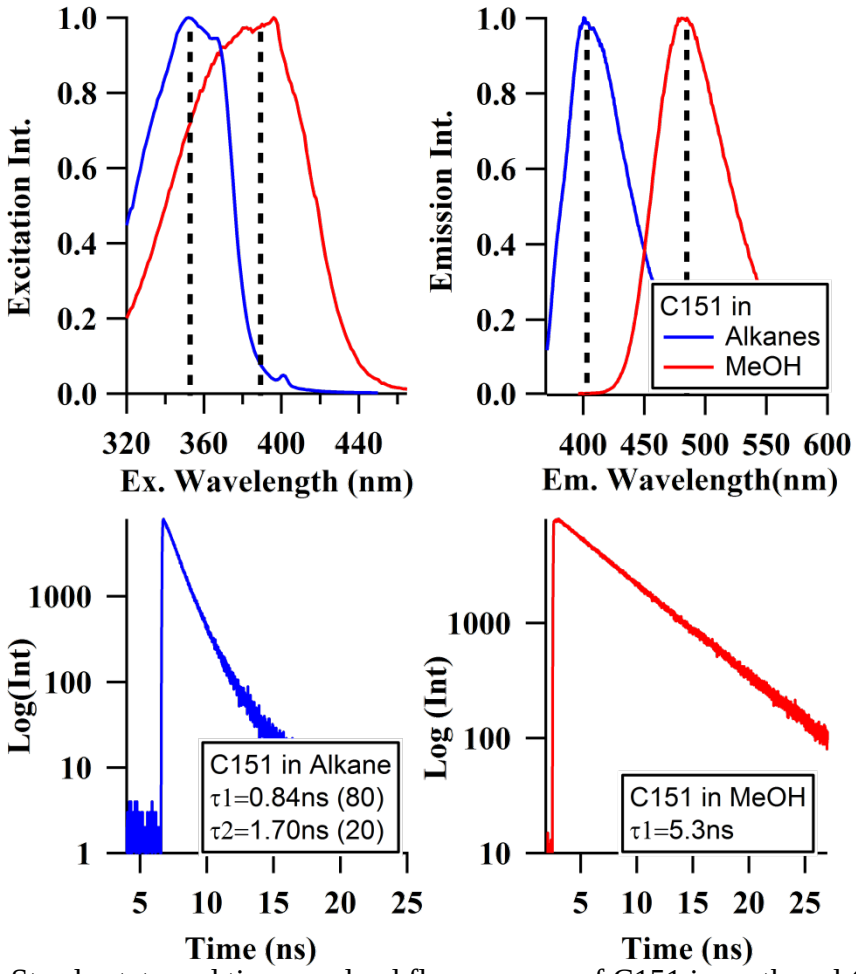

Figure 3.4: Steady state and time resolved fluorescence of C151 in methanol (red) and in alkanes (blue).

3.4.1 SHG Spectra

Figure 4.4 shows the steady state and time resolved fluorescence emission of a 10 µM solution of C151 in bulk methanol and in alkanes for comparison. The lifetime data in methanol fit to a single exponential decay having a lifetime of 5.4 ± 0.2 ns. This result matches the value reported by Nad, *et al.*, and the relatively long lifetime has been attributed to C151's formation of a planar ICT state in polar solvents.[166] When the ICT state cannot be stabilized, the primary amine has an additional degree of freedom

and the hydrogens can be either above or below the plane, resulting in two very short lifetimes of about 1 ns.[153, 155, 159, 178] The differences in lifetimes and the solvatochromatic range of C151 are found in Figure 3.4.

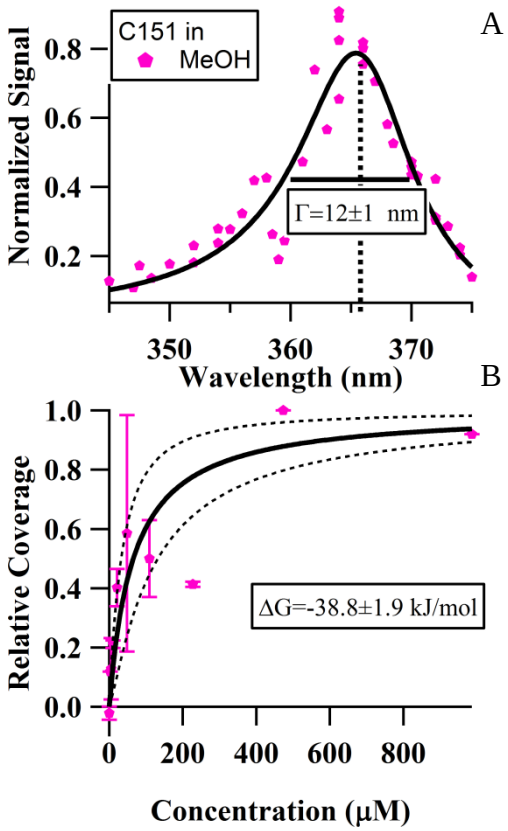

Figure 3.5: SHG spectra of coumarin 151 in methanol (A) isothermal spectrum taken at the methanol/silica interface

The SHG spectrum of C151 adsorbed to the silica/methanol interface from a 20 μM solution of C151 in methanol is shown in Figure 4.5A. Fitting the SHG data to Equations 1.2-1.5 from Chapter 1 results in an excitation wavelength of 364 nm for adsorbed C151, a value very close to the nonpolar, alkane limit. The 12 nm (FWHM)

Line width is quite narrow suggesting a very small degree of inhomogeneous broadening. (For comparison, the width of the bulk solution excitation spectrum in Figure 4.4 is ~75 nm.)

Figure 4.5B shows adsorption data for C151 as a function of C151 bulk concentration. The square root of I(2ω) is proportional to the C151 surface coverage, and assuming monolayer coverage and a homogenous surface, the isotherm can be fitted the Langmuir isotherm (Equation 1.7). Fitting the data led to a calculated adsorption energy of -38.8 ± 1.9 kJ/mol This value compares favorably with data for other aromatic species adsorbed to silica surfaces and would suggest a relatively strong adsorption mechanism.[179]

3.4.2 TCSPC of C151 in Bulk Methanol and Adsorbed to the Silica/Methanol Interface

Shown on Figure 3.6 and in Table 3.3 are TCSPC data acquired in a TIR geometry from the silica/methanol interface for C151 solutions of 0.2 to 10 μM. Relative to the bulk methanol TCSPC data, TIR data show a distinct difference at early time from the bulk solution data, especially for the 0.2 μM solution. Specifically, the TIR data require that a second emission pathway with a lifetime of 1.2 ± 0.2 ns be included in the fit while the original 5.34 ns lifetime remains relatively unchanged for higher concentrations. The shorter lifetime matches the dominant emission lifetime of C151 in alkane solvents and has been ascribed to facile inversion (or "flip-flop") about the sp^3 hybridized amine with a correspondingly more rapid, non-radiative decay.[166] Additionally, this second, shorter lifetime has increasing contribution as concentration

decreases, indicating the interfacial photodynamics can become overwhelmed by bulk contribution if concentrations are too high.

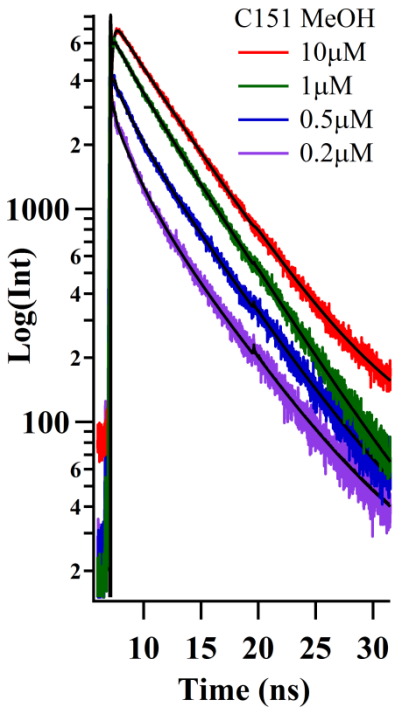

Figure 3.6: TR-TIR decays of the silica/methanol interface at various concentrations of C151.

With these considerations in mind, we assign the long-lived lifetime measured in the TIR experiments to C151 in a bulk solution environment excited by the evanescent wave of the incident light. The shorter lifetime is assigned to interfacial C151, constrained to keep sp^3 hybridization about the amine following photoexcitation. This assignment is supported by the observation that the short lifetime is more pronounced at lower bulk concentrations (corresponding to lower surface coverage) whereas at a concentration slightly above the monolayer limit, the bulk solution lifetime becomes more dominant. We note that the amplitudes of the two lifetimes measured under TIR

conditions cannot be assigned directly to relative surface coverage. The penetration depth of the evanescent wave used to excite the C151 depends sensitively on the angle of incidence so small variations in optical alignment from experiment to experiment may disproportionately weight one lifetime contribution over the other. Furthermore, quantum yields of the two populations are likely to be different[21] meaning that the relative amplitudes reported in Table 3.3 will not correspond directly to relative concentrations. Nevertheless, the data reported in Figure 3.6 and Table 3.3 provide consistent evidence that the silica/methanol interface is dominated by an environment that promotes fast radiative decay of adsorbed C151 solutes.

Taken together, the SHG spectrum and the time resolved fluorescence data show that the silica/methanol interface creates an environment that is decidedly less polar than the bulk solution. The question of how a nonpolar environment arises is yet unresolved. As previously mentioned, two possible descriptions could explain these results: the solute in its excited state could retain its sp^3 hybridization through strong, specific hydrogen bonding interactions with surface silanol groups (an "additive model") *or* the nonplanar solute could be subject to a low-polarity region created by surface induced changes in long range solvent organization (a "cooperative model"). To determine whether the observed changes in solute properties result from an additive or cooperative model of surface adsorption, methanol structure at the silica/methanol interface was characterized using MD simulations.

Table 3.3: Time resolved results of C151 at the silica/MeOH interface with χ^2 of 1.0-1.3 and uncertainties of ± 0.07 for the amplitude and ± 0.20 ps for the lifetimes shown.

	a	τ(ns)		
Bulk	1	5.34		
TIR	a_1	τ_1	a_2	τ_2
0.2 (μM)	0.54	5.85	0.46	1.83
0.5	0.72	5.60	0.28	1.17
1	0.82	5.23	0.18	1.04
10	0.94	5.40	0.06	1.22

Simulations performed by Weeks and coworkers are found in Reference 2. Their simulation data show that near the silica surface, all atom densities drop to their minimum at about 3.1 Å, indicating the existence of a tightly-bound layer at the methanol-silica interface. This is defined as the first layer of liquid/solid interface. The O-H density inside this layer exhibit two peaks: a large peak near the silica surface, indicating strong hydrogen bonding interaction between methanol and surface hydroxyl groups, and a small second peak, which presumably maintains the hydrogen bonding between methanol molecules in the surface layer and those in the bulk. Therefore, the O-H density profile indeed suggests that at the methanol-silica liquid-solid interface, there exist sublayer structures. The computational results predict that O-H bonds in this sublayer tend to point towards methanol molecules in the first sublayer so as to form additional hydrogen bonds rather than exploiting van der Waals attractions between methyl groups in adjacent sublayers.

This detailed examination of the silica/methanol interface implies that unless an adsorbed solute enjoys strong local bonding to the silica surface it will not displace

methanol from the first sublayer. Thus the solute will be subject to a local environment that has lower solvent density, slower relaxation, and fewer hydrogen bonding opportunities relative to the bulk methanol solution. This environment significantly shifts C151's electronic excitation energy to significantly shorter wavelengths. Furthermore, hindered motion of the interfacial solvent limits the ability of the interfacial environment to stabilize C151's planar, ICT state resulting in faster radiative decay relative to what is observed in bulk solution. Collectively these observations support a cooperative description of solute adsorption and solvation at a strongly associating silica/methanol interface.

Computational and experimental data, both steady state and time resolved, have shown the silica/methanol interface presents a nonpolar adsorption environment. Although one would assume by comparing the methanol data to the propanol findings that the silica/n-alcohol interface would present a nonpolar region, this has been shown not to be the case for even numbered chains.[47-48] The silica/ethanol and silica/butanol interface both appear to form a polar adsorption environment, and were explained by the solvents' larger footprint and the solvent-silica adsorption organization.

3.5 Conclusion

Collectively, the experiments described in this chapter examined the role of solvent structure in molecular adsorption. Resonance enhanced SH spectra measured how a solvent's solvating properties at the interface differ from bulk solution limits. Additionally time resolved fluorescence data were collected at the silica/methanol

interface. Comparing the methanol/silica adsorption environment to the propanol/silica interfaces we can determine the extent the hydrophobic tail of alcohol affects the adsorption environment. Several important findings emerge from these studies.

1. Interfacial solvation depends less on solvent monomer structure and more upon the noncovalent associations between the interfacial liquid and the adjacent substrate. As a result, the least polar liquids studied in this work, cyclohexane and methylcyclohexane create surprisingly polar environments at the silica/alkane interface, whereas 1- and 2-propanol and methanol form interfacial regions having interfacial polarity less than that of what one observes in bulk alkanes.
2. Solute identity did not appear to play an important part in adsorption. With the exception of the silica/mChex interface, SHG spectra appeared to be comparable for both the primary amine coumarin and the tertiary amine.
3. The comparison of propanol to methanol showed little variance in SHG spectra from the small to the longer chain alcohol. Time resolved fluorescence was in agreement with the steady state SHG data, the methanol/silica interface presents a nonpolar environment for the ground electronic state and the excited state for C151.

Since methanol and both 1- and 2- propanol –OH dipoles hydrogen bond strongly to the substrate, adsorbed molecules experience a nonpolar environment and have limited hydrogen bonding opportunities. Cyclohexane and methylcyclohexane

associate only weakly with the silica surface through van der Waals and dispersion forces. As a result, the adsorbates can associate with the silica surface through stronger dipole/dipole interactions and sample a much more polar environment than it would were it solvated in bulk alkane solution. Additional SHG and TIR-TCSPC shows C151 at the silica/methanol interface experiences a nonpolar surface. Furthermore, C151 at the silica/methanol terminates at monolayer coverage, with a relatively strong adsorption, and as Chapter 4 will explain, this behavior differs greatly when the silica/methanol interface is probed using C152.

3.6 References

1. Gobrogge, E. A.; Woods, B. L.; Walker, R. A., Liquid Organization And Solvation Properties At Polar Solid/Liquid Interfaces. *Faraday Discussions* **2013**, *167*, 309-327.

2. Roy, D.; Liu, S. L.; Woods, B. L.; Siler, A. R.; Fourkas, J. T.; Weeks, J. D.; Walker, R. A., Nonpolar Adsorption at the Silica/Methanol Interface: Surface Mediated Polarity and Solvent Density across a Strongly Associating Solid/Liquid Boundary. *Journal of Physical Chemistry C* **2013**, *117*, 27052-27061.

27. Brindza, M. R.; Walker, R. A., Differentiating Solvation Mechanisms at Polar Solid/Liquid Interfaces. *Journal of the American Chemical Society* **2009**, *131*, 6207-6214.

32. Horng, P.; Brindza, M. R.; Walker, R. A.; Fourkas, J. T., Behavior of Organic Liquids at Bare and Modified Silica Interfaces. *Journal of Physical Chemistry C* **2010**, *114*, 394-402.

33. Isaienko, O.; Nihonyanagi, S.; Sil, D.; Borguet, E., Observation of the Bending Mode of Interfacial Water at Silica Surfaces by Near-Infrared Vibrational Sum-Frequency Generation Spectroscopy of the Stretch plus Bend Combination Bands. *Journal of Physical Chemistry Letters* **2013**, *4*, 531-535.

37. Roy, D.; Piontek, S.; Walker, R. A., Surface Induced Changes In Coumarin Solvation And Photochemistry At Polar Solid/Liquid Interfaces. *Physical Chemistry Chemical Physics* **2011**, *13*, 14758-14766.

41. Zhang, X. Y.; Cunningham, M. M.; Walker, R. A., Solvent Polarity At Polar Solid Surfaces: The Role Of Solvent Structure. *Journal of Physical Chemistry B* **2003**, *107*, 3183-3195.

43. Zhang, X.; Steel, W. H.; Walker, R. A., Probing Solvent Polarity Across Strongly Associating Solid/Liquid Interfaces Using Molecular Rulers. *Journal Of Physical Chemistry B* **2003**, *107*, 3829-3836.

45. Vazquez, R.; Nogueira, R.; Busquets, S.; Mata, J. L.; Saramago, B., Wetting Films Of Polar And Nonpolar Liquids. *Journal of Colloid and Interface Science* **2005**, *284*, 652-657.

47. Siler, A. R.; Walker, R. A., Effects of Solvent Structure on Interfacial Polarity at Strongly Associating Silica/Alcohol Interfaces. *Journal of Physical Chemistry C* **2011**, *115*, 9637-9643.

48. Shang, X. M.; Benderskii, A. V.; Eisenthal, K. B., Ultrafast Solvation Dynamics At Silica/Liquid Interfaces Probed By Time-Resolved Second Harmonic Generation. *Journal of Physical Chemistry B* **2001**, *105*, 11578-11585.

56. Nad, S.; Kumbhakar, M.; Pal, H., Photophysical Properties Of Coumarin-152 And Coumarin-481 Dyes: Unusual Behavior In Nonpolar And In Higher Polarity Solvents. *Journal of Physical Chemistry A* **2003**, *107*, 4808-4816.

66. Suppan, P., Solvatochromic Shifts - The Influence Of The Medium On The Energy Of Electronic States. *Journal of Photochemistry and Photobiology a-Chemistry* **1990**, *50*, 293-330.

67. Steel, W. H., Y.Y. Lau, C.L. Beildeck, R.A. Walker, Solvent Polarity Across Weakly Associating Interfaces. *Journal Of Physical Chemistry B* **2004**, *108*, 13370-13378.

77. Mondal, S. K.; Yamaguchi, S.; Tahara, T., Molecules at the Air/Water Interface Experience a More Inhomogeneous Solvation Environment than in Bulk Solvents: A Quantitative Band Shape Analysis of Interfacial Electronic Spectra Obtained by HD-ESFG. *Journal of Physical Chemistry C* **2011**, *115*, 3083-3089.

80. Koopal, L. K., Wetting of Solid Surfaces: Fundamentals and Charge effects. *Advances in Colloid and Interface Science* **2012**, *179*, 29-42.

88. Ong, S. W.; Zhao, X. L.; Eisenthal, K. B., Polarization of Water-Molecules at a Charged Interface-2nd Harmonic Studies of Silica Water Interface. *Chemical Physics Letters* **1992**, *191*, 327-335.

107. Alvarezzepeda, A.; Barman, B. N.; Martire, D. E., Thermodynamic Study Of The Marked Differenes Between Acetonitrile Water And Methanol Water Mobile-Phase Systems In Reversed-Phase Liquic Chromatography. *Analytical Chemistry* **1992**, *64*, 1978-1984.

108. Rafferty, J. L.; Siepmann, J. I.; Schure, M. R., Mobile Phase Effects In Reversed-Phase Liquid Chromatography A Comparison Of Acetonitrile/Water And Methanol/Water Solvents As Studied By Molecular Simulation. *Journal of Chromatography A* **2011**, *1218*, 2203-2213.

109. Meyer, T.; Wania, F.; Vreivik, K., Illustrating Sensitivity And Uncertainty In Environmental Fate Models Using Partitioning Maps. *Environmental Science and Technology* **2005**, *39*, 3186-3196.

110. Goss, K. U.; Schwarzenbach, R. P., Linear Free Energy Relationships Used To Evaluate Equilibrium Partitioning Of Organic Compounds. *Environmental Science and Technology* **2001**, *35*, 1-9.

111. Wang, H. F.; Borguet, E.; Eisenthal, K. B., Generalized Interface Polarity Scale Based On Second Harmonic Spectroscopy. *Journal Of Physical Chemistry B* **1998**, *102*, 4927-4932.

112. Yamaguchi, S.; Watanabe, H.; Mondal, S. K.; Kundu, A.; Tahara, T., "Up" Versus "Down" Alignment And Hydration Structures Of Solutes At The Air/Water Interface Revealed By Heterodyne-Detected Electronic Sum Frequency Generation With Classical Molecular Dynamics Simulation. *Journal of Chemical Physics* **2011**, *135*.

113. Farmahini, A. H.; Bhatia, S. K., Differences In The Adsorption And Diffusion Behaviour Of Water And Non-Polar Gases In Nanoporous Carbon: Role Of Cooperative Effects Of Pore Confinement And Hydrogen Bonding. *Molecular Simulation* **2015**, *41*, 432-445.

114. Smith, E. A.; Wirth, M. J., pH Dependence Of Tailing In Reversed-Phase Chromatography Of A Cationic Dye: Measurement Of The Strong Adsorption Site Surface Density. *Journal of Chromatography A* **2004**, *1060*, 127-134.

115. Steel, W. H.; Walker, R. A., Measuring Dipolar Width Across Liquid-Liquid Interfaces With 'Molecular Rulers'. *Nature* **2003**, *424*, 296-299.

116. Zhang, X. Y.; Walker, R. A., Discrete Partitioning Of Solvent Permittivity At Liquid-Solid Interfaces. *Langmuir* **2001**, *17*, 4486-4489.

117. Beaglehole, D.; Christenson, H. K., Vapor Adsorption On Mica And Silicon - Entropy Effects, Layering, And Surface Forces. *Journal of Physical Chemistry* **1992**, *96*, 3395-3403.

118. Schlangen, L. J. M.; Koopal, L. K.; Stuart, M. A. C.; Lyklema, J.; Robin, M.; Toulhoat, H., Thin Hydrocarbon And Water Films On Bare And Methylated Silica - Vapor Adsorption, Wettability, Adhesion, And Surface Forces. *Langmuir* **1995**, *11*, 1701-1710.

119. Tavana, H.; Neumann, A. W., Recent Progress In The Determination Of Solid Surface Tensions From Contact Angles. *Advances in Colloid and Interface Science* **2007**, *132*, 1-32.

120. Fowkes, F. M., Determination Of Interfacial Tensions, Contact Angles, And Dispersion Forces In Surfaces By Assuming Additivity Of Intermolecular Interactions In Surfaces. *Journal of Physical Chemistry* **1962**, *66*, 382-&.

121. Correa, R.; Saramago, B., On The Calculation Of Disjoining Pressure Isotherms For Nonaqueous Films. *Journal of Colloid and Interface Science* **2004**, *270*, 426-435.

122. Levinson, P.; Valignat, M. P.; Fraysse, N.; Cazabat, A. M.; Heslot, F., An Ellipsometric Study Of Adsorption-Isotherms. *Thin Solid Films* **1993**, *234*, 482-485.

123. Bonnet, J. C.; Pike, F. P., Surface Properties Of 9 Liquids. *Journal of Chemical and Engineering Data* **1972**, *17*, 145-&.

124. Chibowski, E.; Holysz, L., Use Of The Washburn Equation For Surface Free-Energy Determination. *Langmuir* **1992**, *8*, 710-716.

125. Chibowski, E.; Holysz, L., On The Use Of Washburn's Equation For Contact Angle Determination. *Journal of Adhesion Science and Technology* **1997**, *11*, 1289-1301.

126. Horr, T. J.; Ralston, J.; Smart, R. S., The Use Of Contact-Angle Measurements To Quantify The Adsorption Density And Thickness Of Organic-Molecules On Hydrophilic Surfaces. *Colloids and Surfaces A - Physicochemical and Engineering Aspects* **1995**, *97*, 183-196.

127. Zhang, X. Y., M.M. Cunningham, R.A. Walker, Solvent Polarity At Polar Solid Surfaces: The Role Of Solvent Structure. *Journal Of Physical Chemistry B* **2003**, *107*, 3183-3195.

128. Benjamin, I., Chemical Reactions And Solvation At Liquid Interfaces: A Microscopic Perspective. *Chemical Reviews* **1996**, *96*, 1449-1475.

129. Yu, C. J., G. Evmenenko, A.G. Richter, A. Datta, J. Kmetko, P. Dutta, Order In Molecular Liquids Near Solid-Liquid Interfaces. *Applied Surface Science* **2001**, *182*, 231-235.

130. Bhattacharyya, K.; Sitzmann, E. V.; Eisenthal, K. B., Study of Chemical-Reactions by Surface 2nd Harmonic Generation-Para-nitrophenol at the Air-Water Interface. *Journal of Chemical Physics* **1987**, *87*, 1442-1443.

131. Ishizaka, S.; Kim, H. B.; Kitamura, N., Time-Resolved Total Internal Reflection Fluorometry Study On Polarity At A Liquid/Liquid Interface. *Analytical Chemistry* **2001**, *73*, 2421-2428.

132. Yanagimachi, M.; Tamai, N.; Masuhara, H., Solvation Dynamics Of A Coumarin Dye At Liquid Solid Interface Layer - Picosecond Total Internal-Reflection Fluorescence Spectroscopic Study. *Chemical Physics Letters* **1992**, *200*, 469-474.

133. Doerr, A. K., M. Tolan, J.P. Schlomaka, W. Press, Evidence For Density Anomalies Of Liquids At The Solid/Liquid Interface. *Europhysics Letter* **2000**, *52*, 330-336.

134. Christenson, H. K., D.W.R. Gruen, R.G. Horn, Structuring In Liquid Alkanes Between Solid Surfaces: Force Measurements And Mean-Field Theory. *Journal of Chemical Physics* **1987**, *87*, 1834-1841.

135. Gao, J. P., W.D. Luedtke, U. Landman, Structure And Solvation Forces In Confined Films: Linear And Branched Alkanes. *Journal of Chemical Physics* **1997**, *106*, 4309-4318.

136. Christenson, H. K., Phase Behavior In Confinement Studied With A Surface Force Apparatus. *Journal of Dispersion Science and Technology* **2006**, *27*, 617-624.

137. Wang, Y.; Hill, K.; Harris, J. G., Comparison Of Branched And Linear Octanes In The Surface Force Apparatus - A Molecular-Dynamics Study. *Langmuir* **1993**, *9*, 1983-1985.

138. Mikulski, P. T.; Herman, L. A.; Harrison, J. A., Odd And Even Model Self-Assembled Monolayers: Links Between Friction And Structure. *Langmuir* **2005**, *21*, 12197-12206.

139. Kanda, Y.; Iwasaki, S.; Higashitani, K., Adhesive Force Between Hydrophilic Surfaces In Alcohol-Water Solutions. *Journal of Colloid and Interface Science* **1999**, *216*, 394-400.

140. Liu, W. T., L.N. Zjang, Y.R. Shen, Interfacial Layer Structure At Alcohol/Silica Interfaces Probed By Sum-Frequency Vibrational Spectroscopy. *Chemical Physics Letters* **2005**, *412*, 206-209.

141. Zobel, M.; Neder, R. B.; Kimber, S. A. J., Universal Solvent Restructuring Induced By Colloidal Nanoparticles. *Science* **2015**, *347*, 292-294.

142. Dolores, E. M.; Rodriguez, J.; Laria, D., Structure And Dynamics Of Liquid Methanol Confined Within Functionalized Silica Nanopores. *Journal of Chemical Physics* **2010**, *133*, 154707.

143. Dolores, E. M.; Rodriguez, J.; Laria, D., Liquid Methanol Confined Within Functionalized Silica Nanopores. 2. Solvation Dynamics Of Coumarin 153. *Journal Of Physical Chemistry B* **2011**, *115*, 12859-12867.

144. Guégan, R.; Morineau, D.; Alba-Simionesco, C., Interfacial Structure Of A H-Bonding Liquid Confined Into Silica Nanopore With Surface Silanols. *Chemical Physics* **2005**, *317*, 236-244.

145. Vartia, A. A.; Thompson, W. H., Solvation and Spectra of a Charge Transfer Solute in Ethanol Confined within Nanoscale Silica Pores. *Journal Of Physical Chemistry B* **2013**, *116*, 5414-5424.

146. Feng, X. B.; Thompson, W. H., Time-Dependent Fluorescence in Nanoconfined Solvents. A Smoluchowski Equation Model Study. *Journal of Physical Chemistry C* **2010**, *114*, 4279-4290.

147. Gomez, J. A.; Tucker, A. K.; Shepherd, T. D.; Thompson, W. H., Conformational Free Energies Of 1,2-Dichloroethane In Nanoconfined Methanol. *Journal of Physical Chemistry B* **2005**, *109*, 17479-17487.

148. Benderskii, A. V.; Henzie, J.; Basu, S.; Shang, X. M.; Eisenthal, K. B., Femtosecond Aqueous Solvation At A Positively Charged Surfactant/Water Interface. *Journal Of Physical Chemistry B* **2004**, *108*, 14017-14024.

149. Shang, X.; Nguyen, K.; Rao, Y.; Eisenthal, K. B., In-Plane Molecular Rotational Dynamics at a Negatively Charged Surfactant/Aqueous Interface. *Journal of Physical Chemistry C* **2008**, *112*, 20375-20381.

150. Abbas, H., First Principle Calculation Of The Photophysical Properties Of Silylated Coumarins 120 And 151. *Computational and Theoretical Chemistry* **2012**, *992*, 55-58.

151. Aono, S.; Minezawa, N.; Kato, S., Electronic Spectra Of Coumarin-151 In Polar Solvents: Linear Response Free Energy Approach. *Chemical Physics Letters* **2010**, *492*, 193-197.

152. Arbeloa, T. L.; Arbeloa, F. L.; Arbeloa, I. L., Influence Of Fluorinated Group On The Photophysics Of 7-Aminocoumarins. *Journal of Luminescence* **1996**, *68*, 149-155.

153. Cave, R. J.; Burke, K.; Castner, E. W., Theoretical Investigation Of The Ground And Excited States Of Coumarin 151 And Coumarin 120. *Journal of Physical Chemistry A* **2002**, *106*, 9294-9305.

154. Cave, R. J.; Castner, E. W., Time-Dependent Density Functional Theory Investigation Of The Ground And Excited States Of Coumarins 102, 152, 153, And 343. *Journal of Physical Chemistry A* **2002**, *106*, 12117-12123.

155. Das, K.; Jain, B.; Patel, H. S., Hydrogen Bonding Properties Of Coumarin 151, 500, And 35: The Effect Of Substitution At The 7-Amino Position. *Journal of Physical Chemistry A* **2006**, *110*, 1698-1704.

156. Krystkowiak, E.; Maciejewski, A., Changes In Energy Of Three Types Of Hydrogen Bonds Upon Excitation Of Aminocoumarins Determined From Absorption Solvatochromic Experiments. *Physical Chemistry Chemical Physics* **2011**, *13*, 11317-11324.

157. Liu, Y.; Ding, J.; Liu, R.; Shi, D.; Sun, J., Revisiting The Electronic Excited-State Hydrogen Bonding Dynamics Of Coumarin Chromophore In Alcohols: Undoubtedly Strengthened Not Cleaved. *Journal of Photochemistry and Photobiology a-Chemistry* **2009**, *201*, 203-207.

158. Liu, Y.-H.; Li, P., Excited-State Hydrogen Bonding Effect On Dynamic Fluorescence Of Coumarin 102 Chromophore In Solution: A Time-Resolved Fluorescence And Theoretical Study. *Journal of Luminescence* **2011**, *131*, 2116-2120.

159. Nad, S.; Pal, H., Unusual Photophysical Properties Of Coumarin-151. *Journal of Physical Chemistry A* **2001**, *105*, 1097-1106.

160. Pedone, A., Role of Solvent on Charge Transfer in 7-Aminocoumarin Dyes: New Hints from TD-CAM-B3LYP and State Specific PCM Calculations. *J. Chem. Theory Comput.* **2013**, *9*, 4087-4096.

161. Rechthaler, K.; Kohler, G., Excited-State Properties And Deactivation Pathways Of 7-Aminocoumarins. *Chemical Physics* **1994**, *189*, 99-116.

162. Corrie, J. E. T.; Munasinghe, V. R. N.; Rettig, W., Synthesis And Fluorescence Properties Of Substituted 7-Aminocoumarin-3-Carboxylate Derivatives. *Journal of Heterocyclic Chemistry* **2000**, *37*, 1447-1455.

163. Forster, Y.; Haas, E., Preparation And Characterization Of 3 Fluorescent Labels For Proteins, Suitable For Structural Studies. *Analytical Biochemistry* **1993**, *209*, 9-14.

164. Shobini, J.; Mishra, A. K.; Sandhya, K.; Chandra, N., Interaction Of Coumarin Derivatives With Human Serum Albumin: Investigation By Fluorescence Spectroscopic Technique And Modeling Studies. *Spectrochimica Acta Part a-Molecular and Biomolecular Spectroscopy* **2001**, *57*, 1133-1147.

165. Das, K.; Jain, B.; Patel, H. S., Hydrogen Bonding Properties Of Coumarin 151, 500, And 35: The Efffect Of Substitution At The 7-Amino Position. *Journal of Physical Chemistry A* **2006**, *110*, 1698-1704.

166. Nad, S.; Pal, H., Unusual Photphysical Properties Of Coumarin-151. *Journal of Physical Chemistry A* **2001**, *105*, 1097-1106.

167. Rechthaler, K.; Kohler, G., Excited State Properties And Deactivation Pathways Of 7-Aminocoumarins. *Chemical Physics* **1994**, *189*, 99-116.

168. Dahiya, P.; Kumbhakar, M.; Mukherjee, T.; Pal, H., Effect Of Protic Solvents On Twisted Intramolecular Charge Transfer State Formation In Coumarin-152 And Coumarin-481 Dyes. *Chemical Physics Letters* **2005**, *414*, 148-154.

169. Siler, A. R., M.R. Brindza, R.A. Walker, Hydrogen-Bonding Molecular Ruler Surfactants As Probes Of Specific Solvation At Liquid/Liquid Interfaces. *Analytical and Bioanalytical Chemistry* **2009**, *395*, 1063-1073.

170. Gayathri, B. R.; Mannekutla, J. R.; Inamdar, S. R., Effect Of Binary Solvent Mixtures (DMSO/Water) On The Dipole Moment And Lifetime Of Coumarin Dyes. *Journal of Molecular Structure* **2008**, *889*, 383-393.

171. Inamdar, S. R.; Gayathri, B. R.; Mannekutla, J. R., Rotational Diffusion of Coumarins in Aqueous DMSO. *Journal of Fluorescence* **2009**, *19*, 693-703.

172. Zhang, L.; Singh, S.; Tian, C.; Shen, Y. R.; Wu, Y.; Shannon, M. A.; Brinker, C. J., Nanoporous Silica-Water Interfaces Studied By Sum-Frequency Vibrational Spectroscopy. *Journal of Chemical Physics* **2009**, *130*.

173. Shen, Y. R.; Ostroverkhov, V., Sum-Frequency Vibrational Spectroscopy On Water Interfaces: Polar Orientation Of Water Molecules At Interfaces. *Chemical Reviews* **2006**, *106*, 1140-1154.

174. Gradl, G.; Kohler, B. E.; Westerfield, C., Electric-Field Splitting of the Octateranene 1 1AG- 2 1AG Transition in n-Hexane. *Journal of Chemical Physics* **1992**, *97*, 6064-6071.

175. Kohler, B. E.; Woehl, J. C., Measuring Internal Electric-Fields With Atomic-Resolution. *Journal of Chemical Physics* **1995**, *102*, 7773-7781.

176. Kohler, B. E.; Woehl, J. C., Effects Of Electrostatic Fields And Potentials On The Electronic Energies Of Conjugated Organic Molecules. *Journal of Physical Chemistry A* **1999**, *103*, 2435-2445.

177. Steel, W. H.; Damkaci, F.; Nolan, R.; Walker, R. A., Molecular Rulers: New Families Of Molecules For Measuring Interfacial Widths. *Journal of the American Chemical Society* **2002**, *124*, 4824-4831.

178. Kina, D.; Arora, P.; Nakayama, A.; Noro, T.; Gordon, M. S.; Taketsugu, T., Ab Initio QM/MM Excited-State Molecular Dynamics Study of Coumarin 151 in Water Solution. *International Journal of Quantum Chemistry* **2009**, *109*, 2308-2318.

179. Bratescu, M. A.; Saito, N.; Takai, O., Attenuated Total Reflectance Spectroscopy Of Coumarin Organosilane Molecules Adsorbed On A Fused Silica Surface. *Applied Surface Science* **2010**, *257*, 1792-1799.

CHAPTER 4

ADSORPTION AND AGGREGATION AT SILICA/METHANOL INTERFACE: THE ROLE OF SOLUTE STRUCTURE

Contributions of Authors and Co-Authors

Manuscript in Chapter 4

Author: B. Lauren Woods

Contributions: Collected and analyzed all SHG experimental data. Designed the TIR geometry and collected time resolved fluorescence.

Author: Jenna K. George

Contributions: Collected time resolved fluorescence

Author: Alex M. Sherman

Contributions: Collected steady state fluorescence at the solid/vapor interface and bulk excitation and emission data

Author: Patrik R. Callis

Contributions: Assisted in performing computational calculations and analysis. Assisted in editing

Co-Author: Rob Walker

Contributions: Assisted with data analysis and edited manuscript at all stages.

Manuscript Information Page

B. Lauren Woods, Jenna K. George, Alex M. Sherman, Patrik R. Callis, and Robert A. Walker
Journal of Physical Chemistry C
Status of Manuscript:
____Prepared for submission to peer-reviewed journal
_X_ Officially submitted to a peer-reviewed journal
____Accepted by a peer-reviewed journal
____Published in a peer-reviewed journal

Publisher: ACS

CHAPTER 4

ADSORPTION AND AGGREGATION AT SILICA/METHANOL INTERFACE: THE ROLE OF SOLUTE STRUCTURE

Abstract

Second harmonic generation (SHG) and time resolved, total internal reflection fluorescence (TR-TIRF) spectroscopy were used to examine the adsorption, solvation and aggregation of a coumarin solute, Coumarin 152 (C152), at the silica/methanol interface. Experiments were performed as a function of bulk C152 concentration with SHG data providing information about relative surface coverage and ground state solvation environment. TR-TIRF data measured emission lifetimes of C152 adsorbed to the silica/methanol interface. SHG spectra show strong resonance enhancement at 365 nm, a result that is blue-shifted considerably from C152's electronic excitation of ~400 nm in bulk methanol. Given C152's solvatochromic behavior, this observation implies that C152 adsorbed to the silica/methanol interface experiences a local dielectric environment that is significantly less polar than in bulk methanol. TR-TIRF decays at sub-μM bulk concentrations were fit to two lifetimes, one assigned to C152 emission in bulk methanol (0.9 ns) and a longer lifetime assigned to contributions from adsorbed C152 (~4 ns). The longer lifetime is similar to C152 in alkanes, a result that is consistent with SHG data. Isothermal data from SHG experiments show unusual behavior as bulk C152 concentration increases. Instead of approaching an asymptotic limit signifying monolayer coverage, the SHG response rises at the lowest C152 concentrations and then

decreases dramatically, suggesting the onset of aggregate formation. Changes in the TR-TIRF emission behavior of C152 at higher C152 bulk concentrations support this hypothesis. These findings are interpreted in terms of C152's ability to self-associate and the energetics of dimer formation are explored using *ab initio* calculations and polarizable continuum models.

4.1 Introduction

Solute adsorption to buried liquid interfaces can be difficult to predict *a priori*. Even simple questions about a solute's tendency to adsorb to solid/liquid interfaces requires knowing about the strength of solute-substrate, solvent-substrate, and solute-solvent energetics. Typically, global questions about solute adsorption to solid/liquid interfaces can be distilled to three specific queries: 1) Will a solute adsorb to a surface from solution? 2) Is adsorption reversible or irreversible? and 3) Does adsorption cease at terminal monolayer coverage or will more solutes continue to accumulate leading to aggregate and/or multi-layer formation? Answers to these questions will depend upon a host of conditions including substrate, solute and solvent identity and local anisotropy induced by the substrate in the adjacent solvent. From this microscopic perspective, adsorption is cast in terms of fundamental, molecular interactions. The consequences of adsorption to buried liquid interfaces, however, are far ranging in a host of fields including groundwater remediation, biofilm formation and chromatographic separations.[8-10, 22-23, 180-181]

Characterizing molecular adsorption is essential to understanding and designing environmental remediation strategies.[8-10] The goal of remediation is often either to immobilize or dilute harmful species in streams and sub-surface ground water sources. Accomplishing this task is difficult if the pollutant's adsorption tendencies are not well characterized.[10] If the pollutant has a strong affinity for a soil substrate, it will not spread significantly, reducing the volume of material in need of remediation. However, failure to remediate a species that adsorbs strongly to soil/liquid interfaces results in a long-lived, persistent source of harmful agents. Weak adsorption leads to rapid dilution of pollutants, but a correspondingly larger volume of material to remediate if regulatory limits are low. Currently, EPA practices require extensive, empirical testing to determine specific remediation strategies for a given site.[21] Little attention has focused on the development of models that can predict molecular mechanisms responsible for solute adsorption to solid/liquid interfaces and the tendencies of solutes to form terminal monolayers or multilayer aggregates. The few experimental and computational studies that have examined adsorption mechanisms at buried interfaces illustrate the difficulties in quantifying forces that contribute to monolayer and aggregate formation.[9-10]

A second application where adsorption plays a central role is chromatographic separation.[22-23] Liquid chromatography uses tailored substrates (stationary phases) and solvent mixtures to separate solutes in solution. Aggregation of molecules can lead to false reporting of size, molecular mass, and poor separation of solutes.[22-23] Separation studies using hydrodynamic chromatography have shown the effect aggregation can have on chromatographic techniques and a procedure to reduce aggregation through altering

the mobile phase.[22] Strategies for improving separation schemes often develop from empirical testing and iteration. Being able to predict or control adsorption and limit aggregation will assist in designing column structures with high selectivity and increased efficiency.

While chromatographic separation applications have readily observable outcomes, the molecular origins of solute dependent, adsorption energetics are less clear. Solvation properties such as polarity, pH, and ion concentration induce changes in surface properties that either promote or inhibit solute adsorption.[1, 3, 37, 41, 47, 93, 182] The silica surface is heterogeneous and, in an aqueous solvation environment, has complicated acid-base and ion-selective adsorption behaviors that can require long equilibration times.[3, 79, 93, 95] In the presence of organic solvents, substrate behavior is less complicated chemically, although the effects of the surface silanol groups on solvent structure and organization can be difficult to predict.[1-3, 27, 37, 47]

Nonlinear optical studies examining the alkane/silica interface showed interfaces formed between silica an nonpolar alkane solvents are very polar.[1] The polar interface can be explained by strong adsorbate-substrate interactions dominated by the hydrogen bond donating properties of surface silanol groups.[27] In contrast, polar, hydrogen bonding solvents such as 1- and 2-propanol, octanol and even methanol create distinctly nonpolar environments, a result that has been interpreted in terms of the solvent hydrogen bonding so strongly to the silica that adsorbed solutes interact primarily with alcohol alkyl groups.[1,2, 27, 43, 47] The work presented here explores the effects of strong hydrogen bonding between silica and methanol on solute adsorption and aggregate formation.

Specifically, resonance enhanced second harmonic generation (SHG) is used to measure how adsorption changes a solute's electronic structure from bulk solution limits and how these changes evolve with increasing surface coverage. Time resolved fluorescence emission collected in a total internal reflection geometry is used to infer details about adsorbate excited state dynamics. The solute used in these studies is Coumarin 152, also called Coumarin 485 or 7-(dimethylamino)-4-(trifluoromethyl)coumarin. (Figure 4.1)

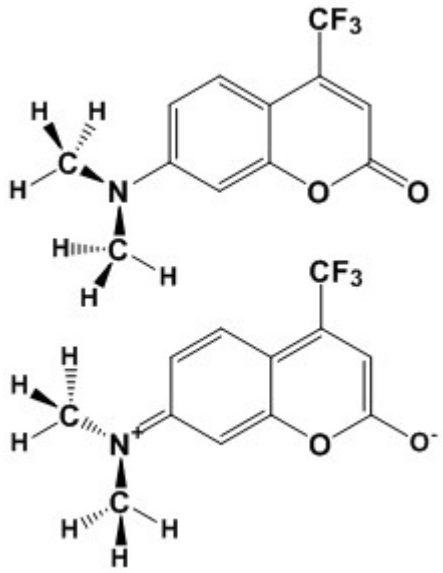

Figure 4.1. A)C152 in a ground state configuration and B) the proposed TICT structure of the excited state in polar solvents.

C152 belongs to the family of 7-aminocoumarins that have been well characterized given their use as laser dyes.[152, 161, 183] With their high quantum yields in appropriate solvents and well-studied excited states, 7-aminocoumarins have also been used as biological markers and fluorescent probes in medical research.[162-164] Many 7-aminocoumarins can form an intramolecular charge transfer excited states in polar media.[155-157, 168] Transient absorption studies have proposed that from its first optically-

accessible excited state, C152 forms a twisted results in a large solvochromatic shift in excitation (and emission) between polar solvents (400 nm excitation/515 nm emission) and non-polar solvents (370 nm/425 nm).[154]

Resonance enhanced SHG measurements are sensitive to the electronic structure of an adsorbed solute in its ground electronic state meaning that the SHG resonance wavelength serves as a sensitive indicator of the interfacial solvation environment. C152's emission lifetime serves as a second, independent indicator of the solute's local dielectric environment. If C152 forms a TICT state at an interface, we expect the solute's emission lifetime to be short. If the interface inhibits TICT formation, C152's emission lifetime will be longer. Recently published results suggest that C152 films at the silica/*vapor* interface consist of either monomers if films were formed from a methanol solution having low C152 concentration or aggregates from high concentration solutions of C152 in methanol.[37] Whether or not aggregates form in the presence of a solvent is a question that motivated the studies presented in this work. Both SHG and time resolved fluorescence emission data support the hypothesis that C152 adsorption to silica methanol interfaces *does not* cease with terminal monolayer coverage. Rather, at concentrations above ~100 μM C152 continues to adsorb in a manner that implies strong adsorbate-adsorbate interactions. Possible C152 aggregation mechanisms of C152 are addressed using *ab inito* computational methods with polarizable continuum models.

ICT (or TICT) state in polar solvents. [1, 37, 160] The stabilization of the TICT results in a low quantum yield of < 0.2 and short (sub-ns) lifetime, while in non-polar solvents quantum yields approach unity with relatively long lifetimes of ~ 4 ns.[56] The large,

~+5 Debye change in C152's dipole moment from the ground state permanent dipole moment following photoexcitation.

4.2 Experimental Considerations

Laser grade Coumarin 152 was purchased and used as received from Exciton. HPLC grade methanol of purity >99% was received from EMD. For fluorescence surface experiments, the Kel-F sample cells use hemispherical fused quartz prisms from ISP Optics. For SHG experiments, fused silica slides were purchased from SPI. To ensure a clean silanol surface, sample preparation includes acid washing both the slides and prisms in a 50/50 sulfuric/ nitric acid mix and rinsing thoroughly with deionized water (Milipore, 18.2 MΩ). The silica surface was then allowed to equilibrate with solutions of C152 in methanol.

Two techniques were used to observe molecular behavior at and near the silica/methanol interface: resonance enhanced Second Harmonic Generation (SHG) and time resolved (TR) fluorescence emission measured using time correlated single photon counting (TCSPC) spectroscopy in a total internal reflection geometry. SHG is inherently surface specific and provides information about a solute's local solvation environment as well as relative surface coverage and adsorption energies. Data from TR-TCSPC emission spectroscopy can be used to infer solvation interactions between the solute in its excited state and changes in the local solvent environment. In order to develop molecular insight into the observed experimental results, computational methods were employed to

explore the tendency for solutes to aggregate in different dielectric continuum environments.

4.2.1 Second Harmonic Generation

Second Harmonic Generation (SHG) is a second order nonlinear optical spectroscopy that is necessarily surface specific within the electric dipole limit.[3, 28, 34, 41, 49] To collect interfacial SH signal, a coherent beam of frequency ω is focused onto a sample and induces a polarization of molecules at the surface at 2ω. The intensity of the SH signal, I(2 ω) is related to the second order polarizability, $P^{(2)}$:

$$I(2\omega) \propto \left|P^{(2)}(2\omega)\right|^2 \qquad \text{Eq. 4.1}$$

where $P^{(2)} = \left|\chi^{(2)}: E(\omega_1)E(\omega_2)\right|$. Since the incident beam is at a single frequency, $\omega_1 = \omega_2$, the electric fields, E, are also equal. SHG's surface specificity arises from $\chi^{(2)}$, the second order nonlinear susceptibility. $\chi^{(2)}$is a third rank tensor that contains 27 matrix elements which is dependent on the anisotropy of a system. In isotropic environments the requirement that $\chi^{(2)}_{i,j,k} = -\chi^{(2)}_{-i,-j,-k}$prevents a SH response from originating in bulk solution within the electric dipole approximation. Only at interfaces where inversion symmetry is broken can elements of the $\chi^{(2)}$ tensor assume nonzero values. The nonzero contribution from $\chi^{(2)}$ elements can also be reduced (or canceled completely) by *local* inversion symmetry. Specifically, if adsorbates adopt an antiparallel structure, dipole moments can cancel resulting in diminished (or nonexistent) SH signal.

Additionally, $\chi^{(2)}$depends on molecular identity. Each $\chi^{(2)}$ element contains nonresonant, NR, and resonant, R, contributions,

$$\chi^{(2)} = \chi_{NR}^{(2)} + \chi_R^{(2)} \qquad \text{Eq. 4.2}$$

The nonresonant factor can be fit to a single value or simple function, depending on its magnitude and frequency dependence. The resonant term is more complex and is related to an adsorbate's molecular hyperpolarizability, β:[67,184]

$$\chi_R^{(2)} = N\langle\beta_{ijk}\rangle,\ \beta = \sum_{k,e} \frac{A}{(\omega_{gk} - \omega_o - i\Gamma)(\omega_{eg} - 2\omega_o + i\Gamma)} \qquad \text{Eq. 4.3}$$

The resonant term is equal to the number of interfacial molecules, N, multiplied the orientational average of $\langle\beta\rangle$, where β is the first order hyperpolarizability. As twice the laser frequency, $2\omega_o$, comes into resonance with the transition frequency, ω_{eg}, the denominator becomes undefined and the magnitude of β is enhanced, resulting in large SH signal. SH signal is measured as a function of wavelength and the resulting spectrum is fitted to Equations 4.2 and 4.3 to calculate the resonance frequency, 2ω, the relative contribution, A, and the line width, Γ. $A = \mu_{gk}\mu_{ke}\mu_{eg}$, where μ_{ij} represents the transition dipole matrix elements from the *i* to the *j* states. The line width provides information about the homogeneity of the solvation environment. More narrow line widths imply increasingly homogeneous solvation across the interface.[50]

Solvatochromic solutes show shifts in excitation wavelength in their SHG spectra and these shifts can be used to infer how the interfacial dielectric environment differs from bulk solution limits.[41, 185-186] Plotting the strength of the generated SH field as a function of bulk concentration creates an isotherm that can be fit to an appropriate equation of state to find ΔG_{ads}^{o}.[3, 105, 187-188]

Resonance-enhanced SHG signal was acquired from an assembly described in detail in Chapter 2. Briefly, experiments used ~3.8 W from an amplified Ti:sapphire

laser (Libra-HE, Coherent, 85 fs pulses, 1 kHz repetition rate, 802 nm) coupled to a visible optical parametric amplifier (Coherent OPerA Solo) and collected using a PMT and photon counting electronics. The incident visible light was attenuated to ~1 μJ/pulse using neutral density filters. Data for individual wavelengths were collected in 3-5 separate 10 sec intervals and then background corrected and averaged.

4.2.2 Time Correlated Single Photon Counting.

TR-TCSPC emission was collected using a Picoquant PicoHarp 300 with FluoTime 200 software. The excitation source for the experiments performed in these studies was a tunable, Ti:sapphire oscillator (Coherent Chameleon, 80 MHz, 12.5 ns rep rate) with a wavelength range of 680-1080 nm. An APE autotracker was used to convert the range using a doubling crystal to create a 350-520 nm range. A schematic of the system is found in Figure 4.2. The excitation wavelength range for C152 requires the use of an electrooptic modulator (Conoptics Model 350-105) to reduce the repetition rate of the 80 MHz Ti:sapphire laser to a repetition rate of 4 MHz for the TR-TIRF measurements.

Bulk and TIR data were analyzed using Picoquant's FluorFit fitting software. The decays were fitted to a multimodal Gaussian distribution after reconvoluting the data to account for scatter from the instrument response function (IRF). After eliminating contributions from the IRF, data were fit to a sum of exponential decays:

$$I(t) = \sum_{i=1}^{n} A_i e^{-t/\tau_i} \qquad \text{Eq. 4.4}$$

The parameters A_i and τ_i are the amplitude and lifetime of the i^{th} component of the decay. Fitting parameters are optimized according to a least squares fit. To test the uniqueness of the results, data are fit several times starting with different sets of initial parameters. In general, data from the TIR assembly can be fit with amplitudes are accurate to ±7 % and lifetimes are accurate to ± 0.20 ns. When making standard, bulk solution measurements, lifetimes can be measured with ±0.05 ns resolution.

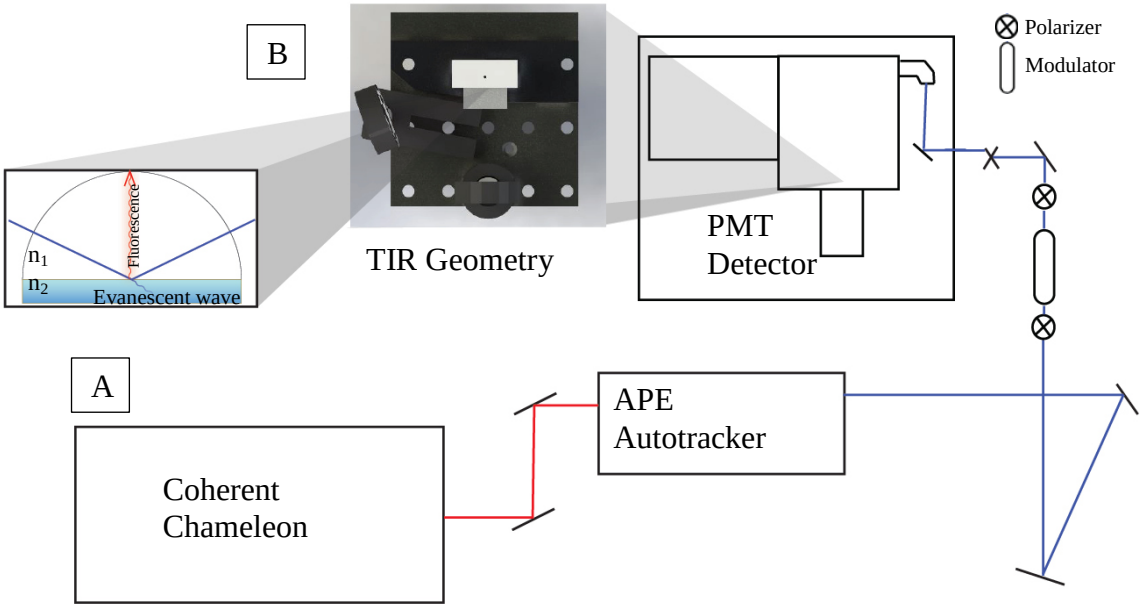

Figure 4.2 A) Schematic of the TCSPC with a diagram of the custom TIR set-up. Shown is the geometry associated with SHG path, a similar set-up is available for THG but was not used for the experiments presented in the paper. B)A schematic of TIR geometry where the incoming angle (θ_i) is greater than θcr, the critical angle. The evanescent wave probes ~100 nm into the bulk before fading.

4.2.3 Total Internal Reflection

Performing experiments in a total internal reflection geometry (TIR) is a strategy used to observe near-surface molecular behavior. (Figure 4.2B) In a TIR geometry, the

incident beam passes through a higher refractive material ($n_2>n_1$) at an angle (θ_i) greater than the critical angle (θ_{cr}). With this geometry the evanescent wave excites only those molecules within the first ~200 nm of the silica/methanol boundary.[57] The sampling depth is dependent on the wavelength, indices of refraction for the chosen media, and the incoming angle. The TR-TIR assembly used in these experiments employed an incident angle range of $72^o \pm 3$, and at a wavelength of 400 nm, the sampling depth is ~125 nm. The resolution for TCSPC decays is dependent on the instrument response function (IRF). For bulk solution measurements, the IRF varies between 20 and 50 ps but additional scatter introduced by the TIR sample cell leads to an IRF in the surface sensitive measurements of ~200 ps.

4.2.4 Computational Methods

Experimental data provide strong indications that C152 adsorption does not cease with terminal monolayer formation and, instead, continues to form aggregates. (*Vide infra.*) We employ density functional theory (DFT) (CAM-B3lyp and M06L) methods to calculate possible aggregation mechanisms. CAM-B3LYP is a range-separated hybrid functional that takes into account dimer interactions while the M06L is a pure local functional that has been shown to be an excellent and accurate method to study noncovalent and weak interactions.[189-190] Monomer and dimer geometries were first optimized using a lower basis set (6-311G(d)) and then optimized again with a higher level basis set that included diffuse functions and orbital interaction terms (6-311+G(d,p)). Calculations began with several different dimer starting geometries and dimer structures were optimized.

The goal of these calculations was to gain a semi-quantitative understanding of the most likely configuration and relative energetics of solute dimers in different polarizable continua. A self-consistent reaction field (SCRF) was used to include an implicit solvent continuum, experiments were performed with continuum dielectric constants of 1.00, 1.88, and 32.61, corresponding to the static dielectric constants of vacuum, hexane and methanol, respectively. The M06L method produced consistently lower energies, both for monomer and dimer calculations. Findings discussed below will focus on results from using this specific functional. Additional calculations of dimer formation using CAM-B3lyp can be found in Appendix B along with a more detailed description of the calculation methods and results.

4.3 Results and Discussion.

4.3.1 Bulk Solution Properties

Understanding how interfacial solvation of C152 changes from bulk solution limits first requires understanding C152's behavior in bulk solution. Figure 4.3 shows the steady state excitation and time resolved spectra of C152 in methanol and in hexane. Wavelengths corresponding to excitation maxima and emission lifetimes are reported in Table 4.1. Given its relatively large change in dipole upon photoexcitation, there is a strong bathochromic shift and its excitation wavelength shifts from 368 nm in nonpolar alkanes to 396 nm in polar, protic solvents such as methanol. Fluorescence emission from C152 in methanol is characterized by a single lifetime of 0.9 ns, while C152 emission in nonpolar solvents is biexponential but dominated by a longer, 3.5 ns lifetime.

Table 4.1. Bulk and Surface Characteristics of C152 in methanol.

	Bulk	SHG
λex(nm)	396	364±2
λem (nm)	511	---
Γ (nm)	77 ±4	15±2

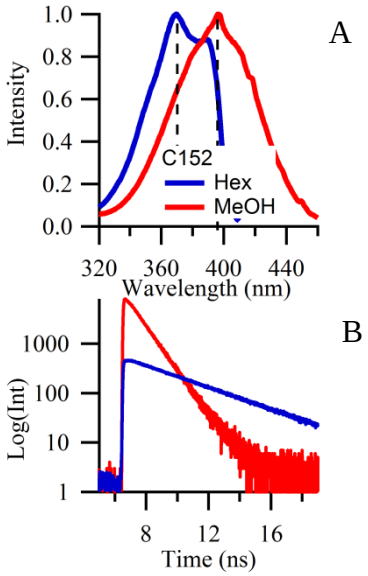

Figure 4.3.A) Bulk excitation spectra for C152 in methanol and hexane B) Time resolved emission of ~20 µM C152 in bulk MeOH and Hex were fit to a single lifetime.

4.3.2 Second Harmonic Generation.

Resonance enhanced SHG measures excitation resonances of molecules in anisotropic environments. A spectrum of C152 adsorbed to the silica/methanol interface from a 30 µM solution is shown in Figure 4.4A. Several features in the spectrum stand out. First, the SH spectrum shows strong resonance enhancement at 364 ± 3 nm, a wavelength that is at the extreme short wavelength edge of C152's solvatochromic

window. This result implies that C152 adsorbed to the silica/methanol interface samples an environment characterized by a very low effective dielectric constant. This shift is not concentration dependent as SHG spectra taken at 30, 80, and 300 μM show no measurable shifts in polarity. (Spectra for these three concentrations are provided in Figure B.1 in Appendix B.) The second aspect of C152's SHG spectrum worth noting is its narrow width. Fitting the data to Equation 3, we calculate a line width (FWHM) of 15 ± 2 nm. This width is much more narrow than its linear excitation spectrum in bulk methanol (~75 nm) but consistent with other SHG linewidths reported in the literature.[43, 191] Part of the line narrowing results from the nonlinear origin of the spectrum, but we also expect that the excitation of C152 adsorbed to the silica surface experiences less inhomogeneous broadening than in bulk methanol.[50, 77]

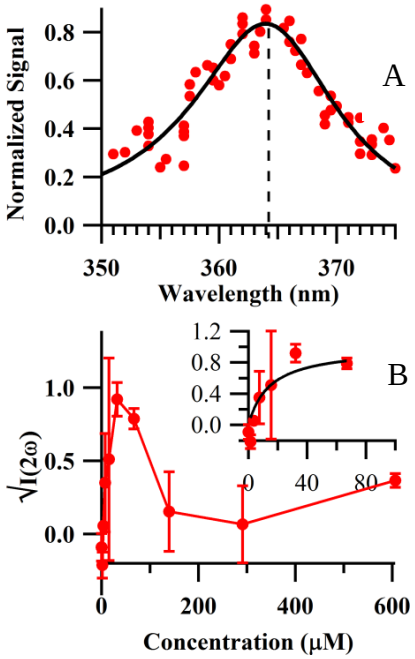

Figure 4.4. A) Resonance enhanced SHG spectrum of ~30μM C152 in methanol B)Isothermal data was collected at resonance wavelength of 364 nm. The data does not obey typical isothermal behavior at higher concentration, the Langmuir equation was fitted to the lower concentration range (inset). A ΔG_{ads}=-35±7kJ/mol was calculated.

Figure 4.4B shows isothermal data recorded at 366 nm as a function of C152 concentration. Data are reported as the square root of the measured SHG signal. Within the limits of small nonresonant contributions and no systematic change in average orientation, the SH field is directly proportional to the number of adsorbed species. From the data in Figure 4.4B, one sees immediately that C152 adsorption cannot be described by any equation of state that assumes adsorption ceases with formation of a full monolayer. The lower concentration range *was* fit to a Langmuir equation leading to a calculated adsorption energy of -35 ± 7 kJ/mol. Importantly, the SHG response falls abruptly at concentrations higher than ~80 μM implying a change in adsorbate surface behavior. At concentrations above ~150 μM, the SHG signal levels out at approximately one third of the maximum intensity. Since SH signal requires a noncentrosymmetric environment, the observed drop in signal implies either a randomization of adsorbed interfacial solutes *or* the creation of local inversion symmetry from dimers or larger adsorbed aggregates.

4.3.3 Fluorescence Studies

Evidence of C152 aggregate formation at silica surfaces has precedent. Earlier studies examining films at solid/vapor interfaces that had been in contact with liquid solutions reported that steady state emission spectra of films formed from low concentration solutions of C152 in methanol showed typical behavior with emission wavelength maximum of ~500 nm and a line width of ~80 nm.[37]

These results were reproduced for this work and the data are shown in Figure 4.5. Films at the solid/vapor interface formed from higher concentration solutions showed

strong emission from a second feature at significantly longer wavelengths with an emission maximum of 574 nm. The lifetime of species responsible for this longer wavelength emission was 5.2 ns (compared to <0.9 ns for the short wavelength emission). These observations were interpreted in terms of aggregate formation between solutes that had adsorbed from the high concentration solutions. Instead of C152 adsorption ceasing once the surface saturated, the data imply that C152 continues to accumulate at the silica surface as bulk concentration increases. Continued accumulation leads to aggregation and the formation of new electronic states comprised of several contributing monomers.

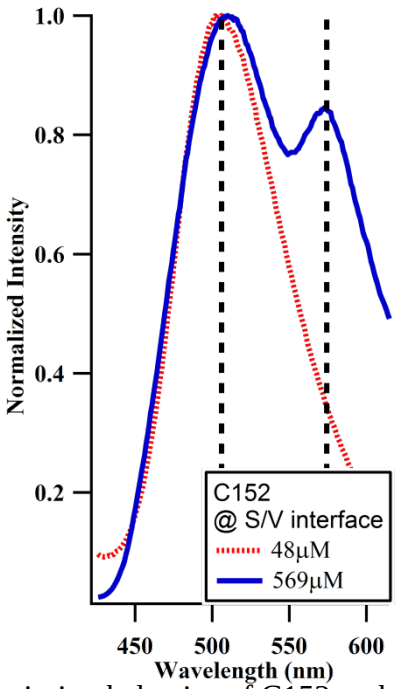

Figure 4.5. Steady state emission behavior of C152 at the silica/vapor interface after allowing silica to equilibrate in a methanol solution.

TIR-TCSPC data in the current studies were collected at both the bulk emission wavelength (513 nm) and at a wavelength associated with emission from molecular aggregates (574 nm). Additional fluorescence emission was collected using two excitation wavelengths, 396 nm, the bulk excitation peak, and 365 nm which arose from the SHG spectral data.[2, 56] The difference in emission behavior was not measurably affected by excitation wavelength, therefore only the decays collected using 396 nm excitation will be presented here. Decays collected with 365 nm excitation can be found in Appendix B (Figure B.2.)

Table 4.2. Emission lifetimes of C152 in bulk methanol and at the methanol/silica interface Lifetimes (τ) and their relative amounts (A) are presented for bulk and from TIR measurements. The concentration range was chosen to represent various positions along the isotherm spectra before and at monolayer coverage. Lifetimes have an accuracy of± 0.20 ns. Amplitudes vary from trial to trial based on laser conditions and position of the TIR cell which explains the large deviation of ±12 %.

Conc. (μM)	τ(ns) (A)	
Bulk	0.94 (100)	
TIR	$\tau_{1\ (ns)}$ (A_1)	$\tau_{2\ (ns)}$ (A_2)
0.4	0.76 (76)	4.39 (24)
2	0.87 (90)	4.18 (10)
5	0.89 (94)	3.80 (6)
27	0.94 (94)	4.56 (6)

At concentrations lower than 30 μM, time resolved emission of C152 collected in a TIR geometry from the silica/methanol interface showed evidence of two lifetimes, one at ~0.9 ns and another at ~4 ns. The shorter lifetime is assigned to emission from C152 solvated in a bulk methanol environment while the longer lifetime corresponds to the

C152's dominant decay lifetime in nonpolar solvents such as alkanes. The magnitude of the longer lifetime's contribution to the emission decay decreases with increasing bulk concentration, consistent with expectations that bulk solution species comprise more of the observed emission at higher concentrations. The time resolved emission data found in Table 4.2 are consistent with SHG results that report extremely nonpolar solvation at the silica/methanol interface.[2, 140]

Similar observations have been made for C151 adsorbed to the silica/methanol interface although the origin of this nonpolar solvation remains subject to debate. Surface specific vibrational studies support a description where weak van der Waals interaction between the first two solvent layers creates an anti-parallel arrangement of opposing methyl groups creating a bilayer structure and corresponding non-polar region.[140] A more recent study combined computational and experimental data and suggested that the second methanol solvent layer hydrogen bonded weakly to the first layer (in contact with the silica substrate).[2] Simulations suggested that strong hydrogen bonding between the first solvent layer and the silica and weaker hydrogen bonding between the second solvent layer and the first created an interfacial region extending up to 1 nm away from the substrate with reduced hydrogen bonding opportunities.

At higher concentrations, the emission data appear dominated by the C152 population in bulk solution. (Figure 4.6) By employing different filter combinations, we were able to isolate different populations of species contributing to the total decay. Specifically, a 420 nm long pass filter (LPF) was employed to collect decays at both the bulk emission wavelength (513 nm) and the emission that had been associated with

aggregates at the solid/vapor interface (574 nm, Figure 4.5). These studies focused on the higher concentration range and representative data of 0.38 μM, 108 μM, and 793 μM C152 at the silica/MeOH interface at 513 nm are shown in Figure 4.6B. To reduce the contribution from the short wavelength emission, additional decays were collected using a 530 nm LPF, as the actual decays are visibly similar to what was shown in Figure 4.6B, decays collected with the 530 nm LPF can be found in Appendix B.

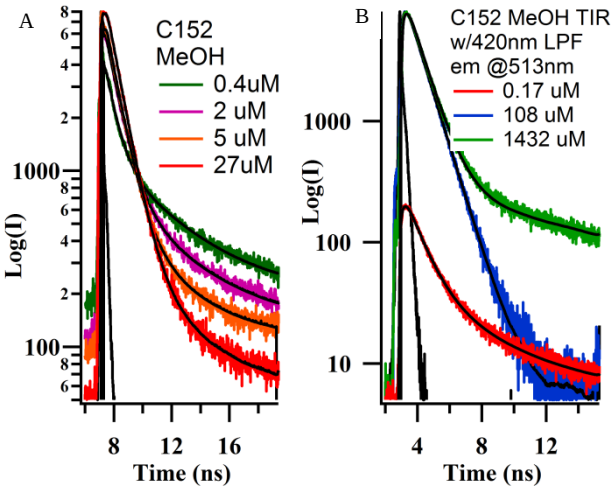

Figure 4.6. A) TIR-TCSPC decays of C152 in methanol for the concentrations shown corresponding to the lifetime data in Table 2. B) Lifetime data were taken for high concentrations with a 420 nm LPF at 513 nm.

We attempted to fit the decays to two lifetimes, the fitted lifetime values and their corresponding contributions, A_i, are reported in Table 3. Three observations stand out from the data reported in Table 3. First, all of the emission decays contain a dominant lifetime of ~0.9 ns. This result is assigned to C152 monomers experiencing a solvation environment equivalent to that in bulk methanol. Second, at the lowest bulk solution concentrations, the emission decays contain a second, longer lifetime consistent with

adsorbed C152 solutes sampling a nonpolar solvation environment. As concentration increases, ($\geq$ 90 μM), the emission decays did not show any evidence of an additional lifetime. Third, at the highest concentrations measured, the emission decays contain a contribution from a long lived species. This long lived (~10 ns) contribution is very small when compared to the total emission sampled by the TIR geometry, but can be isolated by employing filters that remove shorter wavelengths. This last result is consistent with observations made from C152 films adsorbed to silica/vapor interfaces and the emission is assigned to long-lived aggregates or multilayers.[37]

An interesting point is that C151, the primary amine analogue to C152, adsorbs to silica/methanol interfaces forming a terminal monolayer with no evidence in either SHG isotherms or fluorescence emission of aggregate formation.[2] The difference between these solutes is the hydrogen bonding capability. C151 can both donate and accept hydrogen bonds with surface silanol groups. C152 can only accept hydrogen bonds and hydrogen bond accepting through the tertiary amine will be impacted adversely by steric constraints.

Table 4.3. Emission lifetimes of C152 at TIR geometry using different filter combination. Decays were fit with χ^2 of 1.0-1.7 and uncertainties of ± 7 % for the amplitude and ± 0.20 ps for the lifetimes shown.

	420 nm LPF				530 nm LPF	
	513 nm Emission		574 nm emission		574 nm emission	
Conc.(μM)	τ_1(ns)(A_1)	τ_2(ns)(A_2)	τ_1(ns)(A_1)	τ_2(ns)(A_2)	τ_1(ns)(A_1)	τ_2(ns)(A_2)
0.38	0.68 (87)	1.58(13)	0.88(97)	3.33 (3)	0.92(98)	3.20(2)
108	0.99(100)	---	0.96(100)	---	0.97(100)	---
190	0.95(100)	---	0.95 100)	---	0.95 100)	---
381	0.97 (98)	8.94(2)	0.94(99)	8.40 (1)	0.96 (99)	11.02 (1)
793	0.97 (98)	12.11(2)	0.97 (98)	12.27(2)	0.95 (98)	10.79 (2)
1432	0.97 (96)	12.51(2)	0.96 (98)	12.72(2)	0.98 (72)	13.15(28)

4.3.4 Computational Results

In order to better understand mechanisms that could lead to C152 aggregate formation at silica/methanol interfaces, the energetics of C152 dimers having different structures were evaluated using *ab initio* computational methods. The M06L method was used to calculate the optimized geometry for a single C152 molecule and for C152 dimers having constrained geometries. Dimer calculations were performed starting with various initial monomer positions. The self-consistent field energies (SCF) for the dimer formation were calculated for geometries corresponding to stacked dimers, side to side dimers, or in a head (amine) to tail (ester) dimers in an implicit continuum. As C152 has a permanent dipole moment of ~5 Debye,[154] optimized geometries were calculated for dimers with the dipole arranged parallel and anti-parallel for each starting position. To ensure unbiased results, calculations were run starting from several different starting

distances between the two monomers. For a given geometry (i.e. side-to-side or stacked), no distinguishable differences were observed for different starting configurations.

Figure 4.7 shows the results of the M06L calculations for the various starting positions. As previously described, calculations were performed for three implicit continua having dielectric constants corresponding to bulk methanol and hexane as well as vacuum. The SCF energetics of dimer formations were calculated and 2 x monomer energy was subtracted from the energy output of the dimer in the same polarizable continua. The larger difference in formation would imply a stronger association between molecules. Results from these calculations show that a stacked geometry with the C152 dipoles arranged in an antiparallel manner is clearly the most favorable dimer configuration with a stabilization energy (~60 kJ/mole) that is more than two-fold greater than any other arrangement. Not surprisingly, the dimer is most stable in vacuum. The presence of a (continuum) solvent reduces dimerization energy, but only by ~10-20 kJ/mole. These values are reasonable dimerization energies compared to calculations performed with a different coumarin where the energies associated with aggregation were on the order of -200 kJ/mol.[39] These calculations were performed for aggregates (4 to 10 molecules) rather than dimers, which could explain the difference in energies. The stacked geometry optimization was run for C151 in the same continua for comparison and, although not shown in this paper, the dimerization energies were consistently weaker by 10 kJ/mol or more. The M06L calculations consistently predicted dimerization energies ~5 to10 kJ/mole more negative than those using CAM-B3lyp. This is consistent with studies that have found M06L to favor stacking over other modes of interaction.[192-

[193] While this may be true, CAM-B3lyp calculations did show the same trend as the M06L calculations in the present study.

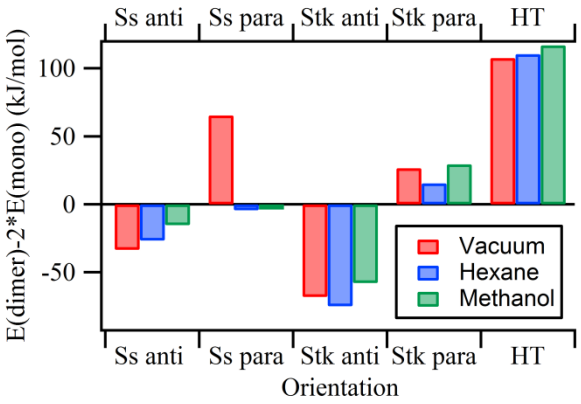

Figure 4.7. M06L/6-311+g(d,p) results for various orientations of stacking patterns. SS is the side to side formation, stck is a stacked geometry, HT is a head to tail arrangement. Anti refers to antiparallel dipoles and para is dipoles facing the same directions. Some computations did not finish completely, if the starting position is too unfavorable, the energetics do not converge and the lowest energy still in the starting orientation was used. The energy represented here is the calculated dimer SCF value minus the energy of a single C152 doubled. Values for calculations can be found in Table B1. in Appendix B.

The calculated hyperpolarizability of an ideal stacked, antiparallel arrangement of two C152 monomers is approximately 14x smaller than the hyperpolarizability of a monomer in vacuum. The hyperpolarizabilities calculated in implicit solvents also showed a decrease in magnitude, however, in methanol the reduction was only about 6 fold while in hexane, the dimerization resulted in a 13 fold decrease in hyperpolarizability. If dimers (or larger aggregates) do begin to form with this general structure, the SH response should diminish rapidly, consistent with the isothermal data

above 100 μM presented in Figure 4.4. The values for the hyperpolarizability calculations and the description of the methods used can be found in Appendix B.

These calculations do not take into account specific solvation forces such as hydrogen bonding, nor do they consider the explicit asymmetry introduced by the silica surface, but these *ab initio* results *do* provide a consistent and insightful description into how association between adsorbates can affect solute accumulation at interfaces and the electronic structure of larger, molecular assemblies. Figure 4.8 shows a schematic illustration that integrates data from experiments and computational analysis. Based on the adsorption, solvatochromic and time-resolved emission data, we propose that C152 first interacts with silica via its ester tail to form the original monolayer. As concentration increases, a second C152 interacts with the primary layer via stacking and creates a local inversion center with a correspondingly low molecular hyperpolarizability and a long emission lifetime. The computational analysis also provides potential insight as to why there is this increase in lifetime as aggregation occurs. Dimer formation can have exciton splitting which would result in an allowed and a forbidden transition, this long lived species could be indicative of this forbidden exciton state. Computational analysis of dimerization-discussed in the Appendix B- suggests this splitting is possible, given the calculated resonance wavelength with the highest oscillator strength was not the lowest state. An additional decay pathway could also be responsible for the long lifetime, where the aggregates interact and form an excited species that must first dissociate into an excited state and ground state monomer before the monomer decays from an emissive state.[194] If the dissociation were rate limiting, then the measured ‘lifetime’ would reflect

dissociation kinetics. Neither the experimental nor computational techniques can distinguish between the possible origins of the long lifetime.

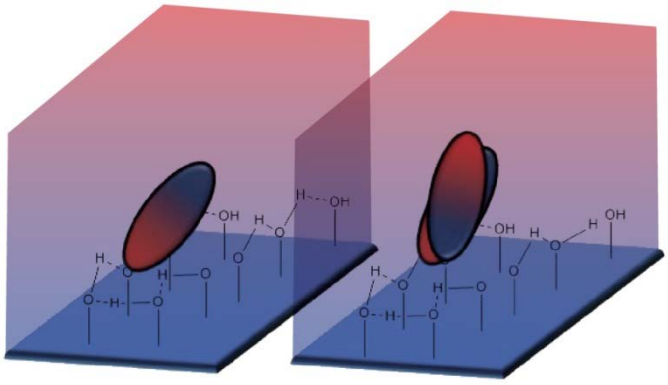

Figure 4.8. Schematic of proposed aggregation of C152 at the silica/methanol interface.

4.4 Conclusions

Experimentally, both SHG and TR-fluorescence data suggests C152 aggregates at the silica/methanol interface at high concentrations. Computational data are also in agreement with experimental data and provides insight into how these aggregates or multilayers are forming. The findings from these experiments suggest the following:

- At low concentrations, C152 experiences a nonpolar region that is consistent with an alkane-like solvation environment.
- SHG spectral data shows the local polarity sampled by the ground electronic state of C152 isn't altered by aggregation, however, the interfacial dynamics appear to be quite concentration dependent.

- As the concentration increases past the point of monolayer coverage, the 2nd lifetime continues to change as concentration increases. In the concentration range directly after monolayer coverage, the 2nd lifetime decreased to <0.2 ns, this short lifetime could imply interfacial C152 molecules must reorient themselves to allow for interactions with another molecule. As aggregation grows, the second lifetime becomes longer, up to 13 ns, suggesting the molecules could be experiencing an extremely nonpolar environment.
- Computational analysis supports our experimental data, C152 prefers to dimerize in nonpolar regimes. Additionally, C152 prefers the stack geometry which would create a local inversion center, reducing the SH signal and would result in a destabilized TICT state and a corresponding long lifetime.

Collectively, these discoveries provide molecular level insight into how an adsorbate's molecular structure can promote aggregation at surfaces. Drawing from previously reported results that implied C152's strong tendency to aggregate at solid/vapor interfaces, SHG and TIR-TCSPC data presented in this work illustrate that the presence of a solute does not mitigate surface aggregation. Furthermore, results from DFT calculations suggest that the most stable structure of these aggregates consists of stacked monomers having anti-parallel orientations and that the strength of dimerization is appreciably larger than monomer adsorption to the surface.

4.5 Acknowledgements

This work was supported by the National Science Foundation through grant CHE-1026870 and through funding by Montana State University Undergraduate Scholars Program. Additionally, the authors would like to thank Mr. Nicholas Woods for assistance with preparation of several figures.

4.6 References

1. Gobrogge, E. A.; Woods, B. L.; Walker, R. A., Liquid Organization And Solvation Properties At Polar Solid/Liquid Interfaces. *Faraday Discussions* **2013**, *167*, 309-327.

2. Roy, D.; Liu, S. L.; Woods, B. L.; Siler, A. R.; Fourkas, J. T.; Weeks, J. D.; Walker, R. A., Nonpolar Adsorption at the Silica/Methanol Interface: Surface Mediated Polarity and Solvent Density across a Strongly Associating Solid/Liquid Boundary. *Journal of Physical Chemistry C* **2013**, *117*, 27052-27061.

3. Woods, B. L.; Walker, R. A., pH Effects on Molecular Adsorption and Solvation of p-Nitrophenol at Silica/Aqueous Interfaces. *Journal of Physical Chemistry A* **2013**, *117*, 6224-6233.

8. Li, W.; Liu, D.; Wu, J.; Kim, C.; Fortner, J. D., Aqueous Aggregation and Surface Deposition Processes of Engineered Superparamagnetic Iron Oxide Nanoparticles for Environmental Applications. *Environmental Science & Technology* **2014**, *48*, 11892-11900.

9. Wu, G.; Zhu, X.; Ji, H.; Chen, D., Molecular Modeling Of Interactions Between Heavy Crude Oil And The Soil Organic Matter Coated Quartz Surface. *Chemosphere* **2015**, *119*, 242-9.

10. Franco, C. A.; Martinez, M.; Benjumea, P.; Patino, E.; Cortes, F. B., Water Remediation Based on Oil Adsorption Using Nanosilicates Functionalized with a Petroleum Vacuum Residue. *Adsorption Science & Technology* **2014**, *32*, 197-207.

21. Soil Screening Guidance: User's Guide. Second Edition ed.; EPA, Ed. Washington, DC, 1996.

22. Grinias, J. P.; Godinho, J. M.; Lunn, D. B.; Jorgenson, J. W., Evaluation Of Preparative Hydrodynamic Chromatography Of Silica Stationary Phase Supports. *Journal of Chromatography A* **2014**, *1370*, 270-273.

23. Lin, M.-C.; Lin, K.-C., Interaction Between Crystal Violet And Anionic Surfactants At Silica/Water Interface Using Evanescent Wave-Cavity Ring-Down Absorption Spectroscopy. *Journal of Colloid and Interface Science* **2012**, *379*, 41-47.

27. Brindza, M. R.; Walker, R. A., Differentiating Solvation Mechanisms at Polar Solid/Liquid Interfaces. *Journal of the American Chemical Society* **2009**, *131*, 6207-6214.

28. Eisenthal, K. B., Second Harmonic Spectroscopy Of Aqueous Nano- And Microparticle Interfaces. *Chemical Reviews* **2006**, *106*, 1462-1477.

34. Marowsky, G.; Steinhoff, R.; Chi, L. F.; Hutter, J.; Wagniere, G., 2ND-Harmonic Generation in Quinquethienyl Monolayers. *Physical Review B* **1988**, *38*, 6274-6278.

37. Roy, D.; Piontek, S.; Walker, R. A., Surface Induced Changes In Coumarin Solvation And Photochemistry At Polar Solid/Liquid Interfaces. *Physical Chemistry Chemical Physics* **2011**, *13*, 14758-14766.

39. Liu, X.; Cole, J. M.; Chow, P. C. Y.; Zhang, L.; Tan, Y.; Zhao, T., Dye Aggregation And Complex Formation Effects In 7-(Diethylamino)-Coumarin-3-Carboxylic Acid. *Journal of Physical Chemistry C* **2014**, *118*, 13042-13051.

41. Zhang, X. Y.; Cunningham, M. M.; Walker, R. A., Solvent Polarity At Polar Solid Surfaces: The Role Of Solvent Structure. *Journal of Physical Chemistry B* **2003**, *107*, 3183-3195.

43. Zhang, X.; Steel, W. H.; Walker, R. A., Probing Solvent Polarity Across Strongly Associating Solid/Liquid Interfaces Using Molecular Rulers. *Journal Of Physical Chemistry B* **2003**, *107*, 3829-3836.

47. Siler, A. R.; Walker, R. A., Effects of Solvent Structure on Interfacial Polarity at Strongly Associating Silica/Alcohol Interfaces. *Journal of Physical Chemistry C* **2011**, *115*, 9637-9643.

49. Bloembergen, N., 2ND Harmonic Reflected Light. *Optica Acta* **1966**, *13*, 311-322.

50. Benjamin, I., Inhomogeneous Broadening Of Electronic Spectra At Liquid Interfaces. *Chemical Physics Letters* **2011**, *515*, 56-61.

56. Nad, S.; Kumbhakar, M.; Pal, H., Photophysical Properties Of Coumarin-152 And Coumarin-481 Dyes: Unusual Behavior In Nonpolar And In Higher Polarity Solvents. *Journal of Physical Chemistry A* **2003**, *107*, 4808-4816.

57. Hecht, E., *Optics*, 4th ed.; Pearson Education, Inc: San Francisco, CA, 2002.

67. Steel, W. H., Y.Y. Lau, C.L. Beildeck, R.A. Walker, Solvent Polarity Across Weakly Associating Interfaces. *Journal Of Physical Chemistry B* **2004**, *108*, 13370-13378.

77. Mondal, S. K.; Yamaguchi, S.; Tahara, T., Molecules at the Air/Water Interface Experience a More Inhomogeneous Solvation Environment than in Bulk Solvents: A Quantitative Band Shape Analysis of Interfacial Electronic Spectra Obtained by HD-ESFG. *Journal of Physical Chemistry C* **2011**, *115*, 3083-3089.

79. Duval, Y.; Mielczarski, J. A.; Pokrovsky, O. S.; Mielczarski, E.; Ehrhardt, J. J., Evidence Of The Existence Of Three Types Of Species At The Quartz-Aqueous Solution

Interface At pH 0-10: XPS Surface Group Quantification And Surface Complexation Modeling. *Journal of Physical Chemistry B* **2002**, *106*, 2937-2945.

93. Azam, M. S.; Weeraman, C. N.; Gibbs-Davis, J. M., Specific Cation Effects on the Bimodal Acid-Base Behavior of the Silica/Water Interface. *Journal of Physical Chemistry Letters* **2012**, *3*, 1269-1274.

95. Zhao, X. L.; Ong, S. W.; Eisenthal, K. B., Polarization of Water-Molecules at a Charged Interface-2nd Harmonic Studies of Charged Monolayers at the Air-Water Interface. *Chemical Physics Letters* **1993**, *202*, 513-520.

105. Malin, J. N.; Geiger, F. M., Uranyl Adsorption and Speciation at the Fused Silica/Water Interface Studied by Resonantly Enhanced Second Harmonic Generation and the Chi((3)) Method. *Journal of Physical Chemistry A* **2010**, *114*, 1797-1805.

140. Liu, W. T., L.N. Zjang, Y.R. Shen, Interfacial Layer Structure At Alcohol/Silica Interfaces Probed By Sum-Frequency Vibrational Spectroscopy. *Chemical Physics Letters* **2005**, *412*, 206-209.

152. Arbeloa, T. L.; Arbeloa, F. L.; Arbeloa, I. L., Influence Of Fluorinated Group On The Photophysics Of 7-Aminocoumarins. *Journal of Luminescence* **1996**, *68*, 149-155.

154. Cave, R. J.; Castner, E. W., Time-Dependent Density Functional Theory Investigation Of The Ground And Excited States Of Coumarins 102, 152, 153, And 343. *Journal of Physical Chemistry A* **2002**, *106*, 12117-12123.

155. Das, K.; Jain, B.; Patel, H. S., Hydrogen Bonding Properties Of Coumarin 151, 500, And 35: The Effect Of Substitution At The 7-Amino Position. *Journal of Physical Chemistry A* **2006**, *110*, 1698-1704.

156. Krystkowiak, E.; Maciejewski, A., Changes In Energy Of Three Types Of Hydrogen Bonds Upon Excitation Of Aminocoumarins Determined From Absorption Solvatochromic Experiments. *Physical Chemistry Chemical Physics* **2011**, *13*, 11317-11324.

157. Liu, Y.; Ding, J.; Liu, R.; Shi, D.; Sun, J., Revisiting The Electronic Excited-State Hydrogen Bonding Dynamics Of Coumarin Chromophore In Alcohols: Undoubtedly Strengthened Not Cleaved. *Journal of Photochemistry and Photobiology a-Chemistry* **2009**, *201*, 203-207.

160. Pedone, A., Role of Solvent on Charge Transfer in 7-Aminocoumarin Dyes: New Hints from TD-CAM-B3LYP and State Specific PCM Calculations. *J. Chem. Theory Comput.* **2013**, *9*, 4087-4096.

161. Rechthaler, K.; Kohler, G., Excited-State Properties And Deactivation Pathways Of 7-Aminocoumarins. *Chemical Physics* **1994**, *189*, 99-116.

162. Corrie, J. E. T.; Munasinghe, V. R. N.; Rettig, W., Synthesis And Fluorescence Properties Of Substituted 7-Aminocoumarin-3-Carboxylate Derivatives. *Journal of Heterocyclic Chemistry* **2000**, *37*, 1447-1455.

163. Forster, Y.; Haas, E., Preparation And Characterization Of 3 Fluorescent Labels For Proteins, Suitable For Structural Studies. *Analytical Biochemistry* **1993**, *209*, 9-14.

164. Shobini, J.; Mishra, A. K.; Sandhya, K.; Chandra, N., Interaction Of Coumarin Derivatives With Human Serum Albumin: Investigation By Fluorescence Spectroscopic Technique And Modeling Studies. *Spectrochimica Acta Part a-Molecular and Biomolecular Spectroscopy* **2001**, *57*, 1133-1147.

168. Dahiya, P.; Kumbhakar, M.; Mukherjee, T.; Pal, H., Effect Of Protic Solvents On Twisted Intramolecular Charge Transfer State Formation In Coumarin-152 And Coumarin-481 Dyes. *Chemical Physics Letters* **2005**, *414*, 148-154.

180. Schach, D.; Globisch, C.; Roeters, S. J.; Woutersen, S., et al., Sticky Water Surfaces: Helix-Coil Transitions Suppressed In A Cell-Penetrating Peptide At The Air-Water Interface. *Journal of Chemical Physics* **2014**, *141*.

181. Azam, M. S.; Gibbs-Davis, J. M., Monitoring DNA Hybridization and Thermal Dissociation at the Silica/Water Interface Using Resonantly Enhanced Second Harmonic Generation Spectroscopy. *Analytical Chemistry* **2013**, *85*, 8031-8038.

182. Sauerbeck, C.; Braunschweig, B.; Peukert, W., Surface Charging and Interfacial Water Structure of Amphoteric Colloidal Particles. *Journal of Physical Chemistry C* **2014**, *118*, 10033-10042.

183. Moog, R. S.; Kim, D. D.; Oberle, J. J.; Ostrowski, S. G., Solvent Effects On Electronic Transitions Of Highly Dipolar Dyes: A Comparison Of Three Approaches. *Journal of Physical Chemistry A* **2004**, *108*, 9294-9301.

184. Shen, Y. R., *The Principles of Nonlinear Optics*; John Wiley and Sons: New York, 1984.

185. Wang, H.; Yan, E. C. Y.; Borguet, E.; Eisenthal, K. B., Second Harmonic Generation From The Surface Of Centrosymmetric Particles In Bulk Solution. *Chemical Physics Letters* **1996**, *259*, 15-20.

186. Wang, H. F.; Borguet, E.; Eisenthal, K. B., Polarity Of Liquid Interfaces By Second Harmonic Generation Spectroscopy. *Journal of Physical Chemistry A* **1997**, *101*, 713-718.

187. Achtyl, J. L.; Vlassiouk, I. V.; Surwade, S. P.; Fulvio, P. F.; Dai, S.; Geiger, F. M., Interaction of Magnesium Ions with Pristine Single-Layer and Defected

Graphene/Water Interfaces Studied by Second Harmonic Generation. *Journal of Physical Chemistry B* **2014**, *118*, 7739-7749.

188. Li, Z.; Weeraman, C. N.; Gibbs-Davis, J. M., Ketone Binding at Amino and Ureido Monolayer/Solvent Interfaces Studied by Nonlinear Optical Techniques. *Journal of Physical Chemistry C* **2014**, *118*, 28662-28670.

189. Frisch, M. J.; Trucks, G. W.; Schlegel, H. B.; Scuseria, G. E., et al. *Gaussian 09*, D.01; Gaussian, INC Wallingford CT: 2009.

190. Zhao, Y.; Truhlar, D. G., A New Local Density Functional For Main-Group Thermochemistry, Transition Metal Bonding, Thermochemical Kinetics, And Noncovalent Interactions. *Journal of Chemical Physics* **2006**, *125*.

191. Shi, X.; Borguet, E.; Tarnovsky, A. N.; Eisenthal, K. B., Ultrafast Dynamics And Structure At Aqueous Interfaces By Second Harmonic Generation. *Chemical Physics* **1996**, *205*, 167-178.

192. Roy, D.; Marianski, M.; Maitra, N. T.; Dannenberg, J. J., Comparison Of Some Dispersion-Corrected And Traditional Functionals With CCSD(T) And MP2 Ab Initio Methods: Dispersion, Induction, And Basis Set Superposition Error. *Journal of Chemical Physics* **2012**, *137*.

193. Marianski, M.; Oliva, A.; Dannenberg, J. J., A Reinvestigation of the Drimer of para-Benzoquinone and Pyrimidine with MP2, CCSD(T), and DFT Using Functionals Including Those Designed to Describe Dispersion. *Journal of Physical Chemistry A* **2012**, *116*, 8100-8105.

194. Nguyen, T. Q.; Doan, V.; Schwartz, B. J., Conjugated Polymer Aggregates In Solution: Control Of Interchain Interactions. *Journal of Chemical Physics* **1999**, *110*, 4068-4078.

CHAPTER 5

SPECTROSCOPIC SOLVATION MECHANISMS AT SILICA/ACETONITRILE INTERFACES

Contributions of Authors and Co-Authors

Manuscript: Liquid Organization and Solvation Properties at Polar Solid/Liquid Interfaces

Author: B. Lauren Woods

Contributions: Collected and analyzed all Second Harmonic experimental data and collected and analyzed time resolved fluorescence data.

Author: Jenna K. George

Contributions: Collected time resolved fluorescence

Co-Author: Rob Walker

Contributions: Assisted with data analysis and edited manuscript at all stages.

Manuscript Information Page

B. Lauren Woods, Jenna K. George, and Robert Walker
Physical Chemistry and Chemical Physics
Status of Manuscript:
_X__ Prepared for submission to a peer-reviewed journal
____ Officially submitted to a peer-review journal
____ Accepted by a peer-reviewed journal
____ Published in a peer-reviewed journal

Publisher: Royal Society of Chemistry

CHAPTER 5

SPECTROSCOPIC SOLVATION MECHANISMS AT SILICA/ACETONITRILE INTERFACES

Abstract

Second harmonic generation (SHG) and time resolved total internal reflection fluorescence (TR-TIRF) spectroscopy were used to examine the solvating properties of acetonitrile (ACN) at the silica/liquid interface. SHG experiments measured the resonant excitation wavelength of adsorbed coumarin solutes, Coumarin 151 (C151) and Coumarin 152 (C152), while TR-TIRF data measured the emission lifetimes of the adsorbates as a function of bulk concentration. At the ACN/silica interface with adsorbed C151, SHG measurements report an excitation wavelength of 400 nm, which is consistent with solvation in an extremely polar environment. Similarly, adsorbed C152 experiences a polar region. In bulk ACN solution, the time dependent fluorescence can be fit with a single exponential decay that corresponds to a lifetime of 5.3 ns and 2.1 ns for C151 and C152, respectively. The interfacial fluorescence decays, however, required an additional exponential term with a lifetime of 1.0 ns for C151 and a shorter lifetime of 0.5 ns for C152. These short lifetime are indicative of C151 experiencing an alkane-like environment, while C152 experiences a water-like environment. Although SHG and fluorescence data of C152 in ACN are in agreement, the C151 silica/acetonitrile fluorescence data appear to contradict findings from SHG measurements: fluorescence lifetimes show little evidence of the polar solvation implied by the SHG excitation

wavelengths of adsorbed C151. We propose that this discrepancy may reflect differences in the properties measured by the two types of experiments: SHG samples adiabatic excitation energies and is sensitive to the solvent organization around adsorbed solutes in their ground electronic state while TR-TIRF measures the response of solutes surrounded by a solvation structure equilibrated to the solute's excited state. These differences are considered in the context of recently proposed descriptions of ACN structure and dynamics at surfaces and in confinement.

5.1 Introduction

Molecular structure and dynamics at surfaces and interfaces can vary greatly from bulk solution limits. At an interface, competition between solute-substrate, solvent-substrate, and adsorbate-solvent interactions conspire to create local environments having distinctly different properties than might be predicted based on bulk considerations with these effects extending up to several nanometers away from the surface. How these different interactions balance to control interfacial solvation depends on their solvent and substrate identities as well as their contribution to the overall solute adsorption tendencies.[1, 3, 30, 37, 41, 47]

In this chapter, we focus on how the behavior of acetonitrile at hydrophilic silica surfaces changes the solvent's ability to solvate adsorbed coumarin 151 (C151), a primary amine, and coumarin 152 (C152), a tertiary amine. The polar, aprotic solvent acetonitrile (ACN) has been well studied both experimentally and computationally.[195-199] Molecular simulations have shown that ACN forms dipole pairs with itself in bulk

solution.[200-201] Furthermore, in the presence of protic molecules, ACN is able to accept hydrogen bonds via the π orbital of the -CN group, where a hydrogen bond is defined as the ability of the terminal hydrogen of silanols to form weak associating bonds with the polar –CN tail.[202-203]

ACN is a common solvent used in liquid chromatography applications. As a polar, aprotic solvent, ACN is well suited to eluting polar pharmaceuticals and low molecular weight, aprotic compounds off of silica columns.[204-205] Furthermore, ACN is completely miscible with virtually all other organic solvents making it an ideal partner in designing binary solvent mixtures having tuneable solvation properties.[206-207] Based on measured retention rates and the chemical composition of the stationary phase, chromatography data can be used to develop empirical models that describe the thermodynamics and kinetics associated with solute adsorption to solid liquid interfaces. Such models often include empirically derived descriptions of adsorption/desorption mechanisms with the mobile phase of the solute being a primary factor in determining macroscopic retention behavior. Such descriptions, however, contain very little detail of the role played by solute solvation at the interface itself.

As first discussed in Chapter 2, 'solvation' is used to describe the noncovalent interactions a solute experiences with its surroundings, and interfacial solvation can be significantly different from bulk solution limits. The ACN/silica interface has previously been studied via sum frequency generation (SFG) and molecular dynamics simulations.[197, 208-209] Experimental and computational work by Ding *et. al.* have shown that at a planar silica interface, ACN can form extended bilayer structures that extend up

to 4 nm away from the surface.[208] The simulations show that the ACN molecules align perpendicular to the silica surface with the –CN interacting with surface silanol groups and the extended bilayers are formed by slightly overlapping molecules in an antiparallel formation.[208-209] Furthermore, the ACN solvent molecules interacting directly with surface silanol groups have limited mobility at the surface such that the adsorbed ACN molecules are restricted to rotating on the axis perpendicular to the surface normal. Compared to an orientational correlation time of 3.4±2 ps for bulk ACN, ACN molecules at the surface cannot rotate as freely resulting in longer rotational times of 24±4 ps.[208] Optical Kerr Effect (OKE) data have also been used to describe reorientation of ACN at the silica surface and in bulk. The OKE data show different activation energies and behavior of ACN at the surface relative to bulk solution.[196, 210] Taken together, these descriptions of ACN at a silica interface raise questions about the local solvation environment sampled by solutes adsorbed to chromatographic interfaces where ACN is the mobile phase. In the studies described below, the solvating behavior of ACN will be compared to the previously reported solvating behavior of methanol inferred from nonlinear optical and TR-TIRF measurements.[2, 211] (Chapters 3 and 4)

Previous studies of the methanol/silica interface have shown that methanol, a polar protic solvent, forms a nonpolar region directly adjacent to the silica.[2, 211-212] Both equilibrium and time-resolved spectroscopic data reported in Chapters 3 and 4 showed solvation at the silica/methanol interface is dominated by a low dielectric environment with reduced hydrogen bonding opportunities relative to bulk solution.[2] Such reports are consistent with descriptions of methanol structure at silica/methanol interfaces. Two

configurations have been proposed to describe how the nonpolar region is formed. The first model is supported by data from surface specific vibrational spectroscopy experiments. In this model the first methanol solvent layer is strongly bound to the silica surface via hydrogen bonding and the second solvent layer adopts a mirror-like structure, where the methyl groups from the two methanol solvent layers were oriented in approximately opposite directions.[116] Simulations performed by Weeks also show that a second solvent layer is formed but rather than interacting with the first layer via van der Waals interactions, the second layer weakly hydrogen bonds to the first layer to create an interfacial region with reduced solvent density and reduced solute hydrogen bonding opportunities.[2] In either scenario, methanol forms a region across the silica/methanol interface where the solvent's s1olvating capabilities are significantly reduced.

In the experiments described below, we examine solvation at silica/acetonitrile interfaces in order to discover how the structure of ACN controls interfacial polarity and time-dependent photophysical behavior of adsorbed solutes. The comparison to methanol will provide a basis for understanding hydrogen bonding vs. simple dipolar forces in interfacial solvation and surface mediated chemistry. Both solvents have similar polarity where the Onsager constant for acetonitrile is $f(d)=0.96$ and 0.95 for methanol.[64] At the surface, both solvents have restricted dynamics,[116, 208] and both solvents are predicted to form layered structures.[15, 20, 2] The surface induced structuring of MeOH largely vanishes in two layers, whereas ACN bilayer structure is thought to propagate up to ~4 nm away from a planar, silica surface.[208]

Experiments were conducted to focus on how various solvents alter the environment sampled by the adsorbed solute. Two solutes, coumarin 151 (C151) and coumarin 152 (C152), were chosen for the present study. Both chromophores have been discussed in earlier chapters and belong to the family of 7-aminocoumarins with a trifluoro methyl group at the 4^{th} position. C151 has a primary amine at the 7^{th} position whereas C152 has a tertiary amine at this position. (Figure 5.1) Both adsorbates were used in previous studies of methanol/silica interactions.[2] C151 has been extensively studied and bulk characterization has been performed both computationally[151, 156-157] and experimentally.[159, 213] Bulk solution experiments by Nad, *et al.* have shown that C151 has an intramolecular charge transfer (ICT) state that is stabilized in polar solvents.[159] (Figure 5.1A) This stabilization results in a larger dipole that is shown in the resonance structure with a formal positive charge on the nitrogen and formal negative charge on the carbonyl oxygen. In non-polar solvents C151 retains its sp^3 structure about the amine and rapid inversion accelerates non-radiative decay rates. Fluorescence and lifetime data of C151 have been characterized in a variety of solvents ranging from nonpolar (hexane, $f(d) = 0.38$) to polar (acetonitrile, $f(d) = 0.96$).[159] In polar solvents, C151 has longer lifetimes consistent with stabilization of the ICT state, while in nonpolar solvents the lifetime shortens to ~1 ns.

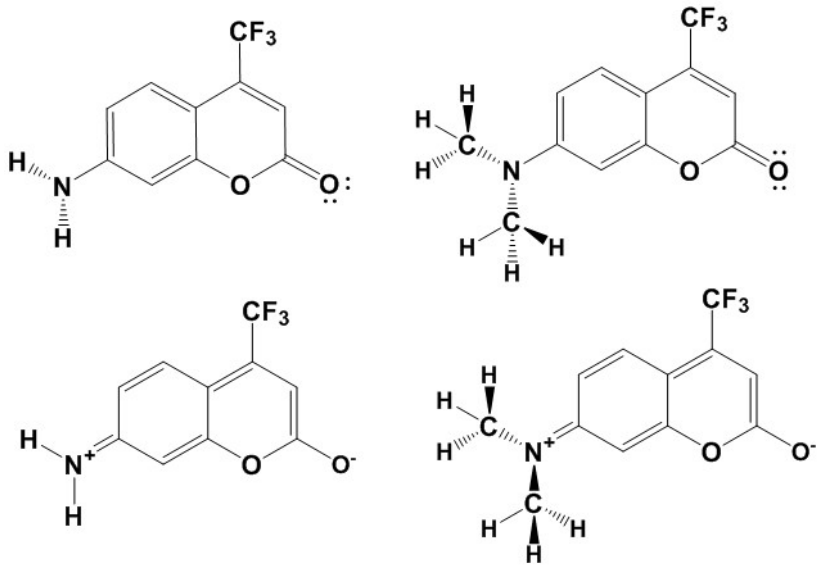

Figure 5.1. Coumarin 151 is a member of the 7-amino-coumarin family. C151 has a primary amine at the 7th position, which is capable of H-bonding. C151 has a ICT state which is stabilized in polar solvents, shown here. In nonpolar solvents, the hydrogens are not secured and are able to go in and out of the plane.

Similarly, the fluorescence behavior of C152 has been well characterized, with a solvatochromatic range from 370 nm in bulk alkanes to 400 nm in polar solvents.[37, 56, 154, 160, 162, 168] Unlike C151, C152 does not have the selectivity to differentiate between polar solvents with varying degrees of hydrogen bonding abilities, as the excitation and emission behavior is similar for water and in DMSO. An additional difference between solutes is that while C152 does have an ICT state in polar solvents, the amine adopts a twisted conformation. (Figure 5.1B) This twisted ICT state, or TICT state, results in a short lifetime in polar solvents and its stabilization depends on the solvent identity.[56, 168] In water, a strong hydrogen bond donator, the lifetime is ~0.5 ns while in methanol the lifetime increases to 0.9 ns and in acetonitrile, a hydrogen bond acceptor, the lifetime increases further to 2.1 ns. Additionally, the quantum yield of C152 depends on the

solvation environment. In bulk MeOH, C152 has a very low value of 0.09 but in ACN, the quantum yield rises to 0.22. Furthermore, the quantum yield of C152 reaches unity in alkanes.[56] Therefore, although our steady state data will be limited in identifying the influence of hydrogen bond acceptors and donators, we do observe some degree of differentiation from the emissive behavior.

We employ resonance enhanced second harmonic generation (SHG) and time resolved fluorescence with a total internal reflection geometry to study the interfacial photophysics and dynamics of C151 and C152 in the presence of ACN. By comparing the data presented with previously reported results from C151 and C152 adsorbed to silica/MeOH interfaces, we will show the importance of solvation effects on adsorption.

5.2 Experimental Section

5.2.1 Materials

Laser grade C151 and C152 were purchased and used as received from Exciton. HPLC grade methanol and acetonitrile of purity >99% were received from EMD and used without further purification. Bulk fluorescence data were taken on a Jobin-Yvon Horiba Fluorolog 3FL3-11. Interfacial studies were performed using total internal reflection geometry (TIR) coupled to a time correlated single photon counting spectroscopy (TIR-TCSPC). TIR-TCSPC experiments were performed using hemispherical fused quartz prisms from ISP Optics. For Second Harmonic Generation (SHG) experiments, silica slides were purchase from SPI. Sample preparation included acid washing slides and prisms and their corresponding Kel-F sample cells in a 50/50

sulfuric/nitric acid mix and rinsing with deionized water (Milipore, 18.2 MΩ). The silica surface was allowed to equilibrate with the solutions for a minimum of 1 hour prior to use.

5.2.2 Techniques

A. Time Correlated Single Photon Counting Spectroscopy. TR-Fluorescence was collected using a Picoquant PicoHarp 300 with the FluoTime 200 software. The experimental details of the TCSPC and TIR geometry have been discussed with greater detail elsewhere.[211] A brief description of these methods is included in this chapter.

TIR fluorescence is a technique used to explore near surface (<200 nm) molecular behavior. In order to observe interfacial dynamics, the incident beam must pass through a higher refractive material ($n_{substrate}>n_{solvent}$) at an angle ($\theta_i$) greater than the critical angle (θ_{cr}). The critical angle is the angle in which the incident light is totally reflected off from a medium with a higher index of refraction. Although the light is reflected, interfacial molecules are excited by the persisting evanescent wave. The strength of the field is exponentially decaying, which results in the evanescent wave exciting molecules in the near surface region. The depth of penetration (d) is dependent on the excitation wavelength (λ), incident angle (θ), and indices of refraction of the substrate and solvent (Equation 5.1).[57]

$$\frac{1}{d} = \frac{2\pi}{\lambda}\left[\frac{sin^2\,\theta}{n_{ti}^2} - 1\right]^{1/2} \qquad \text{Eq. 5.1}$$

The term n_{ti} is the ratio of the indices of refraction of the transmitted medium (solvent) and the initial medium (substrate). Our TIR set-up has an incident angle range of 72^o±3.

For experiments with ACN, λ = 370 nm, the sample depth is ~120 nm. The resolution for TCSPC decay is dependent on the instrument response function (IRF) FWHM. As previously discussed in Chapter 1, the IRF is wider for the TIR geometry than in bulk. ACN bulk decays have an IRF ranging from 20 to 50 ps while the TIR-fluorescence decays have an IRF of ~100-200 ps due to the structure of our TIR system. TIR-fluorescence decays were fit using a sum of exponentials that have been convoluted from the IRF, as discussed in Chapter 1. The fits with a χ^2 of around 1.0±0.2 were deemed acceptable.

B. Second Harmonic Generation. Resonance-enhanced SHG experiments were carried out using a Libra-HE laser (Coherent, 85 fs pulses, 1 kHz repetition rate) coupled to a visible optical parametric amplifier (Coherent OPerA Solo). Data were collected using a PMT and single photon counting electronics. This method has been described in detail in previous reports.[3, 47]

In order to study how the interfacial adsorption and solvation environment differ from the bulk limit, we employed resonance-enhanced SHG.[3, 28, 34, 41, 49] SHG is intrinsically surface specific and allows us to probe only the molecules at the surface. From SHG spectral data, we can collect information about the resonance wavelength (λ_{res}) and the linewidth (Γ). Because the solvochromatic range has been characterized for C151 in bulk solvents, we can compare interfacial λ_{res} with the bulk excitation wavelength (λ_{ex}) to describe the local polarity sampled by solutes at the silica/liquid interface. Additionally, the linewidth can be used to infer heterogeneity at the interface since the inhomogeneous broadening of the spectra is proportional to the linewidth.[50] By

holding the λ_{res} constant and measuring SHG intensity over a range of concentrations, we acquire isothermal data from which the Free Energy of adsorption (ΔG^{o}_{ads}) is calculated.[3] [48]

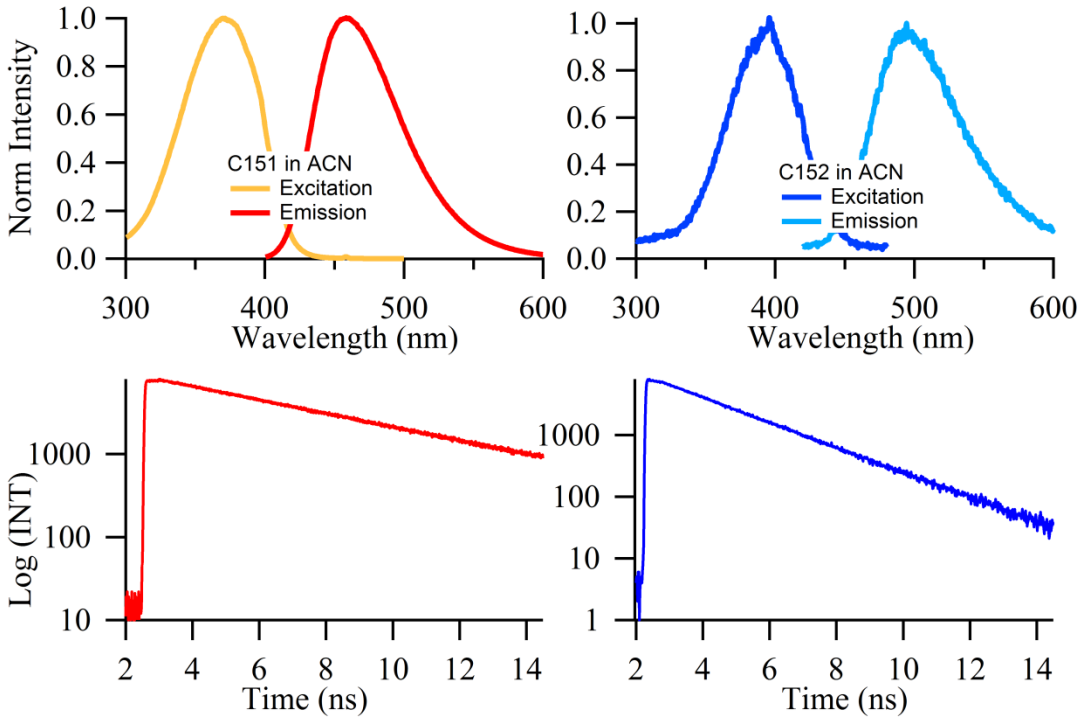

Figure 5.2. Bulk steady state and time resolved data of C151 (A) and C152 (B) in ACN.

5.3 Results

5.3.1 Bulk Behavior of C151 and C152

Understanding the solvating properties of acetonitrile at the silica surface requires an initial characterization of acetonitrile's bulk behavior. Figure 5.2 show the time resolved emission as well as the fluorescence excitation and emission spectra of C151 and C152 in bulk solution. The time resolved emission was found to have a single lifetime of 5.3 ns for C151 and 2.1 ns for C152. The peak emission and excitation

wavelengths for C151 are 456 ± 3 nm and 370 ± 3 nm, respectively. In ACN, C152 has an excitation of 396 nm and an emission peak of 504 nm. The linewidth and wavelengths are reported in Table 5.1. These data are in agreement with previously reported literature values[56, 159, 168, 214-215] and support the model of polar solvation stabilizing the charge transfer states of electronically excited C151 and C152.

5.3.2 SHG Data

By comparing the resonance peak location with the solvochromatic behavior of coumarins in bulk liquids, SHG spectroscopy was used to determine the local solvation environment of adsorbates at the silica/acetonitrile interface. The SHG spectrum of C151 in ACN is shown in Figure 5.3A, along with a concentration dependent isotherm. The resonance peak was found to be 400 ± 2 nm with an extremely narrow linewidth. The shift to longer wavelengths implies C151 is subject to a strongly polar solvation region that extends past the bulk polar limit of 386 nm (in DMSO).[159]

Table 5.1 Steady state data for C151 and C152 in ACN and at the silica/ACN interface.

Bulk	C151	C152	Surface	C151	C152
λ_{em} (nm)	456	494	λ_{res} (nm)	400± 2	401±2
λ_{ex} (nm)	370	396	Γ (nm)	7± 2	6± 2
Γ_{ex} (nm)	66	60	ΔG_{ads} (kJ/mol)	-33.1± 1.5	-31.1± 1.5

C152 has a polar limit of 400 nm, which is similar to the resonance wavelength found at the silica/ACN interface (399 nm). The silica/ACN interface presents a polar environment for both solutes. For both solutes, the line width was narrow, suggesting

this interface is relatively homogeneous with a polar adsorption environment. Linewidth is a useful tool in determining the homogeneity of a molecule's surroundings – the broader the spectrum, the more heterogeneous the environment.[50] At the silica/ACN interface, the SHG linewidth measures 7 ± 2 nm and 6 ± 2 nm for adsorbed C151 and C152, respectively. For comparison, a typical SHG excitation spectrum yields linewidths of 15 to 25 nm.[1-2] However, such narrow line widths do have precedent, and the silica/ACN data would suggest a highly ordered interfacial region produced by the interactions between ACN and silica.[181]

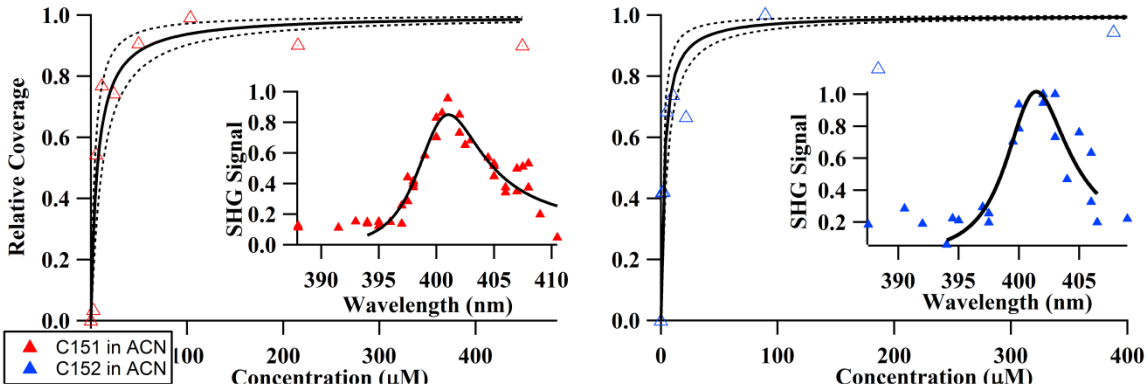

Figure 5.3. SHG isothermal data for C151 (left) and C152 (right) at the silica/ACN interface with insets of their corresponding SHG spectra.

Further adsorption information can be gleaned through SHG isotherm data. Adsorption strengths of the coumarins were measured with the Langmuir method and the ΔG^{o}_{ads} was calculated.[51] The isotherms were consistent with a typical Langmuir model behavior. Adsorption energies were calculated with the assumptions that there was full monolayer coverage at a homogeneous surface and the adsorbates were not interacting with themselves nor undergoing reorganization.[51] The strength of adsorption of C151 in

ACN was -33.1 ± 1.5 kJ/mol. While SHG cannot directly determine the exact association mechanisms between C151 and the surface, the data suggest that C151 – a bidentate-like molecule – has two binding sites at the surface. Given the average strength of an H-bond is approximately -20 kJ/mol, we propose that two weak H-bonds are responsible for C151 adsorption to the surface. The most probable sites would be the H-accepting double bonded oxygen and the H-donating site on the amine at the 7th position.

The tertiary amine has the ability to hinder the hydrogen bonding ability of C152; however, at the silica/ACN interface, the ΔG^{o}_{ads} of -31.1 ± 1.5 kJ/mol, suggesting relatively strong interaction between solute and substrate. Surprisingly, at the silica/ACN interface, C152 terminates at monolayer coverage, a result that is in direct contrast to the silica/MeOH isotherm shown in Chapter 4. The silica/ACN interface does not appear to promote aggregation of C152, indicating that the solvent identity can strongly influence adsorption behavior. If we consider adsorption as reflecting the sum of interactions between the solvent, adsorbate, and substrate, then strong adsorption energies could be a result of a favorable disassociation of the solvent from silica or interactions between the solvent and adsorbate. As discussed previously, however, acetonitrile has a strong association with silica, with a binding energy of about ~-50 kJ/mol[216] so desorption of the solvent molecules would not be favorable. This understanding of the silica/ACN interface leads us to believe that the solute-substrate or the solute-solvent interactions are the major components in influencing adsorption strength. As mentioned in Chapter 4, the steric hindrance of C152's methyl groups on the amine would inhibit hydrogen bonding

opportunities at the 7-position. Therefore we propose C152 interacts with one silanol site, and the strong ΔG^{o}_{ads} is associated with strong solute-solvent interactions.

Additionally, SHG spectra show clearly that the local, effective dielectric constant at the silica/acetonitrile interface is very high. The solvatochromic behavior of C151 indicates the red shift in the SHG spectrum is associated with a hydrogen accepting environment, supporting the theory the solute-solvent interactions are crucial in this adsorption regime. From the SHG spectra of C152, however, one can only say that the silica/ACN environment presents a polar adsorption environment that is independent of solute choice for the ground electronic state of these molecules. We can use the same arguments in Chapter 3 to eliminate the possibility of interference of surface water. The resonance wavelength of C151 at the silica/ACN interface is red shifted from the expected wavelength of C151 in water, meaning that if water were present the SHG data of C151 would have been blue shifted from that of C152 at the silica/ACN interface. The possibility of contaminants can also be dismissed, as the neat silica/ACN SHG spectrum showed no evidence of any resonance enhancement.

5.3.3 TIR-TCSPC Fluorescence

TIR time resolved emission data from C151 adsorbed to silica/acetonitrile interface as a function of bulk solution concentration were collected by monitoring the emission at 461 nm following an excitation of 370 nm. (Figure 5.4A) TIR-TCSPC data for C152 in ACN were collected at 503 nm after exciting at 393 nm. (Figure 5.4B). TIR decays of C151 in ACN show two lifetimes, ~5.1 ns and ~1.0 ns (Table 5.2). The longer lifetime is attributed to the bulk while the shorter lifetime is attributed to C151 in the

near-surface region that is sampled by TIR evanescent field. The value of a_2 decreases as the concentration increases, indicating the contribution from the surface diminishes at high concentration limits. The shorter lifetime of C151 adsorbed to the surface is similar to the average lifetime of C151 in bulk alkanes. In alkane solutions, the shorter lifetime of C151 is attributed to the inability of the solvent to stabilize the excited ICT state, meaning that rapid inversion about the amine can facilitate nonradiative decay. The TIR data from the silica/acetonitrile interface suggest that the interfacial environment cannot support a planar adsorbate structure characteristic of the charge transfer state, despite the apparently high local polarity.

Table 5.2 Time resolved data for C151 in ACN and at the silica/ACN interface with χ^2 of 1.0-1.1 and uncertainties of ± 0.07 for the amplitude and ± 0.20 ps for the lifetimes shown.

	a	τ(ns)		
Bulk	1	5.3		
TIR	a_1	τ_1(ns)	a_2	τ_2(ns)
0.2 (μM)	0.35	4.91	0.65	1.05
0.4	0.52	5.00	0.48	1.01
2	0.89	5.27	0.11	1.01
26	0.99	5.21	0.01	1.02

Table 5.3 Time resolved data for C152 in ACN and at the silica/ACN interface with χ^2 of 1.0-1.2 and uncertainties of ± 0.07 for the amplitude and ± 0.20 ps for the lifetimes shown.

	a	τ (ns)		
Bulk	1	2.11		
TIR	a_1	τ_1(ns)	a_2	τ_2(ns)
0.5 (μM)	0.74	1.9	0.26	0.43
2	0.93	1.89	0.07	0.49
5	0.87	1.93	0.13	0.65
20	0.91	2.09	0.09	0.40

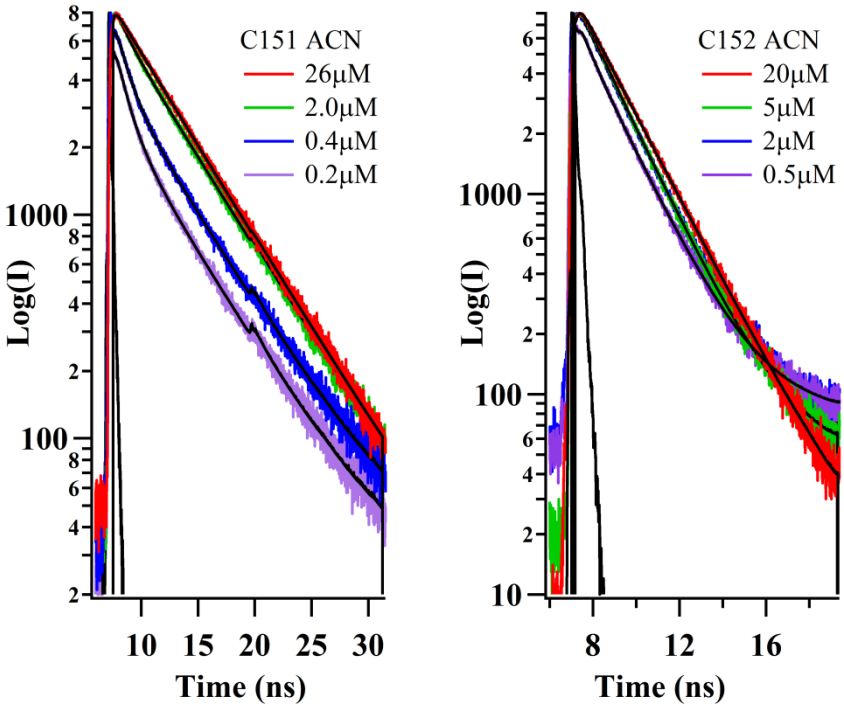

Figure 5.4. TR-TIR data for C151 (left) and C152 (right) at the silica/ACN interface

In contrast, the lifetimes collected for TIR decays of C152 in ACN, were 2.0ns (bulk) and 0.5 ns. (Table 5.3) Although there are some discrepancies, the general trend shows a decreasing contribution from the fast lifetime as concentration increases. The faster lifetime, which is attributed to the interfacial dynamic properties, follows a similar behavior of C152 in water and indicates the stabilization of the TICT state. This conflicting description of the silica/ACN environment between solutes and experimental techniques was initially surprising.

5.4 Discussion

Both steady state SHG and time resolved fluorescence show C152 experiences a polar solvation environment. The behavior of C151 at the silica/ACN interface presents a conundrum for interpretation. Fluorescence data show that the excited state of C151 is destabilized due to an apparent non-polar environment. The SHG measurements, however, indicate the solute experiences a polar environment at the interface. Several possible explanations discussed in detail below may explain the discrepancy between steady state (SHG) and time resolved TIR fluorescence data.

5.4.1 Coumarins at the Silica/ACN Interface

The first explanation involves the different properties measured by the two experimental techniques. While SHG reports the equilibrium solvation environment surrounding the solute in its ground electronic state, fluorescence emission probes the solute in its excited state following solvent reorganization. SHG spectra have shown the ground electronic states of both coumarins are in a polar adsorption environment. The

excited state environment, however, is very different for C151 and C152 as reported by the TR-TCSPC data. The excited state of C152 appears to be stabilized by a combination of the silica surface and interfacial ACN molecules, while C151's ICT state is not stabilized, leading to a correspondingly short (or 'nonpolar') emission lifetime. We propose this difference in emission behavior between the two coumarins arises from the interfacial solvent structuring *and* the difference in solute hydrogen bonding opportunities.

As discussed in the introduction of this chapter, experiments and simulations performed by Ding *et.al* of interfacial ACN molecules indicate the formation of an extended bilayer at the silica surface.[208] In this model, the first layer of solvent molecules arrange themselves with their dipoles perpendicular to the surface while accepting hydrogen bonds through the –CN group. The second layer then forms antiparallel with interdigitating methyl groups. This arrangement would be expected to create a polar interface given the high density of surface dipoles.[208] This bilayer extends multiple layers and results in restricted solvent mobility. ACN solvent molecules in these bilayers have long reorientation times that occur too slowly to reorganize and stabilize the almost instantaneous excitation of C151 to the ICT state following photoexcitation. In this environment, we might expect the resulting decay of C151 to show a short lifetime, not because the surface is non-polar but because the excited state of C151 cannot be stabilized.

This polar region is supported by both the SHG and TIRF data of C152 at the silica/ACN interface. The conflicting fluorescence data between C151 and C152 can be

explained by their differing substituents. As discussed in Section 5.3, we propose that C151 interacts with the surface via hydrogen bonding through two sites, with the primary amine donating and the =O accepting the hydrogen bonds. A schematic of the proposed adsorption mechanism is shown in Figure 5.5. Although, C152 had similar adsorption strength, the tertiary amine cannot donate hydrogen bonds. This behavior led us to suggest that the strong association is due in part to the carbonyl group accepting a hydrogen bond and a favorable interaction between the solvent and C152. (Figure 5.5) This interpretation is supported by the TIRF data that indicates ACN can stabilize the TICT state of C152. If interfacial C152 molecules are hydrogen bonding to silica through only the =O, the amine group would be pointing away from the surface, this geometry would allow the solvent molecules access to stabilize the amine in its twisted conformation.

5.4.2 Comparing Hydrogen Bonding Acceptors and Hydrogen Bonding Donators

If the description of acetonitrile organization at the silica interface presented by Ding, *et al.* is correct, then acetonitrile forms highly ordered, conformationally restricted polar interfacial environment that is unable to stabilize the excited state of C151. By comparing these results to the methanol/silica experiments performed by Roy *et.al*,[2] the solvent structure is thought to play a significant role in molecular adsorption. MeOH and ACN are of similar size and polarity, but ACN has a linear geometry while the –OH group on MeOH has a bent configuration. The methanol behavior at a silica interface was discussed in detailed in Chapter 3 and 4. Those chapters reported how calculations

performed by Weeks show that this geometry allows for the formation of a 2nd less dense layer that weakly H-bonds to the hydroxyl end of the primary methanol layer.[2] In Chapter 3, specifically, the results from these simulations are supported by both SHG and TR-TIR fluorescence data that show C151 experiences a nonpolar surface.[2]

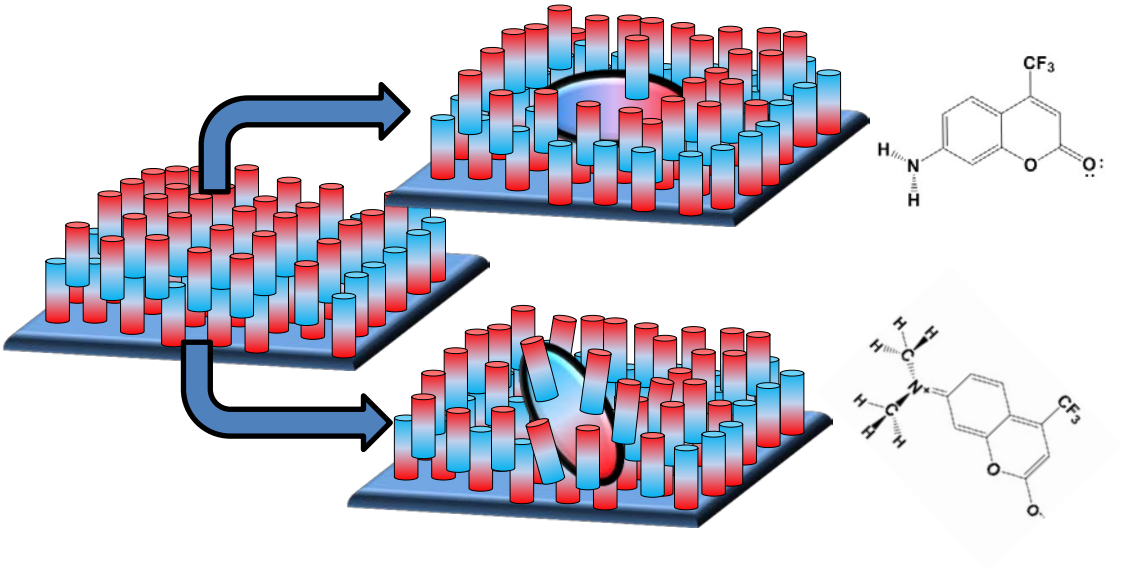

Figure 5.5. A schematic of the silica/ACN interface and its rearrangement for C151 and C152. The red ends on the columns represent the –CN tail, the methyl (blue) terminals of the two layers interlock forming a well-organized bilayer. A single bilayer is shown, but calculations have shown to extend up to 4 nm from the surface. C151 interacts with the surface via two binding sites, (TOP) but C152 only interacts through its carbonyl. (BOTTOM).

A dramatic difference in SHG spectra is observed for the coumarins in methanol and acetonitrile. In addition to a shift in the resonance peak, the SHG spectra of C151 and C152 in methanol exhibit double the linewidth of silica/ACN, suggesting ACN is creating a more homogeneous interfacial solvation environment than MeOH. When comparing dipole interactions versus the H-bonding capabilities of methanol, the data

show C151 in MeOH has a slightly stronger adsorption than in ACN. Additionally, the aggregation of C152 discussed in Chapter 4 was never observed for C152 adsorbed to the silica/ACN interface. The strong association of the bilayer of ACN to the polar nature of the interface does not promote aggregation of C152, as evident by a levelling off of signal on the SHG isotherm spectrum.

The emission lifetimes reflect similar behavior for C151 in both ACN and MeOH but for two different reasons. The interfacial molecular geometry of methanol presents a nonpolar interface that destabilizes the ICT state. Conversely, the short lifetime found at the silica/ACN interface is due to the slow reorganization of solvent molecules, which retains C151 sp^3 structure about the amine, and rapid inversion resulting accelerating non-radiative decay rates.

In summary, slight variations in solvent structure have been shown to create large changes in the solvation environment experienced by an adsorbate. The interfacial behavior of C151 illustrates the importance of solvation environment and the dissimilarity between bulk and surface properties.

5.5 Conclusions

The hydrogen bonding opportunities of the solvent *and* the solute can greatly influence the adsorption behavior. Vibrational data and simulations show that acetonitrile, a hydrogen bond acceptor, forms an extended bilayer system that at the silica interface, creates a polar surface. In contrast, methanol, a hydrogen bonding donator, forms a less organized, nonpolar adsorption environment.

Additionally, by changing the substituents of the solute from a primary amine to a tertiary amine, we observed a change of photodynamic properties. The silica/ACN interface appears to be unable to stabilize the excited state of C151. We propose that the bilayer structure of the interfacial acetonitrile is unable to reorganize around adsorbed C151. Because C151 is able to accept and donate hydrogen bonds, C151 may adsorb to the surface via two different binding mechanisms. This configuration results in a restricted arrangement of interfacial C151 molecules, hindering the ability of ACN to solvate the amine group. The excited state of C152, however, was stabilized at the silica/ACN interface. The only difference between these two systems is the hydrogen bonding abilities of the solutes, where C152 is only able to accept hydrogen bonds. Therefore, C152 binds to only one silica site, this configuration would allow solvent molecules better access to the amine group and a stabilization of the TICT state. Steady state and time resolved data suggests this slight difference in solute substituent alters the adsorption mechanism.

5.6 References

1. Gobrogge, E. A.; Woods, B. L.; Walker, R. A., Liquid Organization And Solvation Properties At Polar Solid/Liquid Interfaces. *Faraday Discussions* **2013**, *167*, 309-327.

2. Roy, D.; Liu, S. L.; Woods, B. L.; Siler, A. R.; Fourkas, J. T.; Weeks, J. D.; Walker, R. A., Nonpolar Adsorption at the Silica/Methanol Interface: Surface Mediated Polarity and Solvent Density across a Strongly Associating Solid/Liquid Boundary. *Journal of Physical Chemistry C* **2013**, *117*, 27052-27061.

3. Woods, B. L.; Walker, R. A., pH Effects on Molecular Adsorption and Solvation of p-Nitrophenol at Silica/Aqueous Interfaces. *Journal of Physical Chemistry A* **2013**, *117*, 6224-6233.

28. Eisenthal, K. B., Second Harmonic Spectroscopy Of Aqueous Nano- And Microparticle Interfaces. *Chemical Reviews* **2006**, *106*, 1462-1477.

30. Gibbs-Davis, J. M.; Kruk, J. J.; Konek, C. T.; Scheidt, K. A.; Geiger, F. M., Jammed Acid-Base Reactions at Interfaces. *Journal of the American Chemical Society* **2008**, *130*, 15444-15447.

34. Marowsky, G.; Steinhoff, R.; Chi, L. F.; Hutter, J.; Wagniere, G., 2ND-Harmonic Generation in Quinquethienyl Monolayers. *Physical Review B* **1988**, *38*, 6274-6278.

37. Roy, D.; Piontek, S.; Walker, R. A., Surface Induced Changes In Coumarin Solvation And Photochemistry At Polar Solid/Liquid Interfaces. *Physical Chemistry Chemical Physics* **2011**, *13*, 14758-14766.

41. Zhang, X. Y.; Cunningham, M. M.; Walker, R. A., Solvent Polarity At Polar Solid Surfaces: The Role Of Solvent Structure. *Journal of Physical Chemistry B* **2003**, *107*, 3183-3195.

47. Siler, A. R.; Walker, R. A., Effects of Solvent Structure on Interfacial Polarity at Strongly Associating Silica/Alcohol Interfaces. *Journal of Physical Chemistry C* **2011**, *115*, 9637-9643.

48. Shang, X. M.; Benderskii, A. V.; Eisenthal, K. B., Ultrafast Solvation Dynamics At Silica/Liquid Interfaces Probed By Time-Resolved Second Harmonic Generation. *Journal of Physical Chemistry B* **2001**, *105*, 11578-11585.

49. Bloembergen, N., 2ND Harmonic Reflected Light. *Optica Acta* **1966**, *13*, 311-322.

50. Benjamin, I., Inhomogeneous Broadening Of Electronic Spectra At Liquid Interfaces. *Chemical Physics Letters* **2011**, *515*, 56-61.

51. Hiemenz, P. C., *Principles Of Colloid And Surface Chemistry*, 2 ed.; Marcel Dekker, Inc: New York 1986; Vol. 9, p 792.

56. Nad, S.; Kumbhakar, M.; Pal, H., Photophysical Properties Of Coumarin-152 And Coumarin-481 Dyes: Unusual Behavior In Nonpolar And In Higher Polarity Solvents. *Journal of Physical Chemistry A* **2003**, *107*, 4808-4816.

57. Hecht, E., *Optics*, 4th ed.; Pearson Education, Inc: San Francisco, CA, 2002.

64. Onsager, L., Electric Moments Of Molecules In Liquids. *Journal of the American Chemical Society* **1936**, *58*, 1486-1493.

116. Zhang, X. Y.; Walker, R. A., Discrete Partitioning Of Solvent Permittivity At Liquid-Solid Interfaces. *Langmuir* **2001**, *17*, 4486-4489.

151. Aono, S.; Minezawa, N.; Kato, S., Electronic Spectra Of Coumarin-151 In Polar Solvents: Linear Response Free Energy Approach. *Chemical Physics Letters* **2010**, *492*, 193-197.

154. Cave, R. J.; Castner, E. W., Time-Dependent Density Functional Theory Investigation Of The Ground And Excited States Of Coumarins 102, 152, 153, And 343. *Journal of Physical Chemistry A* **2002**, *106*, 12117-12123.

156. Krystkowiak, E.; Maciejewski, A., Changes In Energy Of Three Types Of Hydrogen Bonds Upon Excitation Of Aminocoumarins Determined From Absorption Solvatochromic Experiments. *Physical Chemistry Chemical Physics* **2011**, *13*, 11317-11324.

157. Liu, Y.; Ding, J.; Liu, R.; Shi, D.; Sun, J., Revisiting The Electronic Excited-State Hydrogen Bonding Dynamics Of Coumarin Chromophore In Alcohols: Undoubtedly Strengthened Not Cleaved. *Journal of Photochemistry and Photobiology a-Chemistry* **2009**, *201*, 203-207.

159. Nad, S.; Pal, H., Unusual Photophysical Properties Of Coumarin-151. *Journal of Physical Chemistry A* **2001**, *105*, 1097-1106.

160. Pedone, A., Role of Solvent on Charge Transfer in 7-Aminocoumarin Dyes: New Hints from TD-CAM-B3LYP and State Specific PCM Calculations. *J. Chem. Theory Comput.* **2013**, *9*, 4087-4096.

162. Corrie, J. E. T.; Munasinghe, V. R. N.; Rettig, W., Synthesis And Fluorescence Properties Of Substituted 7-Aminocoumarin-3-Carboxylate Derivatives. *Journal of Heterocyclic Chemistry* **2000**, *37*, 1447-1455.

168. Dahiya, P.; Kumbhakar, M.; Mukherjee, T.; Pal, H., Effect Of Protic Solvents On Twisted Intramolecular Charge Transfer State Formation In Coumarin-152 And Coumarin-481 Dyes. *Chemical Physics Letters* **2005**, *414*, 148-154.

181. Azam, M. S.; Gibbs-Davis, J. M., Monitoring DNA Hybridization and Thermal Dissociation at the Silica/Water Interface Using Resonantly Enhanced Second Harmonic Generation Spectroscopy. *Analytical Chemistry* **2013**, *85*, 8031-8038.

195. Rivera, C. A.; Souna, A. J.; Bender, J. S.; Manfred, K.; Fourkas, J. T., Reorientation-Induced Spectral Diffusion in Vibrational Sum-Frequency-Generation Spectroscopy. *Journal of Physical Chemistry B* **2013**, *117*, 15875-15885.

196. Loughnane, B. J.; Farrer, R. A.; Scodinu, A.; Fourkas, J. T., Dynamics Of A Wetting Liquid In Nanopores: An Optical Kerr Effect Study Of The Dynamics Of Acetonitrile Confined In Sol-Gel Glasses. *Journal of Chemical Physics* **1999**, *111*, 5116-5123.

197. Morales, C. M.; Thompson, W. H., Simulations of Infrared Spectra of Nanoconfined Liquids: Acetonitrile Confined in Nanoscale, Hydrophilic Silica Pores. *Journal of Physical Chemistry A* **2009**, *113*, 1922-1933.

198. Gulmen, T. S.; Thompson, W. H., Grand Canonical Monte Carlo Simulations of Acetonitrile Filling of Silica Pores of Varying Hydrophilicity/Hydrophobicity. *Langmuir* **2009**, *25*, 1103-1111.

199. Milischuk, A. A.; Ladanyi, B. M., Polarizability Anisotropy Relaxation in Nanoconfinement: Molecular Simulation Study of Acetonitrile in Silica Pores. *Journal of Physical Chemistry B* **2013**, *117*, 15729-15740.

200. CabaleiroLago, E. M.; Rios, M. A., A Potential Function For Intermolecular Interaction In The Acetonitrile Dimer Constructed From Ab Initio Data. *Journal of Physical Chemistry A* **1997**, *101*, 8327-8334.

201. Takamuku, T.; Tabata, M.; Yamaguchi, A.; Nishimoto, J.; Kumamoto, M.; Wakita, H.; Yamaguchi, T., Liquid Structure Of Acetonitrile-Water Mixtures By X-Ray Diffraction And Infrared Spectroscopy. *Journal of Physical Chemistry B* **1998**, *102*, 8880-8888.

202. Marcus, Y.; Migron, Y., Polarity, Hydrogen-Bonding, And Structure Of Mixtures Of Water And Cyanomethane. *Journal of Physical Chemistry* **1991**, *95*, 400-406.

203. Choi, J.-H.; Oh, K.-I.; Lee, H.; Lee, C.; Cho, M., Nitrile And Thiocyanate IR Probes: Quantum Chemistry Calculation Studies And Multivariate Least-Square Fitting Analysis. *Journal of Chemical Physics* **2008**, *128*.

204. Guo, Y.; Gaiki, S., Retention Behavior Of Small Polar Compounds On Polar Stationary Phases In Hydrophilic Interaction Chromatography. *Journal of Chromatography A* **2005**, *1074*, 71-80.

205. Olsen, B. A., Hydrophilic Interaction Chromatography Using Amino And Silica Columns For The Determination Of Polar Pharmaceuticals And Impurities. *Journal of Chromatography A* **2001**, *913*, 113-122.

206. Reubsaet, J. L. E.; Vieskar, R., Characterisation Of Pi-Pi Interactions Which Determine Retention Of Aromatic Compounds In Reversed-Phase Liquid Chromatography. *Journal of Chromatography A* **1999**, *841*, 147-154.

207. Urban, J.; Skerikova, V.; Jandera, P.; Kubickova, R.; Pospisilova, M., Preparation And Characterization Of Polymethacrylate Monolithic Capillary Columns With Dual Hydrophilic Interaction Reversed-Phase Retention Mechanism For Polar Compounds. *Journal of Separation Science* **2009**, *32*, 2530-2543.

208. Ding, F.; Hu, Z.; Zhong, Q.; Manfred, K.; Gattass, R. R.; Brindza, M. R.; Fourkas, J. T.; Walker, R. A.; Weeks, J. D., Interfacial Organization of Acetonitrile: Simulation and Experiment. *Journal of Physical Chemistry C* **2010**, *114*, 17651-17659.

209. Hu, Z.; Weeks, J. D., Acetonitrile on Silica Surfaces and at Its Liquid-Vapor Interface: Structural Correlations and Collective Dynamics. *Journal of Physical Chemistry C* **2010**, *114*, 10202-10211.

210. Loughnane, B. J.; Farrer, R. A.; Fourkas, J. T., Evidence For The Direct Observation Of Molecular Exchange Of A Liquid At The Solid/Liquid Interface. *Journal of Physical Chemistry B* **1998**, *102*, 5409-5412.

211. Woods, B. L.; George, J. K.; Sherman, A. M.; Callis, P. R.; Walker, R. A., Adsorption and Aggregate Formation at the Silica/Liquid Interface. *Journal of Physical Chemistry C* **2015**, *Submitted*.

212. Liu, W. T.; Zhang, L. N.; Shen, Y. R., Interfacial layer structure at alcohol/silica interfaces probed by sum-frequency vibrational spectroscopy. *Chemical Physics Letters* **2005**, *412*, 206-209.

213. Gayathri, B. R.; Mannekutla, J. R.; Inamdar, S. R., Rotational Diffusion Of Coumarins In Alcohols: A Dielectric Friction Study. *Journal of Fluorescence* **2008**, *18*, 943-952.

214. Pal, H.; Nad, S.; Kumbhakar, M., Photophysical Properties Of Coumarin-120: Unusual Behavior In Nonpolar Solvents. *Journal of Chemical Physics* **2003**, *119*, 443-452.

215. Sharma, V. K.; Saharo, P. D.; Sharma, N.; Rastogi, R. C.; Ghoshal, S. K.; Mohan, D., Influence Of Solvent And Substituent On Excited State Characterstics Of Laser Grade Coumarin Dyes. *Spectrochimica Acta Part a-Molecular and Biomolecular Spectroscopy* **2003**, *59*, 1161-1170.

216. Curthoys, G.; Davydov, V. Y.; Kiselev, A. V.; Kiselev, S. A.; Kuznetso.Bv, Hydrogen-Bonding In Adsorption On Silica. *Journal of Colloid and Interface Science* **1974**, *48*, 58-72.

CHAPTER 6

CONCLUSIONS

Work presented in this thesis investigated the fundamental processes responsible for adsorption to solid/liquid interfaces. Specifically, experiments were designed to determine the roles played by polarity, hydrogen bonding and molecular structure at silica/liquid interfaces.

Initial studies examined the role of hydrogen bonding of the substrate by changing the pH at the silica/aqueous interface. Changing the pH caused the silica surface to become either partially positive at low pH or negatively charged at higher pHs. Altering the ability of the substrate to efficiently hydrogen bond greatly interferes with the adsorption process leading to long equilibration times. This observation was shown in Chapter 2 by examining silica/aqueous interfaces at different pHs by measuring the second harmonic response of adsorbed p-nitrophenol. This charged interface disrupted the solvent's ability to fully interact with the terminal silanols, requiring long equilibration times on the order of hours. At short equilibration times, the solvation environment of pNP was not pH dependent, whereas a large pH dependency was evident at long equilibration times. If the silica/liquid interface examined was neutral - as is the case at the silica/organic solvent interface - a long equilibration times were not evident.

The work presented in Chapter 3 not only showed how interfacial behavior greatly differs from bulk properties, but also the importance of the functionality and identity of the solvent. Although bulk cyclohexane and methylcyclohexane are nonpolar,

at the silica interface both solvents appeared to create a polar adsorption environment for the adsorbates coumarin 151 and coumarin 152. The most probable explanation of this polar interface was the creation of a high density of surface silanol groups that interacted directly and strongly with adsorbed solutes. In contrast, the silica/alcohol interface was probed using the same adsorbates and was shown to present solutes with a nonpolar environment. The size of the alcohol did not influence the nonpolar adsorption environment as evident in the comparison of propanol and methanol at the silica interface. The adsorption environment did not appear to be solute dependent as both C151 and C152 sampled the same local polarity for both the silica/alkane. Additionally, the silica/propanol studies created a nonpolar adsorption environment for both C151 and C152. Time resolved studies of C151 at the silica/methanol interface confirmed the nonpolar interfacial region proposed by the steady state SHG work, and showed that the excited state of C151 also experiences a nonpolar environment.

Comparing C151 behavior at the silica/methanol interface to C152 at the same interface offered insight into the role of the adsorbate in the adsorption process (Chapter 4). Adsorption of C151, a primary amine, terminates at monolayer coverage whereas C152, a tertiary amine, shows evidence suggesting multilayer or aggregate formation. The SHG results, time resolved fluorescence data, and computational simulations all support the hypothesis that C152 continues to adsorb the silica/methanol interface after the first monolayer forms. The data suggest C152 interacts with silica via its hydrogen bond accepting site allowing access for another solute molecule to interact. Furthermore, computational simulations proposed C152 dimers prefer to stack with antiparallel facing

dipoles. This configuration creates an inversion center, which explains the observed decrease in SHG signal as concentration, and therefore aggregation, increases. The silica/methanol interface presents a nonpolar environment independent of solute choice, however, the solute's functionality can greatly affect the adsorption mechanisms.

The interfacial behavior and the difference in adsorption mechanisms between C151 and C152 are clearly illustrated in Chapter 5. The results from the silica/methanol interface were compared to C151 and C152 adsorbed at the silica/acetonitrile interface. This comparison provided insight into the role of hydrogen bonding of solvents. Methanol is polar protic, in contrast, acetonitrile is polar but is only able to accept hydrogen bonds. Both solutes sampled a polar adsorption region at the silica/acetonitrile interface. Clear differences between adsorbates were shown in the time resolved fluorescence data, however. The excited state of C151 was not stabilized by the silica/acetonitrile interface, but the excited state of C152 appeared to be stabilized. Differences in emission behavior were explained by different solute adsorption mechanisms, namely C151 can accept and donate hydrogen bonds while C152 is limited to accepting H-bonds. Computational studies describing solvent structure at the neat silica/acetonitrile interface showed the interfacial solvent molecules create an extended bilayer that can range several nanometers from the surface.[208] This configuration slows the time required for the solvent to reorganize itself around the solute and stabilize the excited state, as implied by C151 lifetime data. In the case of C152, we propose that the =O terminus is hydrogen bonding to a silanol while the (tertiary) amine points away from

the silica surface, allowing acetonitrile more access to stabilized the TICT state of the amine.

Although the work presented successfully showed the importance of the identity and behavior of the substrate, solvent, and solute, there are many questions still left to explore. The coumarin family is quite large and we have already begun collecting steady state and time resolved data on other 7-aminocoumarins with different substituents. Of particular interest is coumarin 500 (C500), a secondary amine with an ethyl group on the nitrogen. C151 and C152 data at the silica/methanol interface showed how a primary amine terminates at a monolayer while a tertiary amine promotes aggregation, an interesting study would be to examine how a secondary (C500) behaves at this interface. Will the secondary amine behave like a primary or tertiary or will C500 experience a different adsorption environment all together? C500 also has the benefit of a larger hyperpolarizability than C151 and C152, that should result in a larger SHG signal. C500 also has larger and more consistent quantum yields in solvents for optimal fluorescence collection. The studies presented in this thesis have brought considerable insight into adsorption, however there is more work to be done. Many solvent properties are left to be examined, such as larger alcohol chains, solvents with different dielectric constants, and/or binary mixtures. Also of great interest is shifting these fundamental experiments to more applicable studies by examining adsorbate behavior in biological membranes, like lipid bilayers.[217-218] Supported bilayer studies via SHG and TIR-TCPSC could provide valuable insight into how molecules are transported, adsorb to and partition into membranes.[219-220]

Adsorption at the silica/liquid is complex, with many variables and interactions to consider. My thesis research provided valuable information and insight into the complexity of solid/liquid interfaces. While my research provides a good start to this objective, much knowledge and understanding remains to be gleaned from studying the intricate behavior and nuances of molecular adsorption.

6.1 References

208. Ding, F.; Hu, Z.; Zhong, Q.; Manfred, K.; Gattass, R. R.; Brindza, M. R.; Fourkas, J. T.; Walker, R. A.; Weeks, J. D., Interfacial Organization of Acetonitrile: Simulation and Experiment. *Journal of Physical Chemistry C* **2010**, *114*, 17651-17659.

217. Nguyen, T. T.; Conboy, J. C., High-Throughput Screening of Drug-Lipid Membrane Interactions via Counter-Propagating Second Harmonic Generation Imaging. *Analytical Chemistry* **2011**, *83*, 5979-5988.

218. Liu, Y.; Yan, E. C. Y.; Eisenthal, K. B., Effects of bilayer surface charge density on molecular adsorption and transport across liposome bilayers. *Biophysical Journal* **2001**, *80*, 1004-1012.

219. Troiano, J. M.; Olenick, L. L.; Kuech, T. R.; Melby, E. S., et al., Direct Probes of 4 nm Diameter Gold Nanoparticles Interacting with Supported Lipid Bilayers. *Journal of Physical Chemistry C* **2015**, *119*, 534-546.

220. Greiner, A. J.; Pillman, H. A.; Worden, R. M.; Blanchard, G. J.; Ofoli, R. Y., Effect of Hydrogen Bonding on the Rotational and Translational Dynamics of a Headgroup-Bound Chromophore in Bilayer Lipid Membranes. *Journal of Physical Chemistry B* **2009**, *113*, 13263-13268.

APPENDICES

APPENDIX A

SUPPORTING INFORMATION

Supplemental Data:

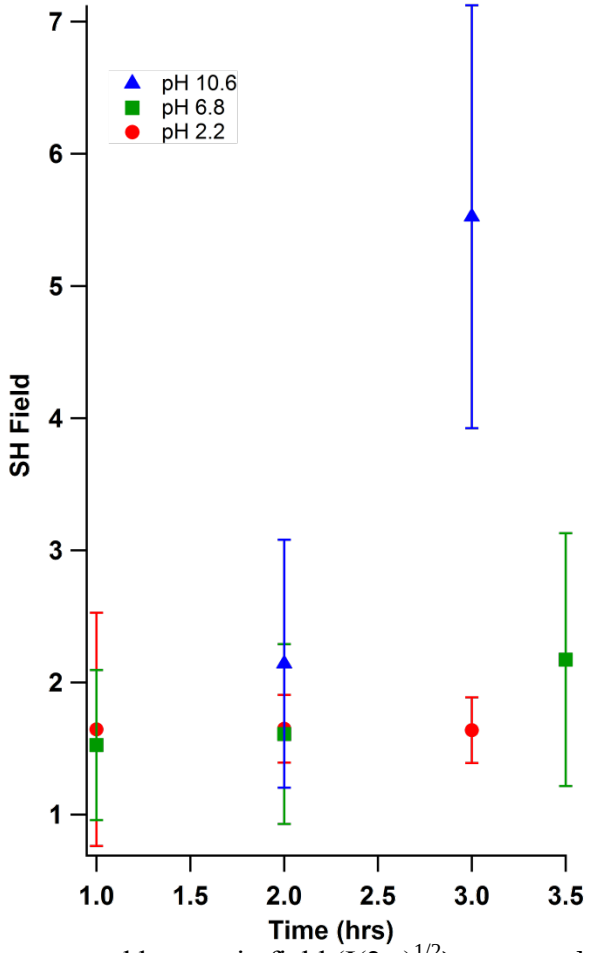

Figure A.1. Nonresonant second harmonic field $(I(2\omega)^{1/2})$ generated by the silica aqueous interface as a function of time.

Spectra were taken at 315 nm and sample preparations were handled as described in the manuscript. Error bars represent the standard deviation from three SH signal acquisitions. These experiments were performed to repeat those of Ong, *et al*. and ensure that high pH conditions enhanced in nonresonant SH field relative to low pH conditions, because we are not studying the ionic behavior in solution our solutions do not have

added salt. Our findings showed that basic conditions did, in fact, enhance the SH field but only after the system had been allowed to equilibrate for ~3 hours.

Working at the silica/aqueous interface, previous work determined a 13:1 increase in field between pH 14 and pH 2. In order to see a 5 fold increase from pH 10.6 to pH 2.2 the solution must equilibrate with the silica slide for at least 3 hours as evident from our experiment. Time did not seem to influence signal strength in acidic and neutral conditions for solid/aqueous interface. Data described in our paper did show that the effect is noticeable when a solute is added.

UV/Vis experiments (not included) shows the addition of NaCl will increase the amount of phenoxide in pH 7 and 10. The nonlinear spectroscopy used in the experiments described in the paper is sensitive to only the neutral pNP. Excess phenoxides will not alter SHG spectra, thus ionic contributions to spectra data can be ignored.

Spectra were taken for 60 mM pNP in pH 7 after allowing the silica slide to equilibrate with water at pH 7 for three hours. SHG spectra of pNP were collected at 1 hour and 3 hours, both equilibration times show similar results. (Figure A.2) The specta presented reinforce the conclusions the authors made, the long equilibration time does reflect the behavior of the solvation environment at the shorter equilibration time.

Orientation data was collected using the SHG set-up described in the experimental section with an additional polarizer added. At the resonance wavelength (317 nm at 1 hour; 310 nm & 330 nm for 3 hours) the incoming polarization was controlled by a half-wave plate and the final polarizer was set as $P_{out.}$

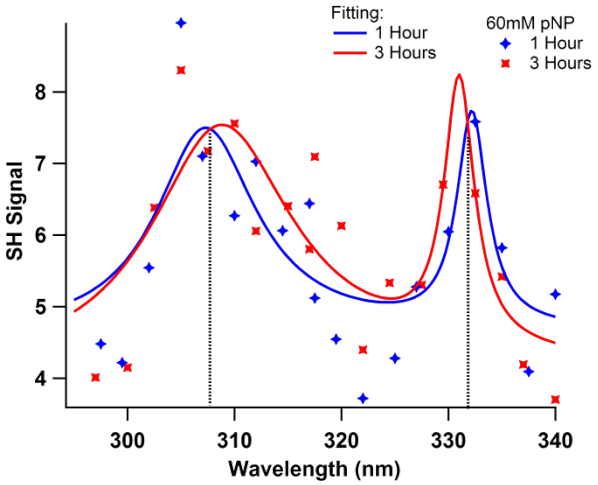

Figure A.2. SHG spectra of pNP at 1 and 3 hours after allowing the interface to equilibrate with water at pH 7.

For calculation purposes, additional data was collected at a Mix_{in}/S_{out} orientation. A detailed description of calculation methods can be found by Higgins and Corn.[31] At a given wavelength the power remained constant throughout the orientation data and was periodically checked to ensure consistency. The large standard deviation is associated with imperfections of the half-wave plate.

SHG orientation data show similar behavior for 50mM pNP in pH 5 at 1 hr and 3 hours. (Figure A-3) Data at 1 hour was taken at peak wavelength (317 nm), the calculated orientation of pNP at the silica/aqueous interface was about 79°. After a ≥3 hour period this angle only slightly decreases to about 75° for both peak wavelengths (310 nm and 330 nm).

Studies at the silica/ air interface have shown that pNP has an orientation of about 70°, from the analysis of these experiments it was concluded that the nitro group is sticking up.[31] If allowances are made for solvation environment, one could interpret Orientation at low and high concentrations were also taken but are not shown, the data

showed no real concentration dependence for orientation of pNP. Data would suggest that equilibration times do not greatly affect the orientation of the adsorbates.

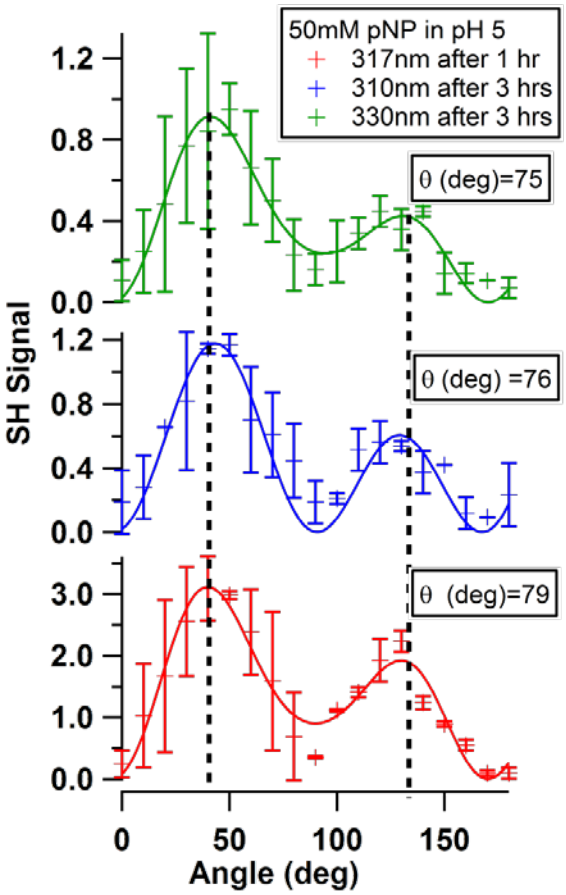

Figure A.3. SHG orientation spectra of pNP at 1 and 3 hours at resonance wavelength.

Experimental Set-up:

Additional parameters for the nonlinear spectroscopy system are listed below. Resolution for incident wavelength of 637 nm has a FWHM of ~10 nm and SHG FWHM is about 3-5 nm. Photons are counted for 10 s, for one experimental run, an average of three cycles are measured.

Raw counts were normalized to power and the spectral data was fitted using Equations 2.1 and 2.2 via a fitting program in Igor. The adjustable parameters were the resonance wavelength (w_0), line width, (w_1), amplitude (w_2) and the nonresonance term (w_3) and initial guesses were the max wavelength, 0.0001, 0.001, and 1, respectively.

Error Analysis:

Error analysis for calculating ΔG^{o}_{ads}. The b parameter was calculated using a 95.4% confidence, below is an example of calculating the error propagation using methods described in Taylor.[52]

$$\Delta G = -RTln(b \pm \delta b) \quad \text{Eq. A.1}$$

Example: b=0.19978 $\pm$ 0.110 Since b has units of mM, we convert to M.

$$\Delta G = -RTln(1.998e^{-4} + 1.100e^{-4}) \quad \text{Eq. A.2}$$

According to Taylor to find error propagation for any function

$$\delta q = \left|\frac{dq}{dx}\right| \delta x \quad \text{Eq. A.3}$$

and for ln(b) this becomes:

$$\delta lnb = \left|\frac{1}{b}\right| \delta b = \frac{1}{1.998e^{-4}} * 1.100e^{-4} \quad \text{Eq. A.4}$$

$$\Delta G = -RTln(8.52 \pm 0.55) \quad \text{Eq. A.5}$$

Measured quantity times exact number:

$$\delta q = |B|\delta q \quad \text{Eq. A.6}$$

where B is RT.

Then divide by 1000 to get units into kJ/mol to get ΔG=-21.03$\pm$1.36 kJ/mol.

APPENDIX B

SUPPORTING INFORMATION

Supporting Information

Computational Data from Different DFT Functionals.

Additional geometry optimization calculations were performed using CAM-B3Lyp, a range separated, hybrid functional. Although CAM-B3Lyp was designed for calculating long range interactions, the M06L method proved to have consistently lower (or more negative) energies, as shown in Table B.1. The 2x the monomer optimized energy was subtracted from the dimer energies to determine the stabilization resulting from dimer formation, ΔE_{dimer}. A large magnitude difference would imply C152 prefers to form dimers in lieu of have single monomers. The table includes the ΔE_{dimer} calculated using both the M06L and CAM-B3Lyp methods, the energetics are given both in units of kJ/mol and a.u. Not all starting orientations converged successfully. Additionally, many unfavorable starting positions resulted in an optimized geometry that was markedly different from the initial arrangement. In Table B.1 if the final geometry was different than the starting geometry, the energy recorded is the optimized energy of the initial geometry. To estimate the effect of aggregation of C152 on the surface, we have examined the computed, frequency dependent hyperpolarizability (β) values in the output from Gaussian 09 calculations for monomer and dimer forms of C152 with input route cards of the form:

 # method/basis polar=dcshg nosym pop=reg

The region of resonance was determined from corresponding calculations with the route card:

 # method/basis td(nstates=N) nosym pop=reg

Table B.1: Calculated energetics of dimers formation with various starting orientations in two different units kJ/mol and au.

	CAM-B3lyp			M06L		
Orientation	Vac (kJ/mol) (au)	Hex (kJ/mol) (au)	MeOH (kJ/mol) (au)	Vac (kJ/mol) (au)	Hex (kJ/mol) (au)	MeOH (kJ/mol) (au)
SS Anti	-23.8120 -0.0091	-16.9597 -0.0065	-6.4297 -0.0025	-33.3696 0.0109	-26.5460 -0.0188	-15.2681 -0.0208
SS para*	86.8137 0.0331	88.0622 0.0336	89.2133 0.0340	65.3521 0.0485	-4.2805 0.0000	-3.8292 -0.0164
Stacked Anti	-23.8120 -0.0091	-17.6623 -0.0067	-6.4297 -0.0025	-74.8892 -0.0285	-68.1592 -0.0260	-57.8589 -0.0220
Stacked para*	234.6826 0.0894	88.0622 0.0331	233.1706 0.0889	26.5751 0.0338	15.4147 -0.0028	29.5416 -0.0037
Head to tail	--- ---	--- ---	--- ---	107.6818 0.0647	110.5058 0.0334	116.9673 0.0296

where N is an integer in the range 3-10 as required to capture the energy of the lowest strongly absorbing excited state. The β term represents the likelihood of inducing a dipole in a molecule and is related to the second order susceptibility $\chi^{(2)}$ through Equation 4.3 in the main text. Although β is a combination of hyperpolarizabilities, experimentally SHG can only detect contributions from 4 unique terms, β_{zzz}, $\beta_{izi,}$, β_{iiz}, and β_{zii}, where the dipole is aligned parallel to β_{zzz}. Computationally, the strongest response came from our assigned β_{zzz}, as expected. The calculations were performed under ideal conditions, where the dimers were overlapped almost completely. Table B.2 shows the calculated resonance wavelength and β_{zzz} for monomer and dimer formation of C152 in vacuum, methanol, and n-hexane. The ratio of the monomer to dimer was also calculated and for direct comparison, the β_{zzz} of the monomer was doubled. The data shows almost a 14-fold decrease in hyperpolarizability values going from a monomer to dimer formation.

As the second harmonic response is proportionally to β^2, the computational data suggests that in ideal conditions, the second harmonic signal should see about a 200-fold decrease in signal in nonpolar environments. In a polar continuum, dimerization resulted in only about a 40-fold decrease in signal. The computational data supports the hypothesis that the dimers are oriented in such a way to form an inversion center which would result in a decrease in SHG response. Experimental methods do not provide the sensitivity to distinguish between individual dimer formations and orientation, computational results can provide insight into the likely dipole-dipole interactions. As the SHG signal did not show a 200-fold decrease in signal, the dipole moments appears not to be overlapped completely.

Table B.2: Calculated hyperpolarizability of monomers and of dimers in vacuum, methanol, and n-hexane.

	Vacuum		Methanol		n-Hexane	
	Monomer	Dimer	Monomer	Dimer	Monomer	Dimer
λres (nm)	785.0	812.9	865.0	868.5	827.0	845.7
$\beta_{(zzz)}$ (au)	4.61E+06	-3.36E+05	3.60E+06	-5.85E+05	8.15E+06	-6.39E+05
Ratio ($\beta_{2xmono}/\beta_{dimer}$)	13.7		6.2		12.8	

Concentration Dependent SHG Measurements

Second Harmonic Generation (SHG) was used to collect spectra of C152 at the methanol/silica interface at three different concentrations. The three concentrations were chosen based on the isotherm spectrum shown in Figure B.1A, the normalized spectra are shown in Figure B.1B. The concentrations were chosen before monolayer coverage

(30 μM), at monolayer coverage (80 μM), and after aggregation (300 μM). As evident from Figure B.1, all three spectra overlaps and there are no discernible differences in line shape. The data suggest that the C152 being sampled in the SHG experiments is experiencing the same solvation environment throughout the aggregation process.

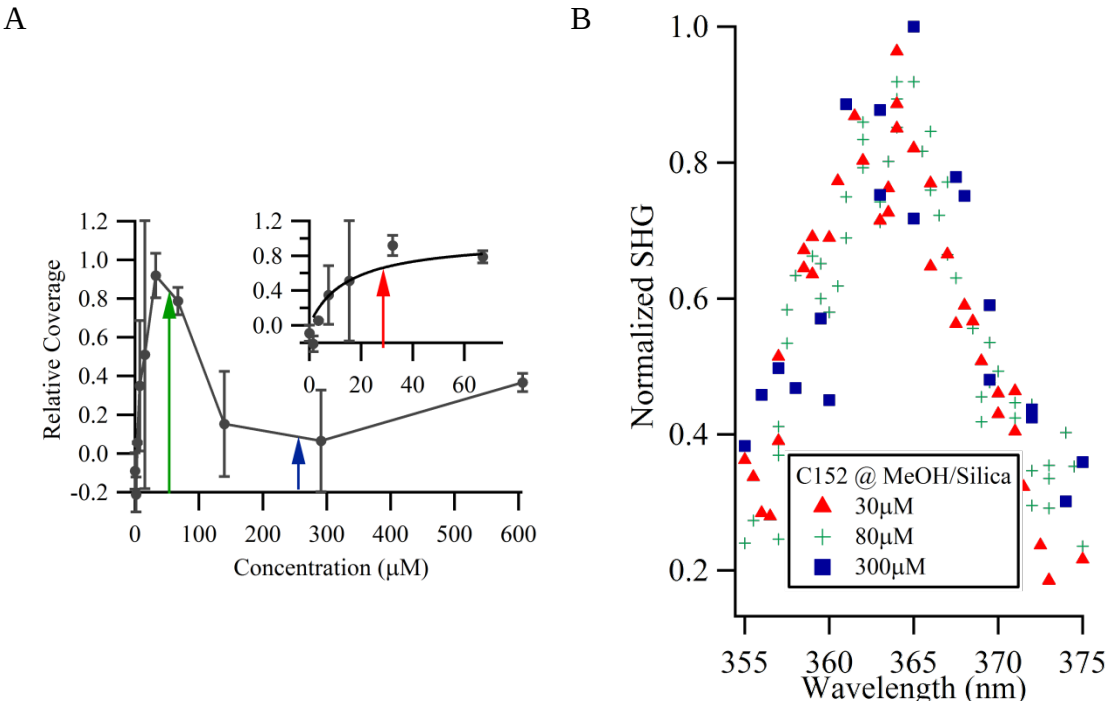

Figure B. 1: SHG spectra of C152 at the MeOH/silica interface at 3 concentrations.

Time Resolved Fluorescence at Different Wavelengths

Time resolved fluorescence data were collected at total internal reflection geometry using the excitation wavelength of 365 nm, the resonance wavelength calculated from SHG data. No filters were added for the decays found in Figure B.2. Fitting the decays to two lifetimes yielded values of ~0.9 ns and ~2 ns at lower concentrations, however as concentration increased the lifetime assigned to the interfacial

behavior, ~3 ns, had diminishing contribution. At concentrations where aggregation is occurring, the decays did not show any distinguishing changes. As reported in the manuscript, when exciting C152 adsorbates at 396 nm, at concentrations >300 μM a second longer lifetime was visible. The lower excitation wavelength did not appear to excite the aggregates efficiently.

Additional decays were taken following excitation at 396 nm using the TIR geometry for a large range of concentrations. Figure A.3 shows the decays taken when monitoring emission at 574 nm, the emission peak assigned to aggregation at the solid/vapor interface. Data on the left were acquired using a 420 nm long pass filter and data on the right resulted from further filtering the emission using a 530 nm long pass filter. These filters allow for separation of the aggregation peak and the bulk emission peak, at 513 nm. The decays collect at 513 nm were shown in the manuscript, but in comparison, the addition of filters did not alter the values of the lifetimes but did make drastic differences in relative contributions, as discussed in the manuscript.

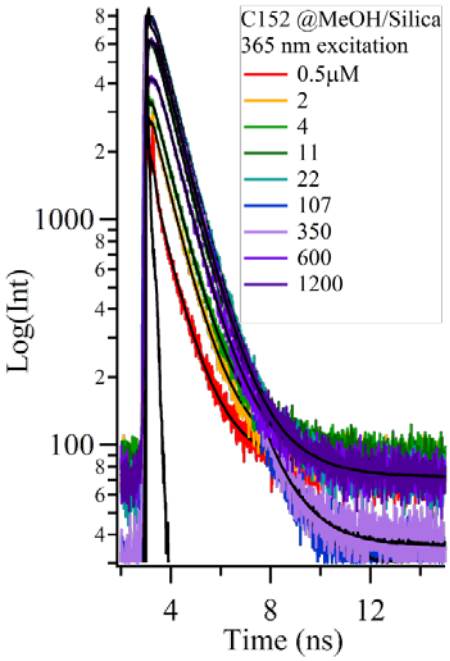

Figure B.2: Time resolved decays for C152 at MeOH/silica interface with an excitation of 365nm and collected at 513nm. The IRF is shown in black.

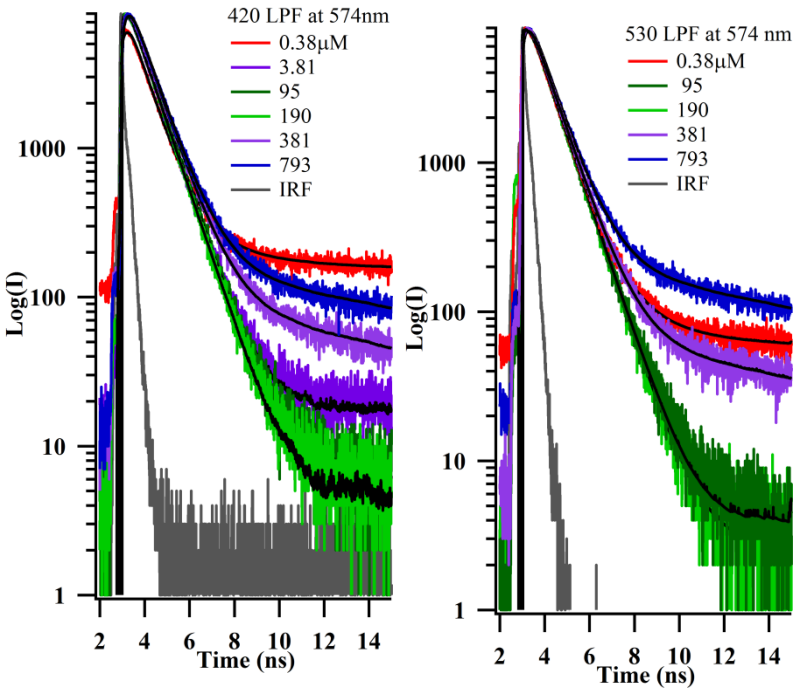

Figure B.3: Time resolved decays for C152 at MeOH/silica interface exciting at 396 nm and collected at 574 nm using two different long pass filters. Fits are shown in black.

References

31. Higgins, D. A.; Abrams, M. B.; Byerly, S. K.; Corn, R. M., Resonant 2nd Harmonic-Generation Studies of p-Nitrophenol Adsorption at Condensed-phase Interfaces. *Langmuir* **1992**, *8*, 1994-2000.

52. Taylor, J. R., *An Introduction To Error Analysis: The Study Of Uncertainties In Physical Measurements*, 2nd ed.; University Science Boooks: Sausalito, Ca, 1997.

REFERENCES CITED

1. Gobrogge, E. A.; Woods, B. L.; Walker, R. A., Liquid Organization And Solvation Properties At Polar Solid/Liquid Interfaces. *Faraday Discussions* **2013**, *167*, 309-327.

2. Roy, D.; Liu, S. L.; Woods, B. L.; Siler, A. R.; Fourkas, J. T.; Weeks, J. D.; Walker, R. A., Nonpolar Adsorption at the Silica/Methanol Interface: Surface Mediated Polarity and Solvent Density across a Strongly Associating Solid/Liquid Boundary. *Journal of Physical Chemistry C* **2013**, *117*, 27052-27061.

3. Woods, B. L.; Walker, R. A., pH Effects on Molecular Adsorption and Solvation of p-Nitrophenol at Silica/Aqueous Interfaces. *Journal of Physical Chemistry A* **2013**, *117*, 6224-6233.

4. Cashman, J. D.; Kennah, E.; Shuto, A.; Winternitz, C.; Springate, C. M. K., Fucoidan Film Safely Inhibits Surgical Adhesions in a Rat Model. *Journal of Surgical Research* **2011**, *171*, 495-503.

5. Bucholz, E. W.; Phillpot, S. R.; Sinnott, S. B., Molecular Dynamics Investigation Of The Lubrication Mechanism Of Carbon Nano-Onions. *Computational Materials Science* **2012**, *54*, 91-96.

6. Picarra, S.; Afonso, C. A. M.; Kurteva, V. B.; Fedorov, A.; Martinho, J. M. G.; Farinha, J. P. S., The Influence Of Nanoparticle Architecture On Latex Film Formation And Healing Properties. *Journal of Colloid and Interface Science* **2012**, *368*, 21-33.

7. Tofan-Lazar, J.; Al-Abadleh, H. A., ATR-FTIR Studies on the Adsorption/Desorption Kinetics of Dimethylarsinic Acid on Iron-(Oxyhydr)oxides. *Journal of Physical Chemistry A* **2012**, *116*, 1596-1604.

8. Li, W.; Liu, D.; Wu, J.; Kim, C.; Fortner, J. D., Aqueous Aggregation and Surface Deposition Processes of Engineered Superparamagnetic Iron Oxide Nanoparticles for Environmental Applications. *Environmental Science & Technology* **2014**, *48*, 11892-11900.

9. Wu, G.; Zhu, X.; Ji, H.; Chen, D., Molecular Modeling Of Interactions Between Heavy Crude Oil And The Soil Organic Matter Coated Quartz Surface. *Chemosphere* **2015**, *119*, 242-9.

10. Franco, C. A.; Martinez, M.; Benjumea, P.; Patino, E.; Cortes, F. B., Water Remediation Based on Oil Adsorption Using Nanosilicates Functionalized with a Petroleum Vacuum Residue. *Adsorption Science & Technology* **2014**, *32*, 197-207.

11. Muncy, B. L.; Price, S. J.; Bonner, S. J.; Barton, C. D., Mountaintop Removal Mining Reduces Stream Salamander Occupancy And Richness In Southeastern Kentucky (USA). *Biological Conservation* **2014**, *180*, 115-121.

12. Perine, A. *An Investigation of Potential Ground and Surface Water Contamination From Stormwater Discharge, City of Missoula, MT.*; Missoula Valley Water Quality District: Missoula, 1998.

13. Tian, F.; Roman, M. J.; Decker, E. A.; Goddard, J. M., Biomimetic Design of Chelating Interfaces. *Journal of Applied Polymer Science* **2015**, *132*.

14. Van Aken, B.; Quaranta, J. D.; Mack, B.; Yu, H.; Ducatman, A. M.; Ziemkiewicz, P. F., Environmental Contaminants in Coal Slurry Intended for Underground Injection in the State of West Virginia. *Journal of Environmental Engineering* **2015**, *141*.

15. EPA Drinking Water Contaminants.

16. Ennist, J. H.; Gobrogge, E. A.; Schlick, K. H.; Walker, R. A.; Cloninger, M. J., Cyclodextrin-Functionalized Chromatographic Materials Tailored for Reversible Adsorption. *Acs Applied Materials & Interfaces* **2014**, *6*, 18087-18097.

17. Arora, P. K.; Bae, H., Bacterial Degradation Of Chlorophenols And Their Derivatives. *Microbial Cell Factories* **2014**, *13*.

18. Corma, A.; Iborra, S.; Velty, A., Chemical Routes For The Transformation Of Biomass Into Chemicals. *Chemical Reviews* **2007**, *107*, 2411-2502.

19. Davis, T. A.; Volesky, B.; Mucci, A., A Review Of The Biochemistry Of Heavy Metal Biosorption By Brown Algae. *Water Research* **2003**, *37*, 4311-4330.

20. Fujishima, A.; Zhang, X.; Tryk, D. A., TiO2 Photocatalysis And Related Surface Phenomena. *Surface Science Reports* **2008**, *63*, 515-582.

21. Soil Screening Guidance: User's Guide. Second Edition ed.; EPA, Ed. Washington, DC, 1996.

22. Grinias, J. P.; Godinho, J. M.; Lunn, D. B.; Jorgenson, J. W., Evaluation Of Preparative Hydrodynamic Chromatography Of Silica Stationary Phase Supports. *Journal of Chromatography A* **2014**, *1370*, 270-273.

23. Lin, M.-C.; Lin, K.-C., Interaction Between Crystal Violet And Anionic Surfactants At Silica/Water Interface Using Evanescent Wave-Cavity Ring-Down Absorption Spectroscopy. *Journal of Colloid and Interface Science* **2012**, *379*, 41-47.

24. Nawrocki, J., The Silanol Group And Its Role In Liquid Chromatography. *Journal of Chromatography A* **1997**, *779*, 29-71.

25. Dawson, R.; Messina, S. M.; Stokes, C.; Salyani, S.; Alcalay, N.; de Fiebre, N. C.; de Fiebre, C. M., Solid-Phase Extraction And HPLC Assay Of Nicotine And Cotinine In Plasma And Brain. *Toxicology Mechanisms and Methods* **2002**, *12*, 45-58.

26. Huber, C. G.; Kleindienst, G.; Bonn, G. K., Application Of Micropellicular Poly-Styrene/Divinylbenzene Stationary Phases For High-Performance Reversed-Phase Liquid Chromotography Electrospray Mass Spectrometry Of Proteins And Peptides. *Chromatographia* **1997**, *44*, 438-448.

27. Brindza, M. R.; Walker, R. A., Differentiating Solvation Mechanisms at Polar Solid/Liquid Interfaces. *Journal of the American Chemical Society* **2009**, *131*, 6207-6214.

28. Eisenthal, K. B., Second Harmonic Spectroscopy Of Aqueous Nano- And Microparticle Interfaces. *Chemical Reviews* **2006**, *106*, 1462-1477.

29. Esenturk, O.; Walker, R. A., Indoline: A Versatile Probe Of Specific And Non-Specific Solvation Forces. *Physical Chemistry Chemical Physics* **2003**, *5*, 2020-2026.

30. Gibbs-Davis, J. M.; Kruk, J. J.; Konek, C. T.; Scheidt, K. A.; Geiger, F. M., Jammed Acid-Base Reactions at Interfaces. *Journal of the American Chemical Society* **2008**, *130*, 15444-15447.

31. Higgins, D. A.; Abrams, M. B.; Byerly, S. K.; Corn, R. M., Resonant 2nd Harmonic-Generation Studies of p-Nitrophenol Adsorption at Condensed-phase Interfaces. *Langmuir* **1992**, *8*, 1994-2000.

32. Horng, P.; Brindza, M. R.; Walker, R. A.; Fourkas, J. T., Behavior of Organic Liquids at Bare and Modified Silica Interfaces. *Journal of Physical Chemistry C* **2010**, *114*, 394-402.

33. Isaienko, O.; Nihonyanagi, S.; Sil, D.; Borguet, E., Observation of the Bending Mode of Interfacial Water at Silica Surfaces by Near-Infrared Vibrational Sum-Frequency Generation Spectroscopy of the Stretch plus Bend Combination Bands. *Journal of Physical Chemistry Letters* **2013**, *4*, 531-535.

34. Marowsky, G.; Steinhoff, R.; Chi, L. F.; Hutter, J.; Wagniere, G., 2ND-Harmonic Generation in Quinquethienyl Monolayers. *Physical Review B* **1988**, *38*, 6274-6278.

35. Verma, P.; Pal, H., Intriguing H-Aggregate and H-Dimer Formation of Coumarin-481 Dye in Aqueous Solution As Evidenced from Photophysical Studies. *Journal of Physical Chemistry A* **2012**, *116*, 4473-4484.

36. Verma, P.; Pal, H., Unusual H-Type Aggregation of Coumarin-481 Dye in Polar Organic Solvents. *Journal of Physical Chemistry A* **2013**, *117*, 12409-12418.

37. Roy, D.; Piontek, S.; Walker, R. A., Surface Induced Changes In Coumarin Solvation And Photochemistry At Polar Solid/Liquid Interfaces. *Physical Chemistry Chemical Physics* **2011**, *13*, 14758-14766.

38. Ariga, K.; Lvov, Y.; Kunitake, T., Assembling Alternate Dye-Polyion Molecular Films By Electrostatic Layer-By-Layer Adsorption. *Journal of the American Chemical Society* **1997**, *119*, 2224-2231.

39. Liu, X.; Cole, J. M.; Chow, P. C. Y.; Zhang, L.; Tan, Y.; Zhao, T., Dye Aggregation And Complex Formation Effects In 7-(Diethylamino)-Coumarin-3-Carboxylic Acid. *Journal of Physical Chemistry C* **2014**, *118*, 13042-13051.

40. Pant, D.; Le Guennec, M.; Illien, B.; Girault, H. H., The pH Dependent Adsorption Of Coumarin 343 At The Water/Dichloroethane Interface. *Physical Chemistry Chemical Physics* **2004**, *6*, 3140-3146.

41. Zhang, X. Y.; Cunningham, M. M.; Walker, R. A., Solvent Polarity At Polar Solid Surfaces: The Role Of Solvent Structure. *Journal of Physical Chemistry B* **2003**, *107*, 3183-3195.

42. Zhang, X. Q.; Yang, W. Y.; You, X. Z.; Wei, Y., Preparation And Characterization Of Self-Assembly Organic Multilayer Films On Silica Surface. *Applied Surface Science* **1995**, *84*, 267-271.

43. Zhang, X.; Steel, W. H.; Walker, R. A., Probing Solvent Polarity Across Strongly Associating Solid/Liquid Interfaces Using Molecular Rulers. *Journal Of Physical Chemistry B* **2003**, *107*, 3829-3836.

44. Wirth, M. J.; Burbage, J. D., Adsorbate Reorientation At A Water(Octadecylsilyl) Silica Interface. *Analytical Chemistry* **1991**, *63*, 1311-1317.

45. Vazquez, R.; Nogueira, R.; Busquets, S.; Mata, J. L.; Saramago, B., Wetting Films Of Polar And Nonpolar Liquids. *Journal of Colloid and Interface Science* **2005**, *284*, 652-657.

46. Vartia, A. A.; Thompson, W. H., Solvation and Spectra of a Charge Transfer Solute in Ethanol Confined within Nanoscale Silica Pores. *Journal of Physical Chemistry B* **2012**, *116*, 5414-5424.

47. Siler, A. R.; Walker, R. A., Effects of Solvent Structure on Interfacial Polarity at Strongly Associating Silica/Alcohol Interfaces. *Journal of Physical Chemistry C* **2011**, *115*, 9637-9643.

48. Shang, X. M.; Benderskii, A. V.; Eisenthal, K. B., Ultrafast Solvation Dynamics At Silica/Liquid Interfaces Probed By Time-Resolved Second Harmonic Generation. *Journal of Physical Chemistry B* **2001**, *105*, 11578-11585.

49. Bloembergen, N., 2ND Harmonic Reflected Light. *Optica Acta* **1966**, *13*, 311-322.

50. Benjamin, I., Inhomogeneous Broadening Of Electronic Spectra At Liquid Interfaces. *Chemical Physics Letters* **2011**, *515*, 56-61.

51. Hiemenz, P. C., *Principles Of Colloid And Surface Chemistry*, 2 ed.; Marcel Dekker, Inc: New York 1986; Vol. 9, p 792.

52. Taylor, J. R., *An Introduction To Error Analysis: The Study Of Uncertainties In Physical Measurements*, 2nd ed.; University Science Boooks: Sausalito, Ca, 1997.

53. Lakowicz, J., *Principles of Fluorescence Spectroscopy*, Third ed.; Springer Science +Business Media, LLC: New York, 2006.

54. Becker, W., Advanced Time Correlated Single Photon Counting Techniques. In *Advanced Time Correlated Single Photon Counting Techniques*, A.W. Castleman, J., J.P. Toennies, and W. Zinth, Ed. Springer Berlin, Germany, 2006; p 414.

55. Harris, D. C., *Exploring Chemical Analysis*, 3rd ed.; W.H. Freeman and Company: New York, NY, 2005.

56. Nad, S.; Kumbhakar, M.; Pal, H., Photophysical Properties Of Coumarin-152 And Coumarin-481 Dyes: Unusual Behavior In Nonpolar And In Higher Polarity Solvents. *Journal of Physical Chemistry A* **2003**, *107*, 4808-4816.

57. Hecht, E., *Optics*, 4th ed.; Pearson Education, Inc: San Francisco, CA, 2002.

58. Buncel, E.; Rajagopal, S., Studies Of Azo And Azoxy Dyestuffs .19. Solvatochromic Studies Of Novel Azo Merocyanine Dyes - The Pi-Star-Azo-Scale Of Solvent Polarity. *Journal of Organic Chemistry* **1989**, *54*, 798-809.

59. Marcus, Y., The Effectiveness Of Solvents As Hydrogen-Bond Donors. *Journal of Solution Chemistry* **1991**, *20*, 929-944.

60. Freed, B. K.; Biesecker, J.; Middleton, W. J., Spectral Polarity Index - A New Method For Determining The Relative Polarity Of Solvents 1. *Journal of Fluorine Chemistry* **1990**, *48*, 63-75.

61. Kosower, E. M., The Effect Of Solvent On Spectra .1. A New Empirical Measure Of Solvent Polarity - Z-Values. *Journal of the American Chemical Society* **1958**, *80*, 3253-3260.

62. Reichardt, C., Solvatochromic Dyes As Solvent Polarity Indicators. *Chemical Reviews* **1994**, *94*, 2319-2358.

63. Mellein, B. R.; Aki, S. N. V. K.; Ladewski, R. L.; Brennecke, J. F., Solvatochromic Studies Of Ionic Liquid/Organic Mixtures. *Journal of Physical Chemistry B* **2007**, *111*, 131-138.

64. Onsager, L., Electric Moments Of Molecules In Liquids. *Journal of the American Chemical Society* **1936**, *58*, 1486-1493.

65. *CRC Handbook of Chemistry and Physics*, 90 ed.; Taylor and Francis Group, LLC: Boca Raton, Fl, 2009-2010.

66. Suppan, P., Solvatochromic Shifts - The Influence Of The Medium On The Energy Of Electronic States. *Journal of Photochemistry and Photobiology a-Chemistry* **1990**, *50*, 293-330.

67. Steel, W. H., Y.Y. Lau, C.L. Beildeck, R.A. Walker, Solvent Polarity Across Weakly Associating Interfaces. *Journal Of Physical Chemistry B* **2004**, *108*, 13370-13378.

68. Urio, R. d. P.; Masini, J. C., Evaluation Of Sequential Injection Chromatography For Reversed Phase Separation Of Triazine Herbicides Exploiting Monolithic And Core-Shell Columns. *Talanta* **2015**, *131*, 528-534.

69. Escudero, C.; Salmeron, M., From Solid-Vacuum To Solid-Gas And Solid-Liquid Interfaces: In Situ Studies Of Structure And Dynamics Under Relevant Conditions. *Surface Science* **2013**, *607*, 2-9.

70. Weetall, H. H., Preparation of Immobilized Proteins Covalently Coupled Through Silane Coupling Agents to Inorganic Supports. *Applied Biochemistry and Biotechnology* **1993**, *41*, 157-188.

71. Chen, Z.; Li, Z.; Lin, Y.; Yin, M.; Ren, J.; Qu, X., Biomineralization Inspired Surface Engineering Of Nanocarriers For pH-Responsive, Targeted Drug Delivery. *Biomaterials* **2013**, *34*, 1364-71.

72. Mann, S., Molecular Technntonics in Biomineralization and Biomimetic Materials Chemistry. *Nature* **1993**, *365*, 499-505.

73. Znidarsic, W. J.; Chen, I. W.; Shastri, V. P., Influence Of Surface Charge And Protein Intermediary Layer On The Formation Of Biomimetic Calcium Phosphate On Silica Nanoparticles. *Journal of Materials Chemistry* **2012**, *22*, 19562-19569.

74. Yang, H.; Vovk, G.; Coombs, N.; Sokolov, I.; Ozin, G. A., Synthesis Of Mesoporous Silica Spheres Under Quiescent Aqueous Acidic Conditions. *Journal of Materials Chemistry* **1998**, *8*, 743-750.

75. Destoop, I.; Ghijsens, E.; Katayama, K.; Tahara, K.; Mali, K. S.; Tobe, Y.; De Feyter, S., Solvent-Induced Homochirality In Surface-Confined Low-Density Nanoporous Molecular Networks. *Journal of the American Chemical Society* **2012**, *134*, 19568-71.

76. Hopkins, A. J.; McFearin, C. L.; Richmond, G. L., Investigations Of The Solid-Aqueous Interface With Vibrational Sum-Frequency Spectroscopy. *Current Opinion in Solid State & Materials Science* **2005**, *9*, 19-27.

77. Mondal, S. K.; Yamaguchi, S.; Tahara, T., Molecules at the Air/Water Interface Experience a More Inhomogeneous Solvation Environment than in Bulk Solvents: A Quantitative Band Shape Analysis of Interfacial Electronic Spectra Obtained by HD-ESFG. *Journal of Physical Chemistry C* **2011**, *115*, 3083-3089.

78. Jena, K. C.; Covert, P. A.; Hore, D. K., The Effect of Salt on the Water Structure at a Charged Solid Surface: Differentiating Second- and Third-order Nonlinear Contributions. *Journal of Physical Chemistry Letters* **2011**, *2*, 1056-1061.

79. Duval, Y.; Mielczarski, J. A.; Pokrovsky, O. S.; Mielczarski, E.; Ehrhardt, J. J., Evidence Of The Existence Of Three Types Of Species At The Quartz-Aqueous Solution Interface At pH 0-10: XPS Surface Group Quantification And Surface Complexation Modeling. *Journal of Physical Chemistry B* **2002**, *106*, 2937-2945.

80. Koopal, L. K., Wetting of Solid Surfaces: Fundamentals and Charge effects. *Advances in Colloid and Interface Science* **2012**, *179*, 29-42.

81. Liu, Q.; Yuan, S. L.; Yan, H.; Zhao, X., Mechanism of Oil Detachment from a Silica Surface in Aqueous Surfactant Solutions: Molecular Dynamics Simulations. *Journal of Physical Chemistry B* **2012**, *116*, 2867-2875.

82. Manne, S.; Gaub, H. E., Molecular-Organization Of Surfactants At Solid-Liquid Interfaces. *Science* **1995**, *270*, 1480-1482.

83. Tiberg, F.; Jonsson, B.; Tang, J.; Lindman, B., Ellipsometry Studies Of The Self-Assembly Of Nonionic Surfactants At The Silica Water Interface-Equilibrium Aspects. *Langmuir* **1994**, *10*, 2294-2300.

84. Brown, M. A.; Huthwelker, T.; Redondo, A. B.; Janousch, M.; Faubel, M.; Arrell, C. A.; Scarongella, M.; Chergui, M.; van Bokhoven, J. A., Changes in the Silanol Protonation State Measured In Situ at the Silica-Aqueous Interface. *Journal of Physical Chemistry Letters* **2012**, *3*, 231-235.

85. Drach, M.; Andrzejewska, A.; Narkiewicz-Michalek, J.; Rudzinski, W.; Koopal, L. K., Theoretical Modeling Of Cationic Surfactants Aggregation At The Silica/Aqueous Solution Interface: Effects Of pH And Ionic Strength. *Physical Chemistry Chemical Physics* **2002**, *4*, 5846-5855.

86. Pokrovsky, O. S.; Golubev, S. V.; Mielczarski, J. A., Kinetic Evidences Of The Existence Of Positively Charged Species At The Quartz-Aqueous Solution Interface. *Journal of Colloid and Interface Science* **2006**, *296*, 189-194.

87. Sulpizi, M.; Gaigeot, M. P.; Sprik, M., The Silica-Water Interface: How the Silanols Determine the Surface Acidity and Modulate the Water Properties. *J. Chem. Theory Comput.* **2012**, *8*, 1037-1047.

88. Ong, S. W.; Zhao, X. L.; Eisenthal, K. B., Polarization of Water-Molecules at a Charged Interface-2nd Harmonic Studies of Silica Water Interface. *Chemical Physics Letters* **1992**, *191*, 327-335.

89. Allen, L. H.; Matijevi.E, Stability of Colloidal Silica: Effect of Hydroyzable Cations. *Journal of Colloid and Interface Science* **1971**, *35*, 66-&.

90. Allen, L. H.; Matijevi.E; Meties, L., Exchange Of Na+ For Silanolic Protons Of Silica. *Journal of Inorganic & Nuclear Chemistry* **1971**, *33*, 1293-&.

91. Horiuchi, H.; Nikolov, A.; Wasan, D. T., Calculation Of The Surface Potential And Surface Charge Density By Measurement Of The Three-Phase Contact Angle. *Journal of Colloid and Interface Science* **2012**, *385*, 218-224.

92. Iler, R. K., *The Chemistry Of Silica: Solubility, Polymerization, Colloid And Surface Properties, And Biochemistry* John Wiley & Sons, 1979.

93. Azam, M. S.; Weeraman, C. N.; Gibbs-Davis, J. M., Specific Cation Effects on the Bimodal Acid-Base Behavior of the Silica/Water Interface. *Journal of Physical Chemistry Letters* **2012**, *3*, 1269-1274.

94. Li, I.; Bandara, J.; Shultz, M. J., Time Evolution Studies Of The H2O/Quartz Interface Using Sum Frequency Generation, Atomic Force Microscopy, And Molecular Dynamics. *Langmuir* **2004**, *20*, 10474-10480.

95. Zhao, X. L.; Ong, S. W.; Eisenthal, K. B., Polarization of Water-Molecules at a Charged Interface-2nd Harmonic Studies of Charged Monolayers at the Air-Water Interface. *Chemical Physics Letters* **1993**, *202*, 513-520.

96. Zhao, X. L.; Ong, S. W.; Wang, H. F.; Eisenthal, K. B., New Method For Determination Of Surface pKa Using 2nd Harmonic Generation. *Chemical Physics Letters* **1993**, *214*, 203-207.

97. Green, J. S.; Jorgenson, J. W., Minimizing Adsorption Of Proteins On Fused-Silica In Capillary Zone Electrophoresis By The Addition Of Alkali-Metal Salts To The Buffers. *Journal of Chromatography* **1989**, *478*, 63-70.

98. Yakovleva, J.; Davidsson, R.; Lobanova, A.; Bengtsson, M.; Eremin, S.; Laurell, T.; Emneus, J., Microfluidic Enzyme Immunoassay Using Silicon Microchip With Immobilized Antibodies And Chemiluminescence Detection. *Analytical Chemistry* **2002**, *74*, 2994-3004.

99. Busson, B.; Tadjeddine, A., Non-Uniqueness of Parameters Extracted from Resonant Second-Order Nonlinear Optical Spectroscopies. *Journal of Physical Chemistry C* **2009**, *113*, 21895-21902.

100. Can, S. Z.; Chang, C. F.; Walker, R. A., Spontaneous Formation Of DPPC Monolayers At Aqueous/Vapor Interfaces And The Impact Of Charged Surfactants. *Biochimica Et Biophysica Acta-Biomembranes* **2008**, *1778*, 2368-2377.

101. Moridani, M. Y.; Siraki, A.; Chevaldina, T.; Scobie, H.; O'Brien, P. J., Quantitative Structure Toxicity Relationships For Catechols In Isolated Rat Hepatocytes. *Chemico-Biological Interactions* **2004**, *147*, 297-307.

102. Mazumder, M.; Bhushan, B., Propensity And Geometrical Distribution Of Surface Nanobubbles: Effect Of Electrolyte, Roughness, pH, And Substrate Bias. *Soft Matter* **2011**, *7*, 9184-9196.

103. Yang, J.; Duan, J.; Fornasiero, D.; Ralston, J., Kinetics Of Co2 Nanobubble Formation At The Solid/Water Interface. *Physical Chemistry Chemical Physics* **2007**, *9*, 6327-6332.

104. Yang, C. S. C.; Richter, L. J.; Stephenson, J. C.; Briggman, K. A., In Situ, Vibrationally Resonant Sum Frequency Spectroscopy Study Of The Self-Assembly Of Dioctadecyl Disulfide On Gold. *Langmuir* **2002**, *18*, 7549-7556.

105. Malin, J. N.; Geiger, F. M., Uranyl Adsorption and Speciation at the Fused Silica/Water Interface Studied by Resonantly Enhanced Second Harmonic Generation and the Chi((3)) Method. *Journal of Physical Chemistry A* **2010**, *114*, 1797-1805.

106. Steinhurst, D. A.; Owrutsky, J. C., Second Harmonic Generation From Oxazine Dyes At The Air/Water Interface. *Journal of Physical Chemistry B* **2001**, *105*, 3062-3072.

107. Alvarezzepeda, A.; Barman, B. N.; Martire, D. E., Thermodynamic Study Of The Marked Differenes Between Acetonitrile Water And Methanol Water Mobile-Phase Systems In Reversed-Phase Liquic Chromatography. *Analytical Chemistry* **1992**, *64*, 1978-1984.

108. Rafferty, J. L.; Siepmann, J. I.; Schure, M. R., Mobile Phase Effects In Reversed-Phase Liquid Chromatography A Comparison Of Acetonitrile/Water And Methanol/Water Solvents As Studied By Molecular Simulation. *Journal of Chromatography A* **2011**, *1218*, 2203-2213.

109. Meyer, T.; Wania, F.; Vreivik, K., Illustrating Sensitivity And Uncertainty In Environmental Fate Models Using Partitioning Maps. *Environmental Science and Technology* **2005**, *39*, 3186-3196.

110. Goss, K. U.; Schwarzenbach, R. P., Linear Free Energy Relationships Used To Evaluate Equilibrium Partitioning Of Organic Compounds. *Environmental Science and Technology* **2001**, *35*, 1-9.

111. Wang, H. F.; Borguet, E.; Eisenthal, K. B., Generalized Interface Polarity Scale Based On Second Harmonic Spectroscopy. *Journal Of Physical Chemistry B* **1998**, *102*, 4927-4932.

112. Yamaguchi, S.; Watanabe, H.; Mondal, S. K.; Kundu, A.; Tahara, T., "Up" Versus "Down" Alignment And Hydration Structures Of Solutes At The Air/Water Interface Revealed By Heterodyne-Detected Electronic Sum Frequency Generation With Classical Molecular Dynamics Simulation. *Journal of Chemical Physics* **2011**, *135*.

113. Farmahini, A. H.; Bhatia, S. K., Differences In The Adsorption And Diffusion Behaviour Of Water And Non-Polar Gases In Nanoporous Carbon: Role Of Cooperative Effects Of Pore Confinement And Hydrogen Bonding. *Molecular Simulation* **2015**, *41*, 432-445.

114. Smith, E. A.; Wirth, M. J., pH Dependence Of Tailing In Reversed-Phase Chromatography Of A Cationic Dye: Measurement Of The Strong Adsorption Site Surface Density. *Journal of Chromatography A* **2004**, *1060*, 127-134.

115. Steel, W. H.; Walker, R. A., Measuring Dipolar Width Across Liquid-Liquid Interfaces With 'Molecular Rulers'. *Nature* **2003**, *424*, 296-299.

116. Zhang, X. Y.; Walker, R. A., Discrete Partitioning Of Solvent Permittivity At Liquid-Solid Interfaces. *Langmuir* **2001**, *17*, 4486-4489.

117. Beaglehole, D.; Christenson, H. K., Vapor Adsorption On Mica And Silicon - Entropy Effects, Layering, And Surface Forces. *Journal of Physical Chemistry* **1992**, *96*, 3395-3403.

118. Schlangen, L. J. M.; Koopal, L. K.; Stuart, M. A. C.; Lyklema, J.; Robin, M.; Toulhoat, H., Thin Hydrocarbon And Water Films On Bare And Methylated Silica - Vapor Adsorption, Wettability, Adhesion, And Surface Forces. *Langmuir* **1995**, *11*, 1701-1710.

119. Tavana, H.; Neumann, A. W., Recent Progress In The Determination Of Solid Surface Tensions From Contact Angles. *Advances in Colloid and Interface Science* **2007**, *132*, 1-32.

120. Fowkes, F. M., Determination Of Interfacial Tensions, Contact Angles, And Dispersion Forces In Surfaces By Assuming Additivity Of Intermolecular Interactions In Surfaces. *Journal of Physical Chemistry* **1962**, *66*, 382-&.

121. Correa, R.; Saramago, B., On The Calculation Of Disjoining Pressure Isotherms For Nonaqueous Films. *Journal of Colloid and Interface Science* **2004**, *270*, 426-435.

122. Levinson, P.; Valignat, M. P.; Fraysse, N.; Cazabat, A. M.; Heslot, F., An Ellipsometric Study Of Adsorption-Isotherms. *Thin Solid Films* **1993**, *234*, 482-485.

123. Bonnet, J. C.; Pike, F. P., Surface Properties Of 9 Liquids. *Journal of Chemical and Engineering Data* **1972**, *17*, 145-&.

124. Chibowski, E.; Holysz, L., Use Of The Washburn Equation For Surface Free-Energy Determination. *Langmuir* **1992**, *8*, 710-716.

125. Chibowski, E.; Holysz, L., On The Use Of Washburn's Equation For Contact Angle Determination. *Journal of Adhesion Science and Technology* **1997**, *11*, 1289-1301.

126. Horr, T. J.; Ralston, J.; Smart, R. S., The Use Of Contact-Angle Measurements To Quantify The Adsorption Density And Thickness Of Organic-Molecules On Hydrophilic Surfaces. *Colloids and Surfaces A - Physicochemical and Engineering Aspects* **1995**, *97*, 183-196.

127. Zhang, X. Y., M.M. Cunningham, R.A. Walker, Solvent Polarity At Polar Solid Surfaces: The Role Of Solvent Structure. *Journal Of Physical Chemistry B* **2003**, *107*, 3183-3195.

128. Benjamin, I., Chemical Reactions And Solvation At Liquid Interfaces: A Microscopic Perspective. *Chemical Reviews* **1996**, *96*, 1449-1475.

129. Yu, C. J., G. Evmenenko, A.G. Richter, A. Datta, J. Kmetko, P. Dutta, Order In Molecular Liquids Near Solid-Liquid Interfaces. *Applied Surface Science* **2001**, *182*, 231-235.

130. Bhattacharyya, K.; Sitzmann, E. V.; Eisenthal, K. B., Study of Chemical-Reactions by Surface 2nd Harmonic Generation-Para-nitrophenol at the Air-Water Interface. *Journal of Chemical Physics* **1987**, *87*, 1442-1443.

131. Ishizaka, S.; Kim, H. B.; Kitamura, N., Time-Resolved Total Internal Reflection Fluorometry Study On Polarity At A Liquid/Liquid Interface. *Analytical Chemistry* **2001**, *73*, 2421-2428.

132. Yanagimachi, M.; Tamai, N.; Masuhara, H., Solvation Dynamics Of A Coumarin Dye At Liquid Solid Interface Layer - Picosecond Total Internal-Reflection Fluorescence Spectroscopic Study. *Chemical Physics Letters* **1992**, *200*, 469-474.

133. Doerr, A. K., M. Tolan, J.P. Schlomaka, W. Press, Evidence For Density Anomalies Of Liquids At The Solid/Liquid Interface. *Europhysics Letter* **2000**, *52*, 330-336.

134. Christenson, H. K., D.W.R. Gruen, R.G. Horn, Structuring In Liquid Alkanes Between Solid Surfaces: Force Measurements And Mean-Field Theory. *Journal of Chemical Physics* **1987**, *87*, 1834-1841.

135. Gao, J. P., W.D. Luedtke, U. Landman, Structure And Solvation Forces In Confined Films: Linear And Branched Alkanes. *Journal of Chemical Physics* **1997**, *106*, 4309-4318.

136. Christenson, H. K., Phase Behavior In Confinement Studied With A Surface Force Apparatus. *Journal of Dispersion Science and Technology* **2006**, *27*, 617-624.

137. Wang, Y.; Hill, K.; Harris, J. G., Comparison Of Branched And Linear Octanes In The Surface Force Apparatus - A Molecular-Dynamics Study. *Langmuir* **1993**, *9*, 1983-1985.

138. Mikulski, P. T.; Herman, L. A.; Harrison, J. A., Odd And Even Model Self-Assembled Monolayers: Links Between Friction And Structure. *Langmuir* **2005**, *21*, 12197-12206.

139. Kanda, Y.; Iwasaki, S.; Higashitani, K., Adhesive Force Between Hydrophilic Surfaces In Alcohol-Water Solutions. *Journal of Colloid and Interface Science* **1999**, *216*, 394-400.

140. Liu, W. T., L.N. Zjang, Y.R. Shen, Interfacial Layer Structure At Alcohol/Silica Interfaces Probed By Sum-Frequency Vibrational Spectroscopy. *Chemical Physics Letters* **2005**, *412*, 206-209.

141. Zobel, M.; Neder, R. B.; Kimber, S. A. J., Universal Solvent Restructuring Induced By Colloidal Nanoparticles. *Science* **2015**, *347*, 292-294.

142. Dolores, E. M.; Rodriguez, J.; Laria, D., Structure And Dynamics Of Liquid Methanol Confined Within Functionalized Silica Nanopores. *Journal of Chemical Physics* **2010**, *133*, 154707.

143. Dolores, E. M.; Rodriguez, J.; Laria, D., Liquid Methanol Confined Within Functionalized Silica Nanopores. 2. Solvation Dynamics Of Coumarin 153. *Journal Of Physical Chemistry B* **2011**, *115*, 12859-12867.

144. Guégan, R.; Morineau, D.; Alba-Simionesco, C., Interfacial Structure Of A H-Bonding Liquid Confined Into Silica Nanopore With Surface Silanols. *Chemical Physics* **2005**, *317*, 236-244.

145. Vartia, A. A.; Thompson, W. H., Solvation and Spectra of a Charge Transfer Solute in Ethanol Confined within Nanoscale Silica Pores. *Journal Of Physical Chemistry B* **2013**, *116*, 5414-5424.

146. Feng, X. B.; Thompson, W. H., Time-Dependent Fluorescence in Nanoconfined Solvents. A Smoluchowski Equation Model Study. *Journal of Physical Chemistry C* **2010**, *114*, 4279-4290.

147. Gomez, J. A.; Tucker, A. K.; Shepherd, T. D.; Thompson, W. H., Conformational Free Energies Of 1,2-Dichloroethane In Nanoconfined Methanol. *Journal of Physical Chemistry B* **2005**, *109*, 17479-17487.

148. Benderskii, A. V.; Henzie, J.; Basu, S.; Shang, X. M.; Eisenthal, K. B., Femtosecond Aqueous Solvation At A Positively Charged Surfactant/Water Interface. *Journal Of Physical Chemistry B* **2004**, *108*, 14017-14024.

149. Shang, X.; Nguyen, K.; Rao, Y.; Eisenthal, K. B., In-Plane Molecular Rotational Dynamics at a Negatively Charged Surfactant/Aqueous Interface. *Journal of Physical Chemistry C* **2008**, *112*, 20375-20381.

150. Abbas, H., First Principle Calculation Of The Photophysical Properties Of Silylated Coumarins 120 And 151. *Computational and Theoretical Chemistry* **2012**, *992*, 55-58.

151. Aono, S.; Minezawa, N.; Kato, S., Electronic Spectra Of Coumarin-151 In Polar Solvents: Linear Response Free Energy Approach. *Chemical Physics Letters* **2010**, *492*, 193-197.

152. Arbeloa, T. L.; Arbeloa, F. L.; Arbeloa, I. L., Influence Of Fluorinated Group On The Photophysics Of 7-Aminocoumarins. *Journal of Luminescence* **1996**, *68*, 149-155.

153. Cave, R. J.; Burke, K.; Castner, E. W., Theoretical Investigation Of The Ground And Excited States Of Coumarin 151 And Coumarin 120. *Journal of Physical Chemistry A* **2002**, *106*, 9294-9305.

154. Cave, R. J.; Castner, E. W., Time-Dependent Density Functional Theory Investigation Of The Ground And Excited States Of Coumarins 102, 152, 153, And 343. *Journal of Physical Chemistry A* **2002**, *106*, 12117-12123.

155. Das, K.; Jain, B.; Patel, H. S., Hydrogen Bonding Properties Of Coumarin 151, 500, And 35: The Effect Of Substitution At The 7-Amino Position. *Journal of Physical Chemistry A* **2006**, *110*, 1698-1704.

156. Krystkowiak, E.; Maciejewski, A., Changes In Energy Of Three Types Of Hydrogen Bonds Upon Excitation Of Aminocoumarins Determined From Absorption Solvatochromic Experiments. *Physical Chemistry Chemical Physics* **2011**, *13*, 11317-11324.

157. Liu, Y.; Ding, J.; Liu, R.; Shi, D.; Sun, J., Revisiting The Electronic Excited-State Hydrogen Bonding Dynamics Of Coumarin Chromophore In Alcohols: Undoubtedly

Strengthened Not Cleaved. *Journal of Photochemistry and Photobiology a-Chemistry* **2009**, *201*, 203-207.

158. Liu, Y.-H.; Li, P., Excited-State Hydrogen Bonding Effect On Dynamic Fluorescence Of Coumarin 102 Chromophore In Solution: A Time-Resolved Fluorescence And Theoretical Study. *Journal of Luminescence* **2011**, *131*, 2116-2120.

159. Nad, S.; Pal, H., Unusual Photophysical Properties Of Coumarin-151. *Journal of Physical Chemistry A* **2001**, *105*, 1097-1106.

160. Pedone, A., Role of Solvent on Charge Transfer in 7-Aminocoumarin Dyes: New Hints from TD-CAM-B3LYP and State Specific PCM Calculations. *J. Chem. Theory Comput.* **2013**, *9*, 4087-4096.

161. Rechthaler, K.; Kohler, G., Excited-State Properties And Deactivation Pathways Of 7-Aminocoumarins. *Chemical Physics* **1994**, *189*, 99-116.

162. Corrie, J. E. T.; Munasinghe, V. R. N.; Rettig, W., Synthesis And Fluorescence Properties Of Substituted 7-Aminocoumarin-3-Carboxylate Derivatives. *Journal of Heterocyclic Chemistry* **2000**, *37*, 1447-1455.

163. Forster, Y.; Haas, E., Preparation And Characterization Of 3 Fluorescent Labels For Proteins, Suitable For Structural Studies. *Analytical Biochemistry* **1993**, *209*, 9-14.

164. Shobini, J.; Mishra, A. K.; Sandhya, K.; Chandra, N., Interaction Of Coumarin Derivatives With Human Serum Albumin: Investigation By Fluorescence Spectroscopic Technique And Modeling Studies. *Spectrochimica Acta Part a-Molecular and Biomolecular Spectroscopy* **2001**, *57*, 1133-1147.

165. Das, K.; Jain, B.; Patel, H. S., Hydrogen Bonding Properties Of Coumarin 151, 500, And 35: The Efffect Of Substitution At The 7-Amino Position. *Journal of Physical Chemistry A* **2006**, *110*, 1698-1704.

166. Nad, S.; Pal, H., Unusual Photphysical Properties Of Coumarin-151. *Journal of Physical Chemistry A* **2001**, *105*, 1097-1106.

167. Rechthaler, K.; Kohler, G., Excited State Properties And Deactivation Pathways Of 7-Aminocoumarins. *Chemical Physics* **1994**, *189*, 99-116.

168. Dahiya, P.; Kumbhakar, M.; Mukherjee, T.; Pal, H., Effect Of Protic Solvents On Twisted Intramolecular Charge Transfer State Formation In Coumarin-152 And Coumarin-481 Dyes. *Chemical Physics Letters* **2005**, *414*, 148-154.

169. Siler, A. R., M.R. Brindza, R.A. Walker, Hydrogen-Bonding Molecular Ruler Surfactants As Probes Of Specific Solvation At Liquid/Liquid Interfaces. *Analytical and Bioanalytical Chemistry* **2009**, *395*, 1063-1073.

170. Gayathri, B. R.; Mannekutla, J. R.; Inamdar, S. R., Effect Of Binary Solvent Mixtures (DMSO/Water) On The Dipole Moment And Lifetime Of Coumarin Dyes. *Journal of Molecular Structure* **2008**, *889*, 383-393.

171. Inamdar, S. R.; Gayathri, B. R.; Mannekutla, J. R., Rotational Diffusion of Coumarins in Aqueous DMSO. *Journal of Fluorescence* **2009**, *19*, 693-703.

172. Zhang, L.; Singh, S.; Tian, C.; Shen, Y. R.; Wu, Y.; Shannon, M. A.; Brinker, C. J., Nanoporous Silica-Water Interfaces Studied By Sum-Frequency Vibrational Spectroscopy. *Journal of Chemical Physics* **2009**, *130*.

173. Shen, Y. R.; Ostroverkhov, V., Sum-Frequency Vibrational Spectroscopy On Water Interfaces: Polar Orientation Of Water Molecules At Interfaces. *Chemical Reviews* **2006**, *106*, 1140-1154.

174. Gradl, G.; Kohler, B. E.; Westerfield, C., Electric-Field Splitting of the Octateranene 1 1AG- 2 1AG Transition in n-Hexane. *Journal of Chemical Physics* **1992**, *97*, 6064-6071.

175. Kohler, B. E.; Woehl, J. C., Measuring Internal Electric-Fields With Atomic-Resolution. *Journal of Chemical Physics* **1995**, *102*, 7773-7781.

176. Kohler, B. E.; Woehl, J. C., Effects Of Electrostatic Fields And Potentials On The Electronic Energies Of Conjugated Organic Molecules. *Journal of Physical Chemistry A* **1999**, *103*, 2435-2445.

177. Steel, W. H.; Damkaci, F.; Nolan, R.; Walker, R. A., Molecular Rulers: New Families Of Molecules For Measuring Interfacial Widths. *Journal of the American Chemical Society* **2002**, *124*, 4824-4831.

178. Kina, D.; Arora, P.; Nakayama, A.; Noro, T.; Gordon, M. S.; Taketsugu, T., Ab Initio QM/MM Excited-State Molecular Dynamics Study of Coumarin 151 in Water Solution. *International Journal of Quantum Chemistry* **2009**, *109*, 2308-2318.

179. Bratescu, M. A.; Saito, N.; Takai, O., Attenuated Total Reflectance Spectroscopy Of Coumarin Organosilane Molecules Adsorbed On A Fused Silica Surface. *Applied Surface Science* **2010**, *257*, 1792-1799.

180. Schach, D.; Globisch, C.; Roeters, S. J.; Woutersen, S., et al., Sticky Water Surfaces: Helix-Coil Transitions Suppressed In A Cell-Penetrating Peptide At The Air-Water Interface. *Journal of Chemical Physics* **2014**, *141*.

181. Azam, M. S.; Gibbs-Davis, J. M., Monitoring DNA Hybridization and Thermal Dissociation at the Silica/Water Interface Using Resonantly Enhanced Second Harmonic Generation Spectroscopy. *Analytical Chemistry* **2013**, *85*, 8031-8038.

182. Sauerbeck, C.; Braunschweig, B.; Peukert, W., Surface Charging and Interfacial Water Structure of Amphoteric Colloidal Particles. *Journal of Physical Chemistry C* **2014**, *118*, 10033-10042.

183. Moog, R. S.; Kim, D. D.; Oberle, J. J.; Ostrowski, S. G., Solvent Effects On Electronic Transitions Of Highly Dipolar Dyes: A Comparison Of Three Approaches. *Journal of Physical Chemistry A* **2004**, *108*, 9294-9301.

184. Shen, Y. R., *The Principles of Nonlinear Optics*; John Wiley and Sons: New York, 1984.

185. Wang, H.; Yan, E. C. Y.; Borguet, E.; Eisenthal, K. B., Second Harmonic Generation From The Surface Of Centrosymmetric Particles In Bulk Solution. *Chemical Physics Letters* **1996**, *259*, 15-20.

186. Wang, H. F.; Borguet, E.; Eisenthal, K. B., Polarity Of Liquid Interfaces By Second Harmonic Generation Spectroscopy. *Journal of Physical Chemistry A* **1997**, *101*, 713-718.

187. Achtyl, J. L.; Vlassiouk, I. V.; Surwade, S. P.; Fulvio, P. F.; Dai, S.; Geiger, F. M., Interaction of Magnesium Ions with Pristine Single-Layer and Defected Graphene/Water Interfaces Studied by Second Harmonic Generation. *Journal of Physical Chemistry B* **2014**, *118*, 7739-7749.

188. Li, Z.; Weeraman, C. N.; Gibbs-Davis, J. M., Ketone Binding at Amino and Ureido Monolayer/Solvent Interfaces Studied by Nonlinear Optical Techniques. *Journal of Physical Chemistry C* **2014**, *118*, 28662-28670.

189. Frisch, M. J.; Trucks, G. W.; Schlegel, H. B.; Scuseria, G. E., et al. *Gaussian 09*, D.01; Gaussian, INC Wallingford CT: 2009.

190. Zhao, Y.; Truhlar, D. G., A New Local Density Functional For Main-Group Thermochemistry, Transition Metal Bonding, Thermochemical Kinetics, And Noncovalent Interactions. *Journal of Chemical Physics* **2006**, *125*.

191. Shi, X.; Borguet, E.; Tarnovsky, A. N.; Eisenthal, K. B., Ultrafast Dynamics And Structure At Aqueous Interfaces By Second Harmonic Generation. *Chemical Physics* **1996**, *205*, 167-178.

192. Roy, D.; Marianski, M.; Maitra, N. T.; Dannenberg, J. J., Comparison Of Some Dispersion-Corrected And Traditional Functionals With CCSD(T) And MP2 Ab Initio Methods: Dispersion, Induction, And Basis Set Superposition Error. *Journal of Chemical Physics* **2012**, *137*.

193. Marianski, M.; Oliva, A.; Dannenberg, J. J., A Reinvestigation of the Drimer of para-Benzoquinone and Pyrimidine with MP2, CCSD(T), and DFT Using Functionals

Including Those Designed to Describe Dispersion. *Journal of Physical Chemistry A* **2012**, *116*, 8100-8105.

194. Nguyen, T. Q.; Doan, V.; Schwartz, B. J., Conjugated Polymer Aggregates In Solution: Control Of Interchain Interactions. *Journal of Chemical Physics* **1999**, *110*, 4068-4078.

195. Rivera, C. A.; Souna, A. J.; Bender, J. S.; Manfred, K.; Fourkas, J. T., Reorientation-Induced Spectral Diffusion in Vibrational Sum-Frequency-Generation Spectroscopy. *Journal of Physical Chemistry B* **2013**, *117*, 15875-15885.

196. Loughnane, B. J.; Farrer, R. A.; Scodinu, A.; Fourkas, J. T., Dynamics Of A Wetting Liquid In Nanopores: An Optical Kerr Effect Study Of The Dynamics Of Acetonitrile Confined In Sol-Gel Glasses. *Journal of Chemical Physics* **1999**, *111*, 5116-5123.

197. Morales, C. M.; Thompson, W. H., Simulations of Infrared Spectra of Nanoconfined Liquids: Acetonitrile Confined in Nanoscale, Hydrophilic Silica Pores. *Journal of Physical Chemistry A* **2009**, *113*, 1922-1933.

198. Gulmen, T. S.; Thompson, W. H., Grand Canonical Monte Carlo Simulations of Acetonitrile Filling of Silica Pores of Varying Hydrophilicity/Hydrophobicity. *Langmuir* **2009**, *25*, 1103-1111.

199. Milischuk, A. A.; Ladanyi, B. M., Polarizability Anisotropy Relaxation in Nanoconfinement: Molecular Simulation Study of Acetonitrile in Silica Pores. *Journal of Physical Chemistry B* **2013**, *117*, 15729-15740.

200. CabaleiroLago, E. M.; Rios, M. A., A Potential Function For Intermolecular Interaction In The Acetonitrile Dimer Constructed From Ab Initio Data. *Journal of Physical Chemistry A* **1997**, *101*, 8327-8334.

201. Takamuku, T.; Tabata, M.; Yamaguchi, A.; Nishimoto, J.; Kumamoto, M.; Wakita, H.; Yamaguchi, T., Liquid Structure Of Acetonitrile-Water Mixtures By X-Ray Diffraction And Infrared Spectroscopy. *Journal of Physical Chemistry B* **1998**, *102*, 8880-8888.

202. Marcus, Y.; Migron, Y., Polarity, Hydrogen-Bonding, And Structure Of Mixtures Of Water And Cyanomethane. *Journal of Physical Chemistry* **1991**, *95*, 400-406.

203. Choi, J.-H.; Oh, K.-I.; Lee, H.; Lee, C.; Cho, M., Nitrile And Thiocyanate IR Probes: Quantum Chemistry Calculation Studies And Multivariate Least-Square Fitting Analysis. *Journal of Chemical Physics* **2008**, *128*.

204. Guo, Y.; Gaiki, S., Retention Behavior Of Small Polar Compounds On Polar Stationary Phases In Hydrophilic Interaction Chromatography. *Journal of Chromatography A* **2005**, *1074*, 71-80.

205. Olsen, B. A., Hydrophilic Interaction Chromatography Using Amino And Silica Columns For The Determination Of Polar Pharmaceuticals And Impurities. *Journal of Chromatography A* **2001**, *913*, 113-122.

206. Reubsaet, J. L. E.; Vieskar, R., Characterisation Of Pi-Pi Interactions Which Determine Retention Of Aromatic Compounds In Reversed-Phase Liquid Chromatography. *Journal of Chromatography A* **1999**, *841*, 147-154.

207. Urban, J.; Skerikova, V.; Jandera, P.; Kubickova, R.; Pospisilova, M., Preparation And Characterization Of Polymethacrylate Monolithic Capillary Columns With Dual Hydrophilic Interaction Reversed-Phase Retention Mechanism For Polar Compounds. *Journal of Separation Science* **2009**, *32*, 2530-2543.

208. Ding, F.; Hu, Z.; Zhong, Q.; Manfred, K.; Gattass, R. R.; Brindza, M. R.; Fourkas, J. T.; Walker, R. A.; Weeks, J. D., Interfacial Organization of Acetonitrile: Simulation and Experiment. *Journal of Physical Chemistry C* **2010**, *114*, 17651-17659.

209. Hu, Z.; Weeks, J. D., Acetonitrile on Silica Surfaces and at Its Liquid-Vapor Interface: Structural Correlations and Collective Dynamics. *Journal of Physical Chemistry C* **2010**, *114*, 10202-10211.

210. Loughnane, B. J.; Farrer, R. A.; Fourkas, J. T., Evidence For The Direct Observation Of Molecular Exchange Of A Liquid At The Solid/Liquid Interface. *Journal of Physical Chemistry B* **1998**, *102*, 5409-5412.

211. Woods, B. L.; George, J. K.; Sherman, A. M.; Callis, P. R.; Walker, R. A., Adsorption and Aggregate Formation at the Silica/Liquid Interface. *Journal of Physical Chemistry C* **2015**, *Submitted*.

212. Liu, W. T.; Zhang, L. N.; Shen, Y. R., Interfacial layer structure at alcohol/silica interfaces probed by sum-frequency vibrational spectroscopy. *Chemical Physics Letters* **2005**, *412*, 206-209.

213. Gayathri, B. R.; Mannekutla, J. R.; Inamdar, S. R., Rotational Diffusion Of Coumarins In Alcohols: A Dielectric Friction Study. *Journal of Fluorescence* **2008**, *18*, 943-952.

214. Pal, H.; Nad, S.; Kumbhakar, M., Photophysical Properties Of Coumarin-120: Unusual Behavior In Nonpolar Solvents. *Journal of Chemical Physics* **2003**, *119*, 443-452.

215. Sharma, V. K.; Saharo, P. D.; Sharma, N.; Rastogi, R. C.; Ghoshal, S. K.; Mohan, D., Influence Of Solvent And Substituent On Excited State Characterstics Of Laser Grade Coumarin Dyes. *Spectrochimica Acta Part a-Molecular and Biomolecular Spectroscopy* **2003**, *59*, 1161-1170.

216. Curthoys, G.; Davydov, V. Y.; Kiselev, A. V.; Kiselev, S. A.; Kuznetso.Bv, Hydrogen-Bonding In Adsorption On Silica. *Journal of Colloid and Interface Science* **1974**, *48*, 58-72.

217. Nguyen, T. T.; Conboy, J. C., High-Throughput Screening of Drug-Lipid Membrane Interactions via Counter-Propagating Second Harmonic Generation Imaging. *Analytical Chemistry* **2011**, *83*, 5979-5988.

218. Liu, Y.; Yan, E. C. Y.; Eisenthal, K. B., Effects of bilayer surface charge density on molecular adsorption and transport across liposome bilayers. *Biophysical Journal* **2001**, *80*, 1004-1012.

219. Troiano, J. M.; Olenick, L. L.; Kuech, T. R.; Melby, E. S., et al., Direct Probes of 4 nm Diameter Gold Nanoparticles Interacting with Supported Lipid Bilayers. *Journal of Physical Chemistry C* **2015**, *119*, 534-546.

220. Greiner, A. J.; Pillman, H. A.; Worden, R. M.; Blanchard, G. J.; Ofoli, R. Y., Effect of Hydrogen Bonding on the Rotational and Translational Dynamics of a Headgroup-Bound Chromophore in Bilayer Lipid Membranes. *Journal of Physical Chemistry B* **2009**, *113*, 13263-13268.